Investigation of Advanced Effusion Cooling Technology for Gas Turbine Combustor Liner

Yeongmin Pyo

Thesis submitted to the Department of Mechanical Engineering in partial fulfillment of the requirements for the degree of

MASTER OF APPLIED SCIENCE

Faculty of Engineering - Department of Mechanical Engineering
University of Ottawa
Ottawa, Ontario, Canada

July 2025

Abstract

Effusion cooling represents the forefront of cooling technology for gas turbines, particularly within the hot-gas path components. Traditionally, effusion cooling holes are aligned with the combustor axis, resulting in a nominal zero compound angle, which is defined as the angle between the direction of the effusion jet and the mainstream flow in the lateral (transverse) plane. This alignment is based on the assumption that the swirling nature of the main flow does not significantly affect the cooling effectiveness. However, this study challenges this assumption by investigating the directional effects of effusion cooling under the influence of a swirling main flow, particularly focusing on the adiabatic film cooling effectiveness (AFE).

The research initially explores the isolated impacts of varying compound angles on AFE, deliberately excluding the influences of changing effusion hole spacing called effusion hole pitch. This approach facilitates a clearer understanding of how non-zero compound angles alone affect AFE. Building on this foundation, the study then examines the combined effects of varying pitch and compound angle, aiming to guide future designs of effusion cooling under swirling flow conditions. To achieve this, a novel effusion cooling design was proposed, featuring varying compound angles of 90, 60, and 30 degrees along the main flow direction. This design was compared against conventional methods with fixed compound angles.

Both experimental studies utilized Binary Pressure Sensitive Paint (PSP) and the heat/mass transfer analogy to measure AFE. The results indicate that larger compound angles facilitate quicker initial cooling film build-up, but optimal angles decrease downstream as the cooling film develops. The new effusion cooling design with varying compound angles demonstrated more uniform cooling film coverage and a slight enhancement in AFE compared to traditional designs with fixed angles. These findings suggest that reconsidering the standard alignment and angle of effusion cooling holes, particularly in the context of swirling main flows, can lead to significant improvements in gas turbine cooling efficiency.

Acknowledgments

I extend my profound gratitude to my thesis supervisor, Professor Bertrand Jodoin, whose guidance has been invaluable throughout the duration of this program. It has been a privilege and an enriching experience to learn from and collaborate with him over these years.

My sincere thanks are also due to Dr. Zekai Hong, Senior Research Officer at the National Research Council of Canada, for his supervision and mentorship in this project. His encouragement to delve deeper into my research has enabled me to reach heights previously unimagined.

I am grateful to Dr. Patrick Richer, Assistant Professor, for granting me the opportunity to pursue this project. His insightful suggestions and brilliant ideas have consistently guided me towards the correct path in my research endeavors.

I would like to express my appreciation to all members of the Thermal Management Group of the Zero Carbon Research Team in the Gas Turbine Laboratory at the National Research Council of Canada, including Dr. Mohsen Broumand, Dr. Sean Yun, and Juchan Son, for their valuable suggestions and contributions to this project.

I am thankful to the members of the Cold Spray Laboratory at the University of Ottawa, comprising Dr. Daniel MacDonald, Dr. Aleksandra Nastic, Dr. Leon Guo, Parisa Hasanpour Dastjerdi, Hamid Rahmati, Krutik Mistry, Mihai Stefan Stefanescu, and Juchan Son. Their guidance in the laboratory and the advice provided throughout have been immensely beneficial.

Lastly, but most importantly, I extend my heartfelt gratitude to my parents and to my family, Hanna, Ian, and Ena. Their unwavering love and support have been the cornerstone of my achievements and instrumental in bringing me to this point in my academic career.

Table of Contents

List of Figures

List of Tables

Nomenclature

Latin Letters:

AFE	Adiabatic film cooling effectiveness
BR	Blowing ratio
PSP	Pressure sensitive paint
C	Polynomial constants
d	Effusion cooling hole diameter
I	Luminescent intensity
r	Light intensity ratio
p	Static pressure
S	Henry's law coefficient
K	Stern-Volmer constant
x	Mole fraction of oxygen in air
T	Temperature
U	Velocity
X	Concentration

Greek Letters:

α	Inclination angle
β	Compound angle
η	Film cooling effectiveness
δ	Hole pitch or distance

Subscripts:

ad	Adiabatic state
aw	Adiabatic wall

c	Coolant
$dark$	Camera reading without UV excitation
g	Main gas flow
PT	Pressure signal fluorescence peak near 650 nm
T	Pressure signal fluorescence peak near 560 nm
raw	Raw PSP fluorescence intensity
ref	Standard air condition as the reference point
O_2	Oxygen

1 INTRODUCTION

1.1 Background

The basic theory and development of gas turbine engines were proposed by John Barber in England in 1791, and the first practical turbojet engine was developed by Frank Whittle in England in 1937, with the first successful engine run taking place that year [1]. Since then, with the continuous development of industry, gas turbine engines have become not only the main power source for aircraft but also play a crucial role as a power source for industrial development.

However, with increase in concern over global warming, emissions regulations for aviation gas turbine engines are being strengthened. To comply with these emissions regulations, the use of alternative energy is being explored in the aviation industry. Nevertheless, the aviation sector, which operates powerful air-breathing gas turbine engines on jet fuel to generate the thrust needed for flight, is an area that takes more time to transition from fossil fuels to alternative energy sources according to the development of science. As can be seen in Figure 1, the energy density of kerosene, a fossil fuel commonly used in aircraft, shows about a 40-fold difference from that of Lithium-ion batteries, which can generally be considered in the aviation sector [2-4]. To compensate for this energy gap, installing more batteries would increase the weight, requiring more lift for the airplane to take off and maintain the same speed, thus more thrust. As a result, with the current technology, there is a limit to the maximum size that electric airplanes can reach. Therefore, improving the combustion efficiency of aircraft engines is the best solution to economic and environmental problems because greenhouse gas emissions can be reduced by increasing the efficiency of the engine. Consequently, there is an ongoing interest in gas turbine combustors for aviation with high combustion efficiency that satisfy emissions regulations.

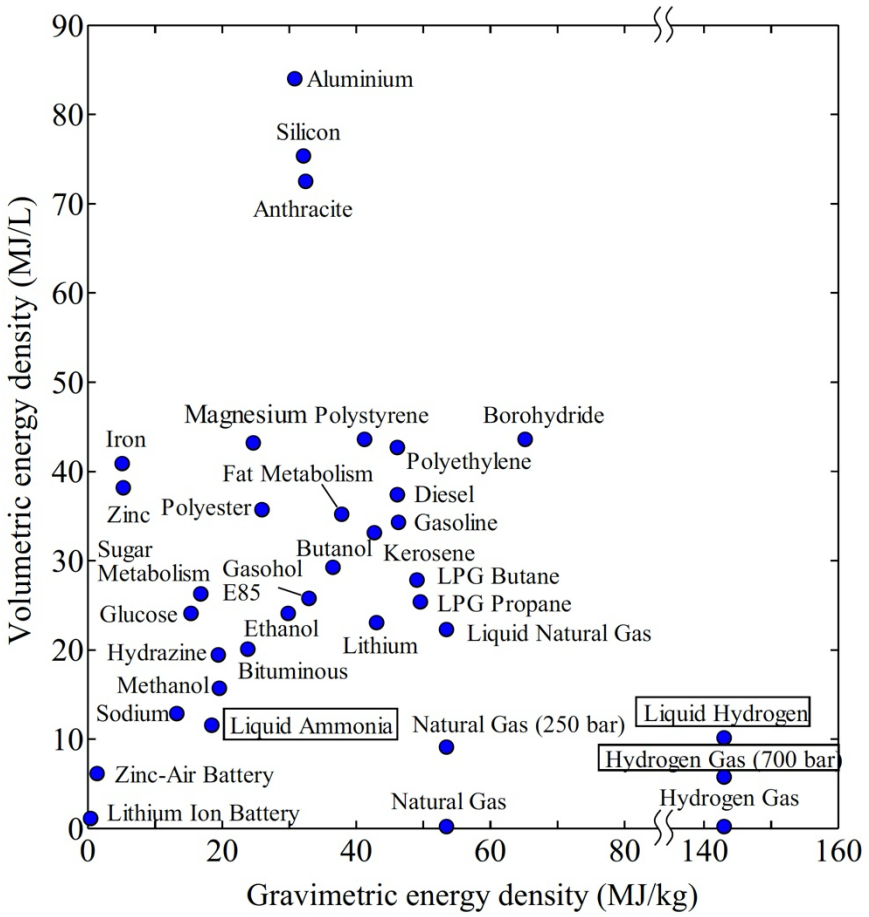

Figure 1. Gravimetric and volumetric energy density chart of combustible materials and batteries [4].

One of the most effective approaches for improving gas turbine efficiency is to reduce the use of cooling air, as the cooling air for components in the hot gas path has to be compressed to the highest-pressure point of the entire engine. Over the years, there has been a constant drive for higher Turbine Inlet Temperatures (TIT) to improve engine power and efficiency. As illustrated in Figure 2, the TIT has significantly increased from the 1960s to the present day, driven by advancements in materials and cooling technologies. This evolution has necessitated greater thermal management needs. Initially, convective cooling techniques were sufficient to handle the temperatures [5]. However, as TITs continued to rise, film cooling and thermal barrier coatings (TBC) became necessary to protect engine components. More recently, the introduction of advanced cooling methods, combined with TBCs and Ceramic Matrix Composites (CMC), has been critical in managing the extreme temperatures associated with modern gas turbines. Furthermore,

rising pressure ratios in modern gas turbine engines make the cooling of components in the hot gas path more challenging because the compressor air is discharged at higher temperatures, making it a less effective coolant for combustor liners and first-stage nozzles. This is because, in a compression process, increasing the pressure ratio across the compressor inherently raises the temperature of the discharge air due to the thermodynamic relationship governed by the ideal gas law and isentropic compression. As such, the development of more efficient gas turbine engines is closely tied to advancements in high-temperature materials, such as nickel-based superalloys and single-crystal alloys, as well as enhanced cooling technologies. These innovations are essential for maintaining the structural integrity and performance of engine components under increasingly demanding conditions.

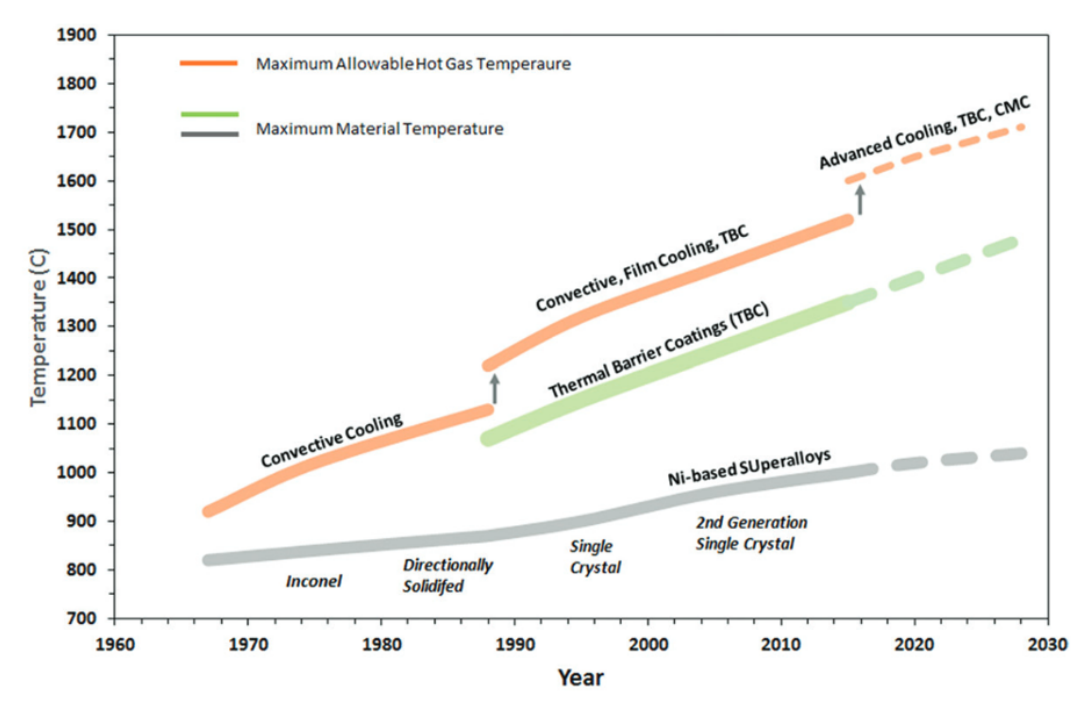

Figure 2. Evolution of turbine inlet temperature (TIT), materials, and cooling technology in the field of gas turbine [5].

Inadequate cooling available for combustor liners leads to reduced combustor life expectancies and premature engine failures [6]. To reduce the metal temperature of combustor liners and to improve the longevity of components in the hot gas path, previous effusion cooling studies have focused on the shape of effusion cooling holes and the

spacing (pitch) of effusion cooling holes [6][7][8]. Effusion cooling is a technique in which coolant air is passed through a dense array of small holes distributed over the surface, creating a thin protective film that insulates the surface from the hot combustion gases. In addition, new ceramic materials are being developed as thermal barrier coatings to protect against high temperatures inside the gas turbine, especially turbine blades [8].

Multi-hole effusion cooling provides thermal protection to combustor liners by forcing air at a higher pressure through a series of pinholes, absorbing heat from the liner while forming a protective fluid film layer to insulate heat on the exposed surface [9]. The portion of air that acts as coolant emanates from the inner surface of the liner through discrete effusion cooling holes as three-dimensional jet columns [10]. Effusion cooling primarily provides thermal protection downstream of the injection location, as the coolant forms a film that travels along the surface after exiting the holes [10]. Effusion cooling holes are typically designed to be in the co-linear direction with the hot main flow.

It is well established that the effusion cooling efficiency is highly dependent on the pattern and diameter of the effusion cooling holes, which govern the formation of protective films over the combustor liner. While studies on the pattern or the shape of effusion cooling holes [8][9][10][11] and coolant blowing ratios [12][13][14] are continuously being conducted, the directional effects of effusion cooling on adiabatic film cooling effectiveness (AFE, or η_{ad}) have not received much attention in past studies. In this thesis, the author asserts the critical importance of comprehending the directional characteristics of effusion cooling within authentic gas turbine combustor environments, underpinned by two primary rationales: Firstly, effusion cooling involves diminutive jets exhibiting pronounced directional properties, whereas the principal combustion flow within gas turbine combustors exhibits a swirling motion essential for flame stabilization. Secondly, contemporary designs of effusion cooling predominantly align the cooling holes with the axis of the combustor. Understanding the directional interaction between effusion cooling jets and the swirling main flow is imperative for optimizing effusion cooling performance and ultimately enhancing the efficiency and durability of gas turbine systems. The swirling main flow including the combustion products induces an angular difference between effusion cooling jets and the swirling main flow. Here compound angle (β) is defined as the angular difference between the main flow and the coolant jets as shown in Figure 3.

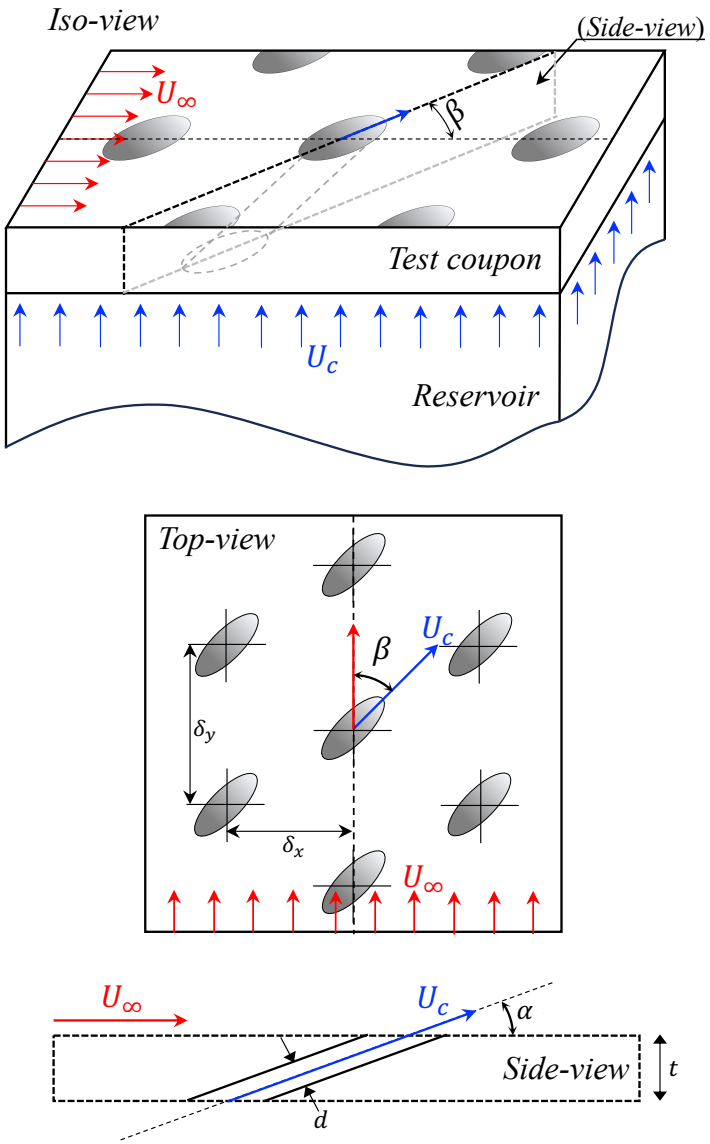

Figure 3. Schematic of the effusion cooling holes with a detailed description. U_c is the speed of coolant flow and U_∞ is the speed of main flow. α is the inclination angle (measured from the surface), and β is the compound angle (measured in the transverse plane, relative to the main flow direction). $\delta_x$is the spanwise pitch and $\delta_y$is the streamwise pitch of holes.

The swirling main flow not only induces a non-zero compound angle for effusion cooling, but it also alters the effective pitch of effusion cooling holes. The hole pitch refers to the spacing between adjacent cooling holes, both in the streamwise and spanwise directions. Figure 3 illustrates the definition of pitch for an effusion cooling configuration. In the example effusion cooling configuration shown in Figure 3, the effusion cooling holes are

staggered with prescribed spanwise separation between effusion hole columns (δ_x) and streamwise separation between effusion hole rows (δ_y). However, the design pitch is only valid under the condition that the main flow is strictly co-linear with effusion cooling jets, as indicated by the red arrow in the figure. Under swirling main flow conditions, the effective pitch is varied. To illustrate this point, an extreme scenario can be considered: if the main flow is introduced at 90° to the direction of the effusion cooling jets, then the effective pitch would be altered such that the streamwise and spanwise pitches would be swapped. In fact, when a swirling main flow induces any non-zero angle between effusion cooling jets and the main flow, the hole pitch is effectively altered.

When the swirling main flow sweeps on the surface of an effusion cooling plate, both compound angle and effective pitch are altered concurrently. A recent study [15] evaluated the two combined effects on AFE from swirling main flow as it is most relevant to practical engine operations. However, it is not clear how a non-zero compound angle and a varied pitch contribute separately to the combined directional effects of effusion cooling.

1.2 Research Objective

The primary aim of this study is to delineate the directional effects on Adiabatic Film Cooling Effectiveness (AFE) attributable to two distinct factors: the non-zero compound angle and the variability of pitch. To isolate the impact of the compound angle, the first phase of the study involves maintaining a constant hole pitch while systematically varying the compound angle in experimental tests. This allows for a clear assessment of how non-zero compound angles influence the performance of the cooling film. Subsequently, the second phase of the study explores the effect of pitch variation on AFE, based on the hypothesis that hole pitch plays a significant role in film development and cooling performance.

Building upon these findings, the secondary objective of this research is to conceptualize, design, and assess an innovative effusion cooling paradigm. This design integrates variable compound angles along the direction of the main flow, a strategy informed by insights gleaned from the initial phase of the study. It is postulated that this novel design will enhance both the uniformity and overall effectiveness of the cooling film on the test surface,

thereby contributing significantly to the advancement of effusion cooling technologies in gas turbine applications.

1.3 Thesis Outline

This thesis is structured into six comprehensive chapters, each of which is briefly summarized in the ensuing subsection.

Chapter 1 serves as an introductory overview, elucidating the central theme of this thesis and delineating the motivating factors that have guided the research presented in the subsequent chapters.

Chapter 2 offers a critical review of existing research in gas turbine cooling technologies, with a focus on effusion cooling. This chapter contextualizes the current study within the broader field of gas turbine engine cooling methods and advancements.

Chapter 3 details the specific aims of the research, elaborating on the intended investigation of compound angles and pitch variation effects on AFE within gas turbine combustor liners.

Chapter 4 describes the comprehensive experimental framework designed to evaluate effusion cooling technologies. This includes a detailed account of the wind tunnel system, coolant reservoir, vent system for boundary layer thickness control, turbulence generator, test coupons, and the use of Pressure Sensitive Paint (PSP) for thermal effectiveness measurement.

Chapter 5 presents the findings from the experimental studies, focusing on the impact of swirling flow and the assessment of a new effusion cooling design employing varying compound angles. This chapter is integral to understanding the practical implications of the research findings.

Following these chapters, the thesis presents the major conclusions of the work, and then includes references and appendices, providing extensive resources for readers to explore the research in greater depth.

2 LITERATURE REVIEW

2.1 Gas Turbine Engine

Gas turbine engines, a cornerstone of modern propulsion and power generation, transform fuel's chemical energy into mechanical energy. This transformation is achieved through a process that involves compressing air, mixing it with fuel, igniting the mixture for combustion, and then expanding the hot gases through a turbine to produce work. Since their inception in the early 20th century, gas turbines have revolutionized industries by providing a reliable source of power for aircraft, ships, electric power plants, and more. In addition, gas turbines' versatility allows their use across numerous applications, from the skies in jet engines to ground-based power generation plants. Their high efficiency, reliability, and ability to operate on a range of fuels make them indispensable in today's energy and transportation sectors [16].

Recent developments in gas turbine technology focus on increasing efficiency, reducing emissions, and enabling the use of alternative fuels. Advances in materials science have led to the creation of superalloys and ceramic matrix composites that withstand higher temperatures, improving efficiency. In addition, to achieve higher efficiency over time, turbine inlet temperature (TIT) has also increased, requiring cooling technology to also evolve in parallel. In other words, cooling technologies, such as film cooling and advanced internal cooling channels, further enhance the durability and performance of the combustion chamber or turbine. The industry is also exploring the use of sustainable fuels, including biofuels and hydrogen, to reduce the environmental impact of gas turbines [5][16].

The operational principle of gas turbine engines is governed by the idealized Brayton cycle, which involves four key processes: intake of air, compression, combustion, and expansion through a turbine as shown in a T-s diagram in Figure 4 [17]. Initially, ambient air is drawn into the engine and compressed, significantly increasing its pressure as in the evolution from 1-2 in Figure 4. This compressed air is then introduced into the combustion chamber, where it is mixed with fuel and ignited as the evolution from 2-3 in Figure 4. The high-pressure, high-temperature gases produced during combustion expand through the turbine as the evolution from 3-4 in Figure 4, generating mechanical power. This expansion cools the gases, which are then expelled through the exhaust system. The turbine not only powers

the compressor but also provides the excess energy for external work, such as propelling an aircraft or driving an electric generator.

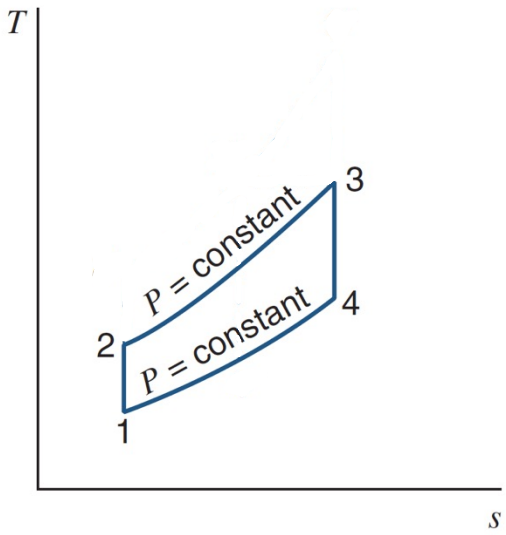

Figure 4. T-s diagram of the air-standard Brayton cycle [17].

Figure 5 shows a gas turbine jet engine and key components: the compressor, combustion chamber, turbine, and exhaust system [16, 17]. The compressor is the first component in the engine's airflow path, and it increases the pressure of the incoming airThe compressors can be axial, centrifugal, or a combination of both, each with its own set of advantages in terms of efficiency, complexity, and suitability for different engine sizes and applications. The combustion chamber is where the compressed air mixes with fuel and is ignited, and the design of the combustion chamber aims to achieve stable and complete combustion, maximizing energy release while minimizing emissions. For this combustion chamber, the challenges include managing high temperatures and avoiding hot spots that could damage the engine. The turbine extracts thermal energy from the combustion gases to drive the compressor and perform external work, and it must withstand extreme temperatures and pressures, necessitating advanced materials and cooling technologies. The efficiency improvements of the gas turbine often focus on turbine blade design and materials that can endure higher temperatures. The exhaust system expels the expanded combustion gases from the engine. In jet engines, the exhaust system's design significantly influences thrust and overall engine performance. In power generation, exhaust heat can be recuperated to improve system efficiency [16].

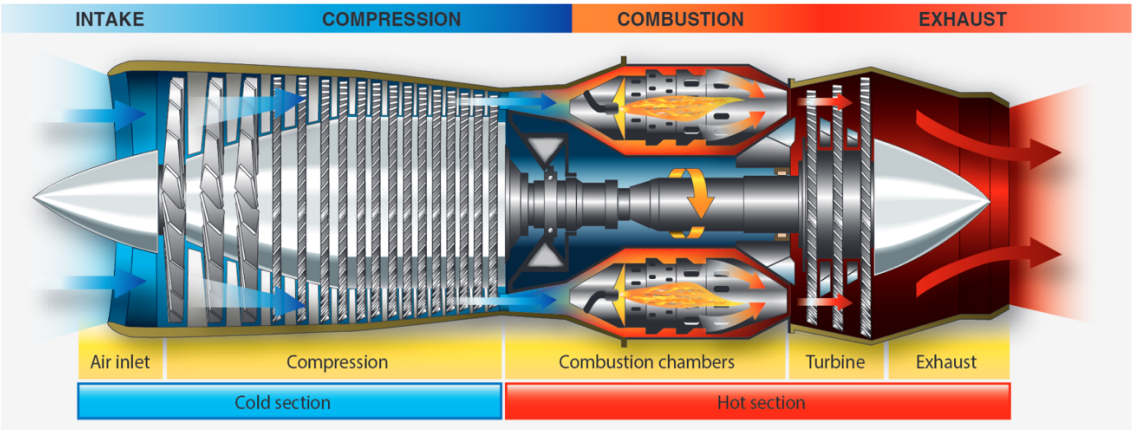

Figure 5. Basic components of a gas turbine jet engine [18].

2.2 Gas Turbine Engine Cooling

In contemporary combustor designs, the temperature of gases resulting from combustion can exceed 2100°C, far surpassing the melting points of materials used in combustor flame tubes and turbine blades [16]. This scenario necessitates the implementation of effective cooling strategies to protect these critical components, ensuring their structural integrity and extending their operational lifespan. Additionally, it's imperative to optimize the use of cooling air to preserve as much air as possible for emissions control. This is because a significant portion of the compressor air is required for complete combustion and dilution, which directly influences the formation of pollutants such as NOx. f the amount of available air for combustion is limited, the local flame temperature increases, which promotes thermal NO_x formation. Conversely, sufficient air helps maintain leaner combustion, reducing peak temperatures and thereby suppressing NO_x generation. Efficient use of cooling air allows more air to be directed toward cleaner and more complete combustion, thereby supporting compliance with increasingly strict environmental regulations.

Although not subjected to the same mechanical stresses as other engine components, the combustor liner must endure extreme temperatures and sharp temperature gradients that could compromise its structural integrity. Achieving a balance to maintain temperatures and temperature gradients within safe limits is crucial. The materials typically used, such

as nickel- or cobalt-based alloys are known to lose significantly mechanical strength at temperatures beyond 1100 K [16]. Traditionally, cooling was facilitated by directing a stream of cool air along the liner's inner surface to carry away heat primarily via radiation and convection [16][19].

Since the 1960s, the push for more advanced cooling solutions for the combustor liner has been driven by several key factors [16][20]:

1) Enhanced engine efficiency through higher pressure ratios and turbine inlet temperatures, — along with the adoption of higher bypass ratios in aircraft engines — has resulted in greater thermal loads on the combustor liner. One consequence is increased radiative heat transfer from the flame to the liner walls. At the same time, the rise in combustor inlet temperatures reduces the temperature difference between the liner and the cooling air flowing through the annular region (annulus), thereby lowering the convective cooling effectiveness. Together, these factors have made it more challenging to maintain liner temperatures within safe limits.
2) Stricter regulations on pollutant emissions over the last two decades have necessitated a shift in air allocation towards combustion to reduce nitric oxide levels. This shift has reduced the volume of air available for cooling, underscoring the need for more air-efficient cooling techniques.
3) The need for improved combustor pattern factors, which refers to the uniformity of the temperature distribution of the hot gases at the exit of the combustor, to safeguard the turbine's hot sections has emerged with rising turbine inlet temperatures. Since film cooling does not contribute to mixing air within the combustor, optimizing cooling air usage directly enhances the pattern factor, facilitating better air mixing in dilution zones.
4) The operational durability of combustor liners has become a more critical expectation among users. Where early engine designs anticipated a few hundred hours between maintenance, the current expectation extends to several thousand hours, reflecting significant advances in material science and cooling technology.

Addressing these challenges calls for not only enhancing the efficiency of existing cooling mechanisms but also inventing new methods that economize the use of cooling air without compromising engine performance or environmental compliance. This approach ensures

that gas turbine engines can meet the dual demands of high efficiency and low emissions, marking a critical area of development in aerospace and power generation industries.

The following sub-section delves into the general approaches to cooling in gas turbine engines, with a specific emphasis on combustor liner cooling, a key area where advanced cooling techniques like effusion cooling play a pivotal role.

2.2.1 Gas Turbine Engine Cooling Methods

Figure 6 shows an example of the combustor liner and the path of the cooling air, the latter coming from the compressor exit. The combustor liner, tasked with containing the combustion process within gas turbines, is subjected to extreme thermal conditions that can significantly impair its lifespan and performance. To mitigate these challenges, several cooling methods have been developed and refined over the years, each tailored to balance cooling effectiveness with the overall efficiency of the engine. This section explores the primary cooling techniques, including film cooling, convective cooling, and effusion cooling, employed for combustor liners, emphasizing their operational principles, advantages, and areas for future advancements [16][20][22].

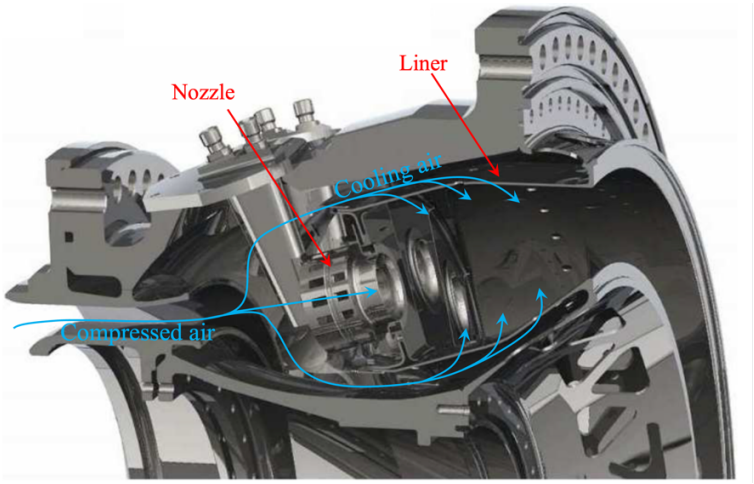

Figure 6. Example of the combustor and the path of the cooling air (adapted from [21]: Reprinted by permission from American Society of Mechanical Engineers ASME: "Numerical and Experimental Investigation on an Effusion-Cooled Lean Burn Aeronautical Combustor: Aerothermal Field and Emissions" Journal of engineering for gas turbines and power, Copyright 2018. All rights reserved)

As shown in Figure 7 and Figure 8(a), film cooling is a widely used technique where cool air is bled from the compressor stage and injected through small holes or slots in the

combustor liner's surface. This creates a protective film of cooler air that shields the liner from the hot combustion gases. Film cooling effectively lowers the surface temperature of the liner, protecting it from thermal stresses and extending its service life. Achieving uniform coverage and preventing the cooling air from mixing too quickly with the hot gases are ongoing challenges. Additionally, excessive reliance on film cooling can lead to a decrease in engine efficiency due to the diversion of air from the combustion process.

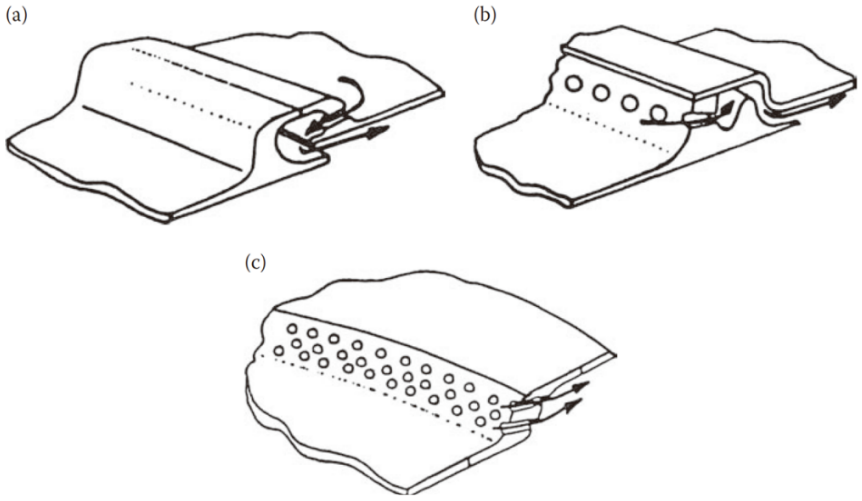

Figure 7. Examples of film cooling devices: (a) GE rolled ring, (b) P&W double-pass wing, (c) RR Z ring (adapted from [16]: Reprinted by permission from American Society of Mechanical Engineers ASME: "Gas Turbine Combustion: Alternative Fuels and Emissions," CRC Press, Boca Raton, FL, Copyright 2010. All rights reserved)

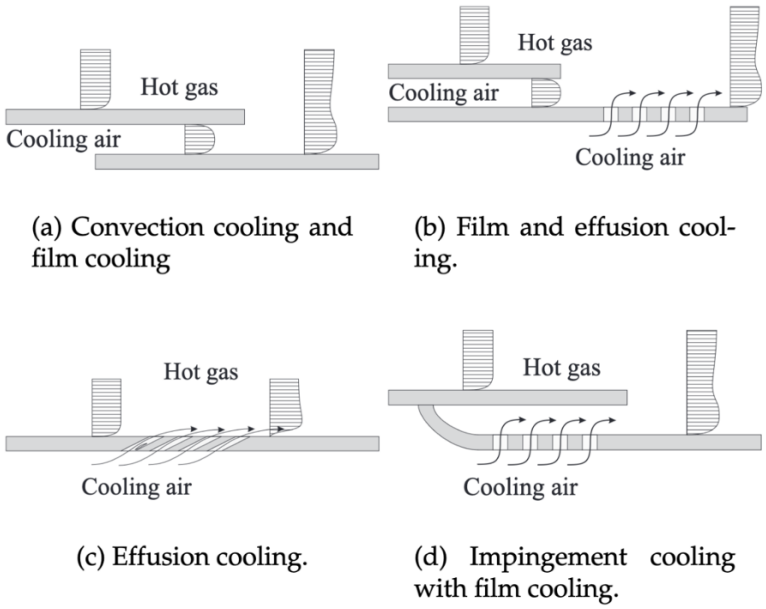

Figure 8. Different cooling methods for combustor liner cooling [22]

Figure 8(a) shows the convective cooling that involves passing cooling air through internal channels within the combustor liner. As the air moves through these channels, it absorbs heat from the liner, carrying it away before being ejected or utilized in another cooling process. This method offers efficient heat transfer and can be particularly effective in areas subjected to the highest temperatures. Designing and manufacturing combustor liners with intricate internal cooling passages is complex and costly. Moreover, ensuring an even flow distribution within these channels to avoid hot spots remains a technical challenge.

The pursuit of effective combustor liner cooling strategies stands at the forefront of advancements in gas turbine technology. The challenge of managing the extreme thermal environment within the combustor necessitates a multifaceted approach, employing a combination of traditional and innovative cooling techniques. Among these, film cooling and convective cooling, which are referred to in previous paragraphs, have laid the foundational principles for thermal management. However, as gas turbines evolve to meet stricter efficiency and emission standards, the limitations of these methods have catalyzed the search for more advanced solutions.

As shown in Figures 8(b), (c), and (d), one such pioneering advancement is effusion cooling, a technique that epitomizes the intersection of innovation and practicality in thermal management. Effusion cooling differs significantly from traditional film and convective cooling methods by utilizing multiple small holes distributed uniformly over the surface of the combustor liner. These holes allow a fine, consistent layer of cooling air to be injected directly onto the liner's surface. Unlike film cooling, which relies on larger, less uniformly distributed holes to create a protective air layer, effusion cooling provides a more evenly distributed cooling effect. This uniformity enhances the overall cooling efficiency and ensures a more consistent temperature profile across the liner. Additionally, compared to convective cooling, which primarily uses air directed along the liner's inner surface, effusion cooling achieves better heat dissipation by directly addressing localized hot spots. Consequently, effusion cooling represents a significant leap forward in our ability to extend component lifespan while enhancing engine performance. This method not only addresses the inherent challenges posed by traditional cooling techniques but also aligns with the overarching goal of achieving higher efficiency and reduced environmental impact in gas turbine operation.

As this thesis delves deeper into the specifics of effusion cooling in the following section, it is essential to appreciate the context in which this technology has emerged. By building upon the principles of film and convective cooling, effusion cooling embodies the culmination of decades of research and development in gas turbine thermal management. It exemplifies how continuous innovation drives the gas turbine industry toward achieving the delicate balance between operational demands and sustainability goals. The ensuing discussion will explain the mechanisms, benefits, and challenges of effusion cooling, highlighting its critical role in shaping the future of combustor liner cooling strategies.

2.3 Effusion Cooling

Effusion cooling, also known as full-coverage film cooling, stands at the cutting edge of thermal management technologies for gas turbine combustor liners [20][22]. This advanced cooling approach involves the ejection of cooling air through a dense array of micro-perforations spread uniformly over the combustor liner surface. The method is indicated for its superior ability to maintain optimal material temperatures under extreme thermal loads, directly addressing the challenges inherent in modern high-efficiency, low-emission gas turbines.

As shown in Figure 6, the essence of effusion cooling lies in its operational mechanism, where cooling air, bled from the compressor, is diffused through thousands of tiny holes on the combustor liner. This creates a thin, protective layer of cooler air that insulates the liner from the hot gases produced during combustion. The key to its effectiveness lies in both the even distribution of perforations—ensuring a uniform cooling effect across the liner—and in promoting the formation of a stable coolant film that resists rapid mixing with the hot mainstream gases. This sustained separation between coolant and combustion flow helps to reduce thermal gradients, prevent hot spots, and maintain material temperatures within safe limits.

Its sophistication and efficacy stem from meticulous control over several key parameters, including hole shape, inclination angle, hole pitch, blowing ratio, turbulence intensity, and compound angle. These factors collectively influence the cooling performance, highlighting the intricate balance required to optimize effusion cooling systems.

2.3.1 Critical Parameters of Effusion Cooling

2.3.1.1 Hole shape

The geometry of the cooling holes significantly influences the trajectory and dispersion of cooling air as it exits into the hot environment of the combustor. Traditional round holes, while simpler to manufacture, offer limited control over the air's spread. Advances in manufacturing technologies have enabled the adoption of complex hole shapes, such as diffuser-shaped and fan-shaped holes as shown in Figure9 [23][24][27]. These configurations expand the cooling air's footprint on the combustor liner, providing a broader and more uniform cooling effect.

Crafting these intricate shapes demands precision engineering and advanced manufacturing techniques, such as laser drilling and electron beam machining. The design process often involves computational fluid dynamics (CFD) simulations to predict the performance of various hole shapes under operational conditions, enabling the optimization of cooling effectiveness and air usage efficiency [23][27].

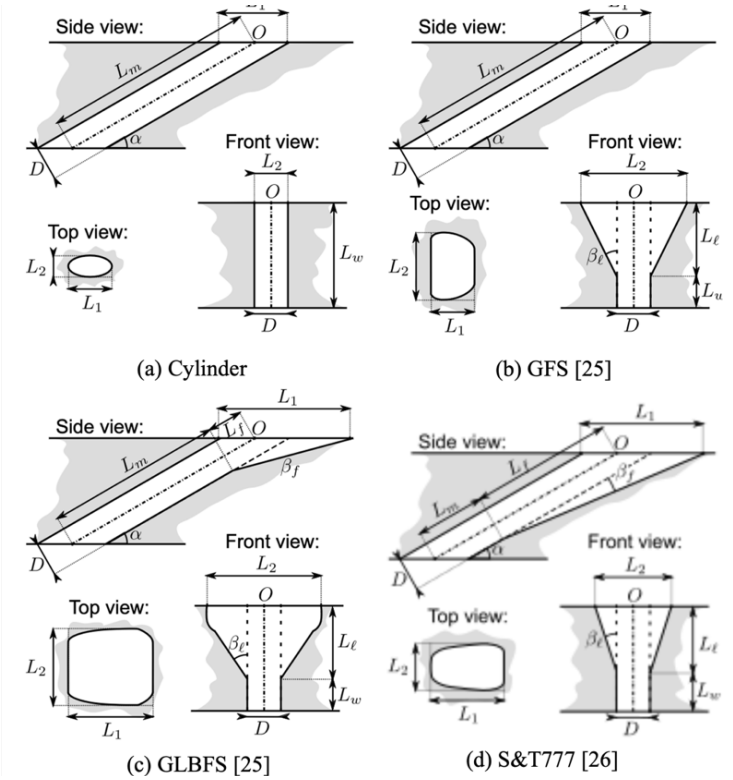

Figure 9. Side, front and top view of the example designs of the effusion cooling holes [23](Reprinted by permission from Elsevier: "Boundary-condition models of film-cooling holes for large-eddy simulation of turbine vanes," International Journal of Heat and Mass Transfer, Volume 166, 2021, 120763, ISSN 0017-9310. Copyright 2021. All rights reserved)

2.3.1.2 Inclination Angle (α)

The inclination angle (α) of the holes—defined as the angle between the cooling air's ejection path and the liner surface as shown in Figure9—affects how effectively the cooling air adheres to the liner, forming a protective layer against the combustion gases. Angles are typically chosen within a range that ensures the ejected air remains close to the surface, enhancing its cooling capability while minimizing the air mixture into the combustion process [27][28].

Selecting the optimal inclination angle requires a delicate balance, considering both the desired cooling impact and the physical constraints of the combustor's design. This balance is achieved through extensive testing and simulation, ensuring that the cooling air provides maximum protective coverage without adversely affecting combustion dynamics [27].

2.3.1.3 Hole Pitch (S)

The spacing or pitch between adjacent cooling holes, as described in Figure2, is critical for ensuring even cooling distribution across the combustor liner. Incorrect spacing can lead to uneven cooling, resulting in hot spots, or excessive cooling air consumption without proportional benefits [29]. The determination of optimal pitch involves a comprehensive analysis of thermal patterns across the liner, aiming for uniform temperature distribution with minimal cooling air usage [5][6]. This parameter becomes even more crucial when considering the effects of swirling flow within the combustor, as it can dramatically affect the distribution and effectiveness of the cooling air [30][31].

The optimal hole pitch is determined by a complex interplay between the cooling air's volume flow rate, the thermal load on the combustor liner, and the physical constraints of the liner design. A pitch that is too narrow may result in excessive cooling and wasted air, while a pitch that is too wide could leave areas of the liner insufficiently cooled, leading to hot spots and potential damage.

Engineers must consider the liner's geometry, the expected thermal loads, and the desired cooling air velocity when determining the hole pitch. Computational fluid dynamics (CFD) simulations often accompany experimental testing to model the thermal and flow dynamics accurately and to predict the cooling performance under various operating conditions [31]. Swirling flows, intentionally introduced into combustors to enhance mixing and combustion efficiency as shown in Figure 10, significantly impact the cooling air's

trajectory and heat transfer characteristics. The centrifugal forces generated by the swirl can push the cooling air against the liner's surface more forcefully, potentially enhancing the cooling effect but also altering the optimal configuration of the hole pitch.

The presence of swirling flows requires a re-evaluation of hole pitch to ensure that the cooling air effectively counters the thermal effects of the hot gases. The swirling motion can lead to uneven cooling distribution if not properly accounted for in the design of the effusion cooling system [30]. Adjusting the hole pitch, in conjunction with the inclination and compound angles of the holes, can mitigate these effects and maintain uniform liner temperatures [32].

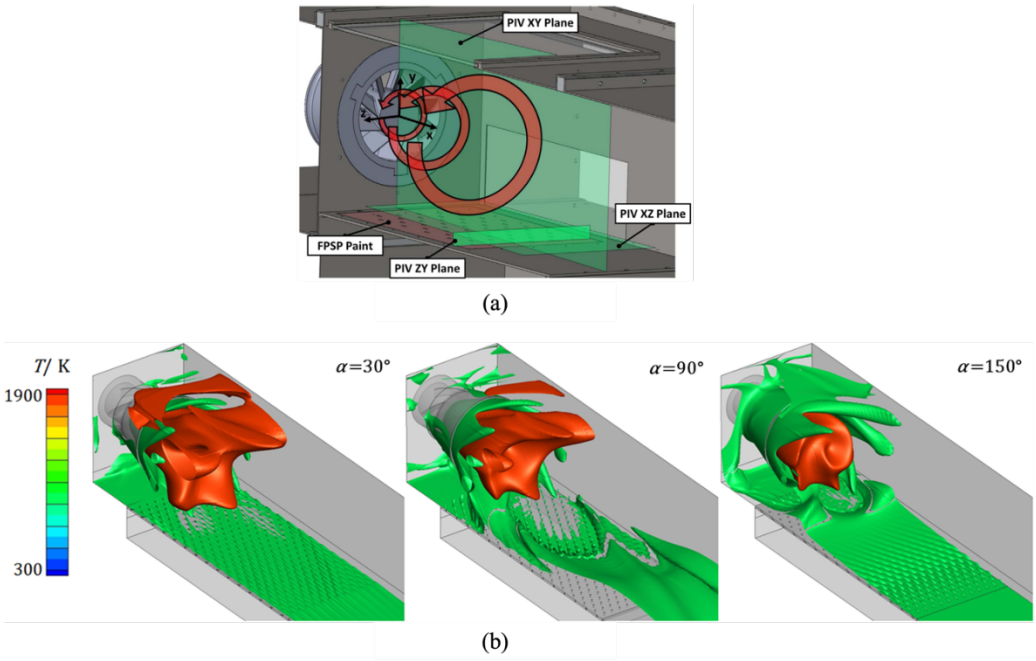

Figure 10. Examples of the swirling flows: (a) schematic of the example experimental setup for generating the swirling flow by the swirler in the nozzle [30] and (b) the iso-temperature 3D contour of CFD simulation results [31]. (Reprinted by permission from Elsevier:[30]"Swirling main flow effects on film cooling: Time resolved adiabatic effectiveness measurements in a gas turbine combustor model," International Journal of Heat and Mass Transfer, Vol. 200, Copyright 2023. [31]"Analysis of effusion cooling under realistic swirl reacting flow in gas turbine combustor," Applied Thermal Engineering, Vol. 216, Copyright 2022. All rights reserved).

2.3.1.4 Blowing Ratio (BR)

The blowing ratio (BR), is a key non-dimensional parameter in effusion cooling representing the momentum ratio between the cooling air and the main hot main gas. An optimal blowing ratio ensures that cooling air effectively shields the liner from heat without

significantly diluting the combustion gases, which could detract from engine performance and efficiency. The blowing ratio is expressed as

$$BR = \frac{\rho_c V_c}{\rho_\infty V_\infty} \tag{2-1}$$

where ρ is density, V is velocity, subscript c is the coolant and ∞ is the main hot gas. Achieving the ideal blowing ratio involves adapting to the gas turbine's operational conditions and the available cooling air supply. This adaptability is crucial for maintaining engine efficiency across various load conditions, making the blowing ratio a dynamic component of the effusion cooling strategy. As shown in Figure 11, Wang et al [33] evaluated the cooling performance of each blowing ratio by measuring the surface film cooling effectiveness. The interaction between the coolant jet and the mainstream flow is strongly influenced by BR, as illustrated in Figure 11. At low BR, the coolant has lower momentum and stays closer to the surface, forming a well-attached cooling film. However, at excessively low BRs, the coolant may not spread sufficiently to provide full coverage, resulting in incomplete surface protection. At high BR, the coolant jet has higher momentum, causing it to penetrate further into the main flow. If BR is too high, the jet may lift off from the surface, reducing its effectiveness in cooling the liner. This behavior highlights the importance of selecting an appropriate BR based on turbine conditions, ensuring that the coolant remains attached to the surface while providing maximum thermal protection.

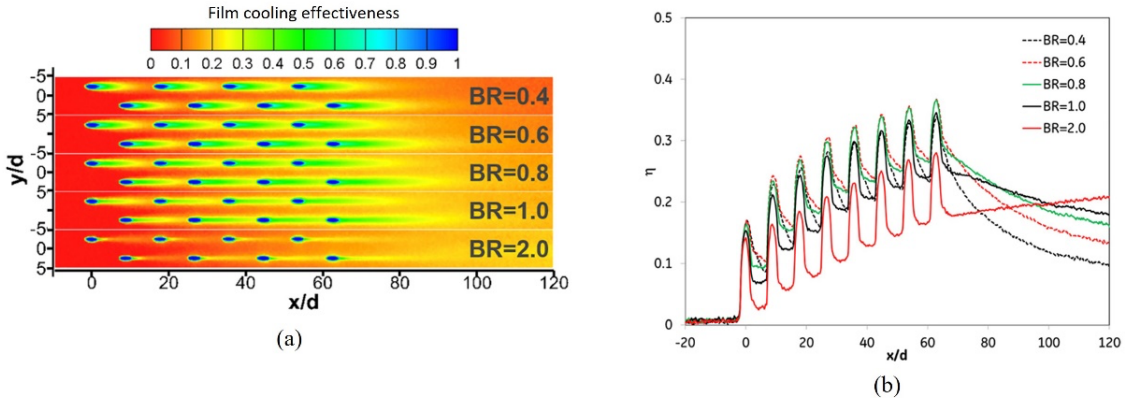

Figure 11. (a) Spatial average one-periodic 2D film cooling effectiveness and (b) spanwise (lateral) average film cooling effectiveness [33] *(Reprinted by permission from American Society of Mechanical Engineers ASME: "Experimental Study of Effusion Cooling with Pressure-Sensitive Paint," Journal of Engineering for Gas Turbines and Power, vol. 139, no. 5, Copyright 2017. All rights reserved))*

2.3.1.5 Turbulence Intensity (Tu)

Turbulence intensity, a measure of the fluctuations in velocity within a gas flow, plays a critical role in the thermal management strategies of gas turbine combustors. In the context of effusion cooling, the turbulence intensity of the main hot gas flow significantly influences the mixing and heat transfer processes between the hot gases and the cooling air [34]. Figure 12 shows the difference in temperature distribution for two different turbulence intensities (5% and 20%), which illustrates how turbulence intensity has a significant impact on cooling performance as higher turbulence intensity makes the initial film attached to the liner surface easier than the lower turbulence intensity case.

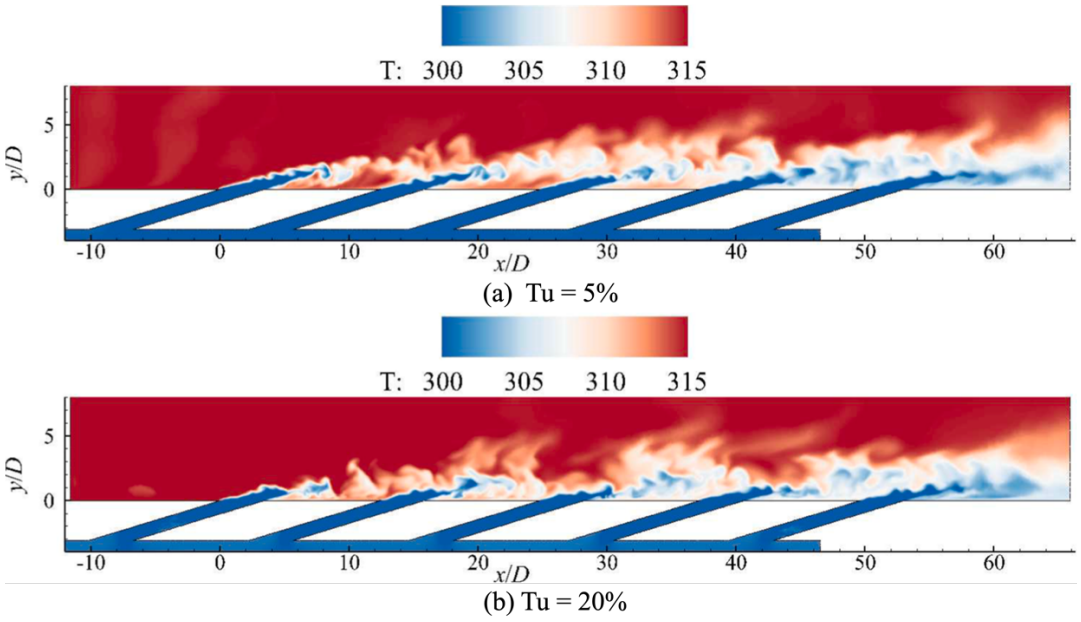

Figure 12. Instantaneous contours of temperature through a column of effusion cooling holes [34]. (Reprinted by permission from Elsevier: "Study of an effusion-cooled plate with high level of upstream fluctuation," Applied Thermal Engineering, Vol. 184, Copyright 2021. All rights reserved).

The challenge lies in balancing the turbulence intensity to optimize cooling without adversely affecting the combustion process or increasing cooling air consumption unnecessarily. Engine designers often leverage turbulence-generating features within the cooling holes or channels to control the turbulence intensity of the cooling air, tailoring it to the specific needs of the combustor liner and the overall engine performance objectives. The incorporation of compound angle and turbulence intensity into the effusion cooling strategy allows for more sophisticated control over the cooling air's behavior as it interacts

with the hot gases and the combustor liner surface. By fine-tuning these parameters, engineers can achieve a delicate balance between cooling effectiveness, engine efficiency, and emissions performance.

2.3.1.6 Compound Angle (β)

The concept of compound angles in effusion cooling systems introduces a critical dimension to the directional control of cooling air, as shown in Figure2 as expressed as β, adding a lateral component that extends beyond the inclination angle. This lateral orientation, determined by the compound angle, significantly enhances the engineer's ability to dictate the dispersion pattern of the cooling air as it exits the effusion holes. In addition, the flow structure by this compound angle would be changed as shown in Figure 13, which implies that the cooling film structure can be a difference between zero and non-zero compound angles [32][35][36].

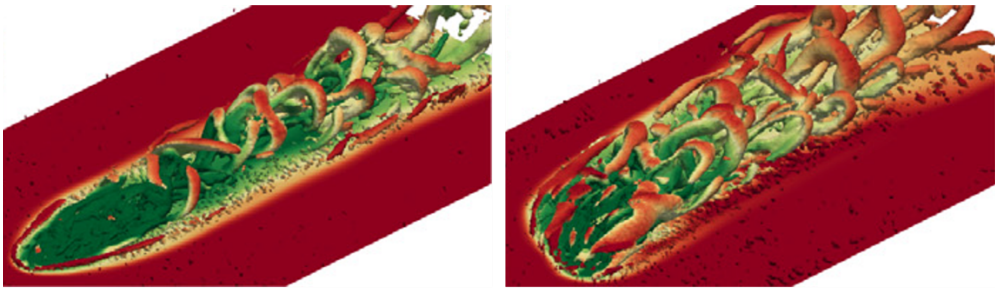

(a) $\beta = 0°$ (b) $\beta = 60°$

Figure 13. 3D vortex structure around hole exit for (a) $\beta = 0°$ and (b) $\beta = 60°$ [23].

The application of compound angles allows for a strategic deployment of cooling air, channeling it precisely to regions where thermal loads peak. This approach is especially advantageous in combustors characterized by intricate geometries or variable airflow dynamics that induce non-uniform temperature fields. Leveraging compound angles facilitates a nuanced cooling strategy, grounded in detailed flow simulations and thermal analyses, to effectively neutralize the detrimental impacts of uneven heat distribution.

The introduction of compound angles as a variable in effusion cooling system design significantly broadens the scope of testing and optimization required. Engineers are tasked with extensive computational modeling and empirical testing to pinpoint the compound

angles that best suit specific combustor configurations. This endeavor, while resource-intensive, is crucial for harnessing the full potential of compound angles in enhancing effusion cooling effectiveness.

The significance of compound angles in effusion cooling has been underscored by pioneering research [35]. Furthermore, the current author's contributions through publications such as [32] and [36] delve into the nuanced impacts of compound angles, offering a foundation for this thesis. Despite the acknowledged importance of compound angles, detailed studies specifically focusing on their effects remain scarce, largely due to the natural occurrence of compound angles in swirling flow scenarios where cooling holes are typically aligned with the combustor's longitudinal axis. This research gap highlights the innovative focus of the current thesis, aiming to isolate and analyze the compound angle's role in optimizing effusion cooling performance within gas turbine combustors.

The exploration of compound angles in effusion cooling represents a frontier in thermal management research, promising enhanced cooling strategies for gas turbine combustors. Through meticulous design, advanced manufacturing, and rigorous testing, the potential of compound angles to significantly improve cooling efficiency is being progressively unlocked, marking a pivotal advancement in the quest for more effective and efficient gas turbine cooling solutions.

3 RESEARCH OBJECTIVES

The primary objective of this research is to elucidate the nuanced effects of effusion cooling technologies on adiabatic film cooling effectiveness (AFE) within gas turbine combustor liners, with a focus on the roles of compound angles and pitch variation. This exploration is motivated by the imperative to optimize gas turbine efficiency amidst the escalating demands for reduced emissions and enhanced durability of components in the hot gas path. Given the intricate dynamics of effusion cooling, influenced by the angular orientation and spatial arrangement of cooling holes, this study seeks to dissect these factors in isolation and in combination, underpinning the development of advanced effusion cooling strategies.

3.1 Directional Effects of Compound Angles on AFE

The first segment of this investigation aims to isolate and analyze the impact of compound angles on AFE. Compound angle, defined as the angle between the coolant jets and the main flow, emerges as a critical variable under the swirling conditions typical of gas turbine operations. Preliminary findings, as discussed in [32] and [36], suggest that varying compound angles along the flow direction can significantly influence the formation and stability of the cooling film. This segment will build upon these insights to establish a comprehensive understanding of how compound angles can be optimized across different sections of the combustor liner to enhance cooling performance.

3.2 Effects of Hole Pitch Variation on Effusion Cooling

Building upon the foundational analysis of compound angles, the second objective delves into the implications of pitch variation on effusion cooling efficiency. The pitch, or spatial arrangement of cooling holes, directly influences the distribution and efficacy of the cooling film. The research in [32] indicates that the effective pitch — altered by the swirling main flow — significantly impacts AFE. This study segment will experimentally and analytically evaluate pitch configurations, striving to decouple the intertwined effects of compound angle variations and pitch alterations. The goal is to delineate their respective contributions to cooling performance, paving the way for effusion cooling designs that are robust against the dynamic conditions within gas turbine combustors.

4 EXPERIMENTAL SETUP

This section delineates the experimental framework devised to investigate advanced effusion cooling technologies for gas turbine combustor liners. The setup's design is established on a holistic approach to simulate operational conditions accurately, enabling a detailed examination of effusion cooling's effectiveness under various configurations.

4.1 Introduction of Experimental Setup

The experimental apparatus is anchored by a state-of-the-art wind tunnel system, facilitating controlled air flow to emulate the environment within a gas turbine combustor accurately. Accompanying this primary system is an array of auxiliary components, including a coolant reservoir, boundary layer thickness control vents, and a turbulence generator, all integral to the setup's functionality. Central to the investigation is the application of Pressure-Sensitive Paint (PSP) technology, providing an innovative method for thermal effectiveness measurement across the test samples. An illustrative schematic of the experimental setup is presented in Figure 14, detailing the integration of these components within the operational framework. The test section has a transparent polycarbonate top panel with a 127-mm square cross-section. To measure the main air flow velocity, the Pitot tube is used. The Pitot tube is located 228.6 mm from the inlet of the square test section after the wind tunnel transition piece that connects the round wind tunnel outlet to the square test section. The reservoir is mounted on the bottom panel of the test section with an inner diameter of 101.6 mm and an internal height of 44.45 mm. This reservoir supplies the cooling gas with a uniform flow distribution using the perforated plate to all the effusion cooling holes. The center of the reservoir is located 406.4 mm from the inlet of the test section. The operating conditions for all cases are shown in Table 1.

Table 1 Summary of test conditions. The coolant flow velocity is calculated at the effusion hole exit based on mass flow rate measurements.

Blowing ratios, -	Main air flow velocity, m/s	Coolant (N_2) flow velocity, m/s
0.6	33.0	20.5
1.0	33.0	34.1
1.4	33.0	47.8

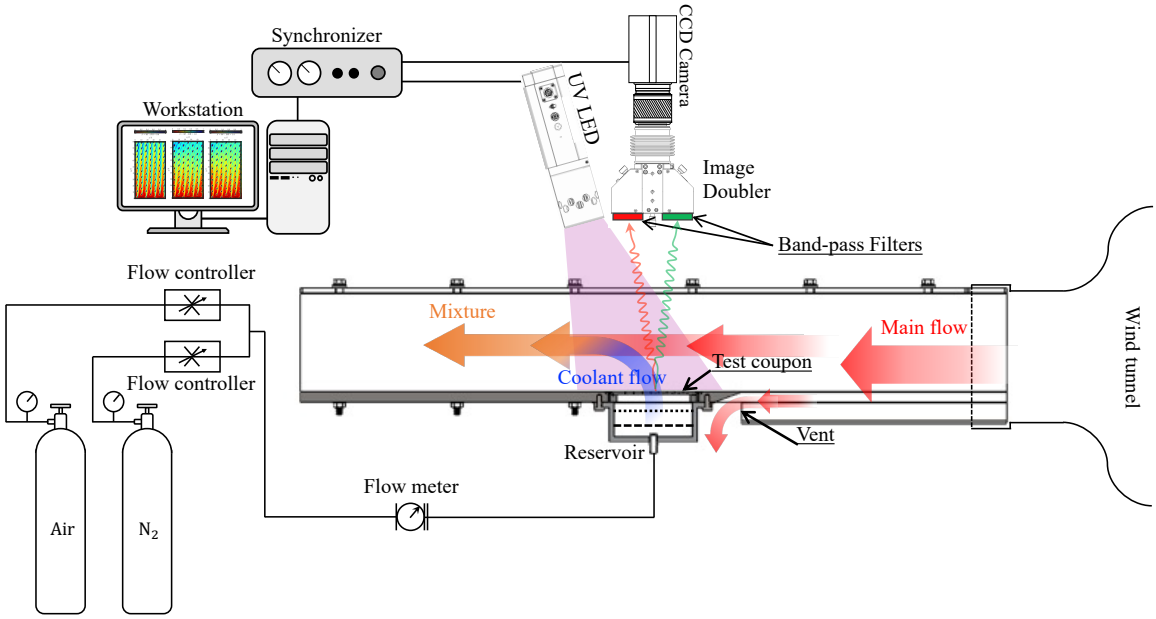

Figure 14. Schematic of the experimental setup and a sectional view of the test section.

4.2 Wind Tunnel

The cornerstone of the experimental investigation is a sophisticated co-annular, low-speed, open circuit wind tunnel, depicted in Figure 15, situated within the Gas Turbine Laboratory at the National Research Council of Canada. This unique setup employs two separate variable-speed radial blowers designed to supply air at room temperature, accommodating the nuanced requirements of gas turbine combustor simulation.

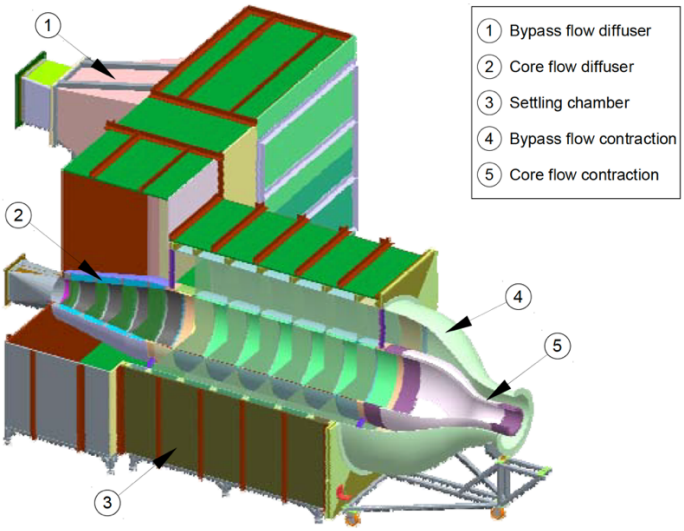

Figure 15. 3D CAD model and it's cutaway of the dual-core wind tunnel [37]

The core flow, essential for replicating the primary airstream within a combustor, is propelled by a 30 kW AC motor-driven blower. This component is adept at delivering airflow up to a maximum of 2.5 kg/s, achieving a total pressure rise of 5 kPa. Complementing this, the bypass flow blower, powered by a 45 kW AC motor, supplies an additional airflow stream, capable of reaching flow rates up to 5.6 kg/s with a pressure rise of 5.6 kPa. The dual-blower system ensures a versatile simulation environment, capable of mimicking various operational conditions encountered in actual turbine operations.

To achieve superior flow uniformity and diminish turbulence length scales, the setup includes meticulously arranged fine wire screens—five in each diffuser and an additional six within the common co-annular settling chamber. This strategic placement of screens, coupled with honeycomb flow straighteners at the settling chamber's inlet, effectively neutralizes any swirl, rendering the airflow exceptionally laminar as it advances through the system.

Following the settling chamber, the conditioned airflows are funneled through two concentric contractions, discharging coaxial air jets at differential velocities into the test section. The core and bypass flows undergo contraction ratios of 10.5:1 and 10:1, respectively, culminating in outlet diameters of 203 mm for the core flow and 320 mm for the bypass flow. This design criterion ensures a ±1% velocity uniformity at the contraction exits for both streams

This wind tunnel arrangement facilitates a well-controlled experimental environment and also mimics the complex airflow dynamics characteristic of gas turbine engines, ensuring the fidelity and relevance of our effusion cooling studies.

4.3 Coolant Reservoir

The coolant reservoir is situated beneath the test section. Its primary function is to deliver pure nitrogen, serving as a coolant proxy, through the porous test samples in a manner that is both controlled and uniform. This ensures that the conditions simulated during the experiments closely replicate those encountered in real-world gas turbine operations.

The reservoir incorporates a honeycomb screen and a perforated plate to condition the coolant flow effectively. This design facilitates an even distribution of nitrogen across the

active area of the test coupons, crucial for accurate simulation and analysis of cooling performance.

The design and performance of the reservoir were initially evaluated through Computational Fluid Dynamics (CFD) simulations using COMSOL Multiphysics 6.0. A detailed description of the simulation setup, mesh design, and flow validation is provided in Appendix A.1. Based on these CFD results, the final reservoir configuration was fabricated and integrated into the experimental test rig. The installed design is shown in Figure 16.

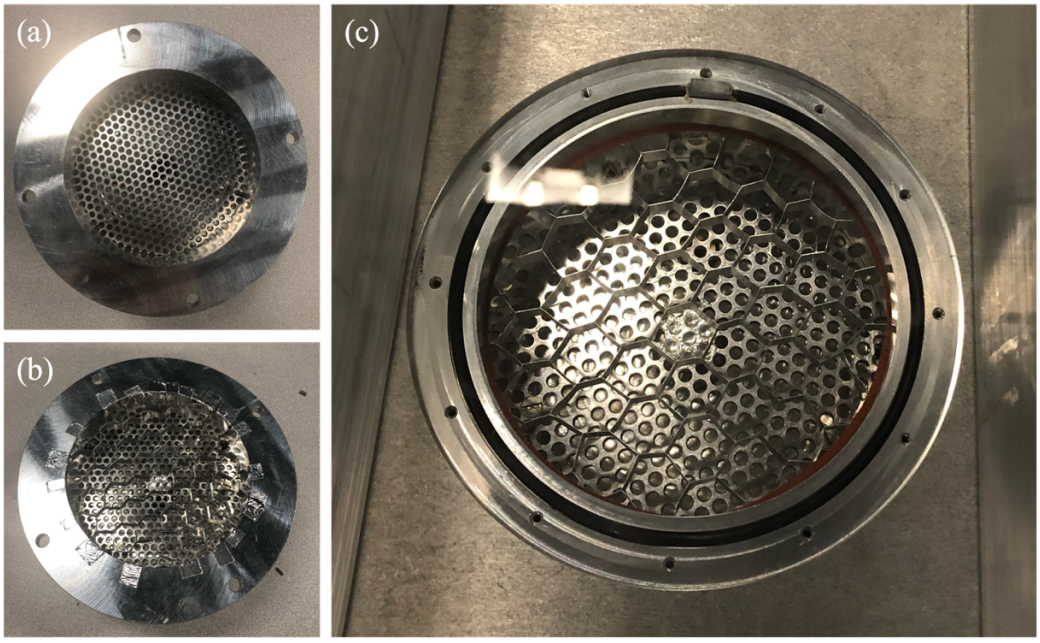

Figure 16. The image of the reservoir installed with (a) the perforated plate and (b) the honeycomb sheet, used in the current experimental setup. (c) The image of the final installation of the reservoir into the current experimental setup.

The dimensions of the coolant reservoir were selected to minimize flux variation across the test surface, thereby enhancing the reliability and accuracy of experimental observations. The internal diameter of the reservoir measures 101.6 mm, with a height of 44.5 mm, dimensions that were found to effectively balance flow distribution and coolant delivery efficiency.

By achieving a uniform distribution of coolant flow, the setup allows for precise simulation of effusion cooling performance, mirroring the operational conditions within gas turbine combustors and minimizing potential measurement errors.

4.4 Vent System for Boundary Layer Thickness Control

The precise regulation of boundary layer thickness within the test section is crucial for simulating real-world gas turbine conditions and accurately assessing effusion cooling performance. In gas turbine applications, the incoming boundary layer directly influences the effectiveness of film cooling and effusion cooling, as it affects coolant jet interactions, coverage, and cooling efficiency. A boundary layer that is too thick may suppress coolant jet penetration, reducing lateral spreading, while an excessively thin boundary layer may lead to increased mixing and coolant dissipation.

To achieve the desired boundary layer conditions, an innovative adjustable vent system was integrated near the leading edge of the test coupon. The vent consists of an opening near the bottom surface of the main flow channel, as seen in Figure 19b, allowing part of the flow to be vented out of the wind tunnel and resetting the boundary layer development (and thickness) in the vicinity of the test sample. This adjustment ensures that the boundary layer thickness at the test section is within the range observed in real gas turbine environments. In this study, the target Reynolds number based on hydraulic diameter was 256,000, which is typical of flow conditions in actual gas turbine combustors. The vent system was specifically designed and positioned to develop a turbulent boundary layer consistent with these conditions, ensuring a representative momentum thickness Reynolds number (Re_θ) and realistic flow development upstream of the test sample. Under this flow regime, the momentum thickness Reynolds number was estimated to fall within the range of 1000–1500, aligning with values reported in the literatures [38][39][40] for combustor liner surfaces.

This subsystem's design and strategic placement allow for dynamic airflow regulation, ensuring that the boundary layer over the test sample closely resembles that in actual gas turbine operation. By maintaining a representative boundary layer profile, the experiment provides realistic cooling performance data, improving the applicability of the results to real-world turbine conditions.

The vent system's effectiveness in controlling the boundary layer thickness was validated against configurations lacking this feature. Comparative analyses highlighted the system's critical role in achieving desired aerodynamic conditions, with Figure 17 illustrating the

vent system's configuration (Figure 17(b)) alongside a setup devoid of the vent mechanism (Figure 17(a)).

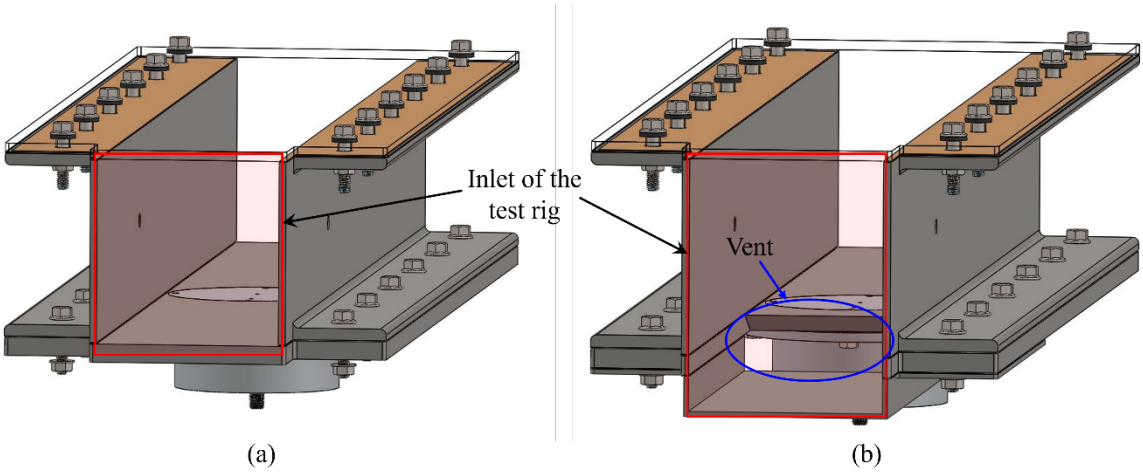

Figure 17. 3D CAD design of the test rig (a) without or (b) with the vent system.

A hot-wire anemometer from Dantec Dynamics [37] was used to measure flow velocity across the main flow channel to obtain precise measurements of boundary layer thickness. The anemometer was positioned as depicted in Figure 18 and arranged as shown in Figure 19, allowing for velocity measurements up to 63.5 mm above the test rig floor.

To accurately capture the boundary layer profile, velocity measurements were conducted at eight or nine discrete heights from the bottom surface of the test section to the centerline of the rig. These measurement points were chosen to provide sufficient resolution of the velocity gradient near the wall, where boundary layer development is most significant. The anemometer probe was incrementally adjusted in height using a precision-controlled traverse system to ensure consistent positioning.

At each measurement height, the mean velocity was recorded over a duration of 30 seconds, with data sampled at a rate of 10 kHz to ensure high temporal resolution and minimize random fluctuations. The collected data was then processed to compute the boundary layer thickness using the conventional definition, where the thickness is determined at the height where the velocity reaches 99% of the freestream velocity.

This measurement approach ensured repeatability and accuracy, allowing for a well-resolved boundary layer velocity profile, which was subsequently used for comparison with CFD predictions and validation of the vent system’s effect on boundary layer control.

A detailed description of the simulation setup, meshing strategy, solver selection, and validation results is provided in Appendix A.2.

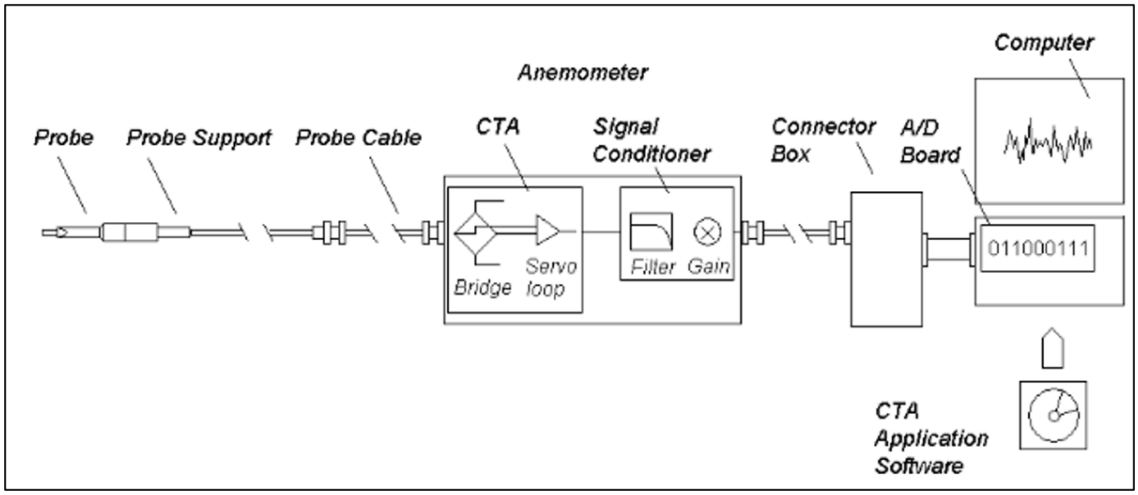

Figure 18. Schematic of the measurement system for the hot-wire anemometer [41].

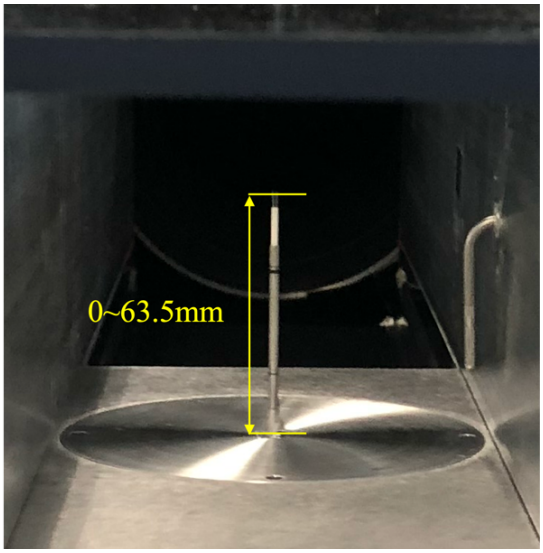

Figure 19. The image of the hot-wire anemometer installed in the test rig.

The comparison results, as plotted in Figure 20, demonstrate that the vent system successfully adjusts the boundary layer thickness to 10 mm, confirming its effectiveness. A comparison between the vented and unvented configurations further highlights the vent system's significant impact on boundary layer development, ensuring the experimental setup closely mimics real-world gas turbine conditions.

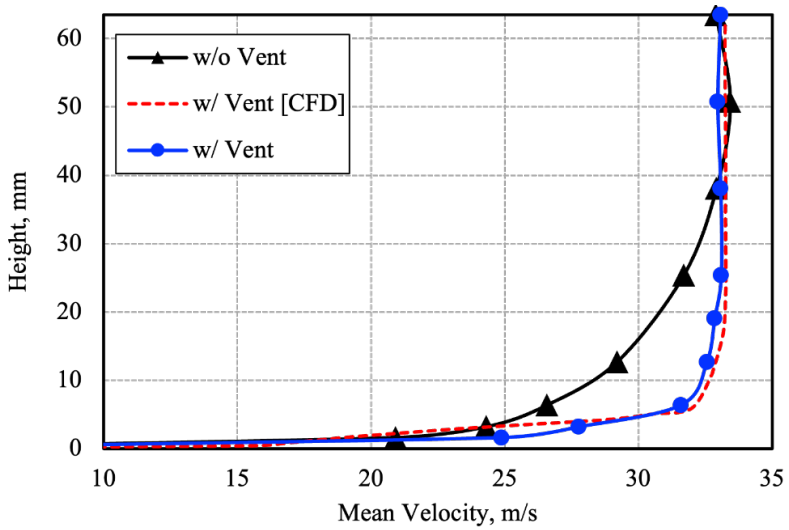

Figure 20. The velocity profiles at the center point of the leading edge of the test coupons in the test rig without and with the vent system, which validate CFD predictions as indicated by the red dotted line in the plot.

The incorporation of the vent system into the experimental setup marks an improvement in replicating the thermal and fluid dynamics characteristic of gas turbine environments. By enabling precise control over the boundary layer thickness, the system significantly enhances the reliability and relevance of the effusion cooling studies. This approach not only aligns the experimental conditions more closely with operational realities but also bolsters the integrity of the data collected, ensuring that subsequent analyses and conclusions are firmly rooted in accurately simulated environments.

4.5 Turbulence Generator

Achieving an accurate representation of the turbulent conditions characteristic of gas turbine operations is pivotal for the meaningful evaluation of effusion cooling technologies. To this end, a turbulence generator, positioned upstream of the vent system, plays an instrumental role in the experimental setup by introducing controlled disturbances into the airflow. For the boundary layer development and vent system validation discussed in the previous section, the turbulence intensity was maintained at approximately 2%, reflecting the undisturbed baseline condition without the turbulence generator.

In operational gas turbines, turbulence intensities can surge up to 35% at the combustor outlet [41][42], with a minimum presence of 10% noted across the board and a typical

intensity of 20% near the combustor walls [43][44]. These conditions, especially the elevated turbulence near the combustor walls, have significant implications for the cooling performance of combustor liners. The turbulence generator employed in this study, therefore, seeks to replicate these conditions to generate a realistic simulation environment for assessing effusion cooling efficacy under varied turbulence intensities.

The selected turbulence generators (which consist of coarse wire mesh screens and round bars, as shown in Figure 21(a)), were designed and strategically positioned to generate turbulence intensities of 5%, 10%, and 20% within the experimental rig as shown in Figure 22, aligning with the range observed in real gas turbine conditions. As depicted in Figure 21(b), the configuration includes two distinct grids—Grid 1 and Grid 2—situated 152 mm and 76 mm from the hot-wire anemometer measurement location, respectively. A composite design, referred to as Design 3, is also placed 76 mm away, effectively replicating the desired turbulence intensities. The hot-wire anemometer, previously introduced in Figure 18 and positioned as per Figure 19, was used to measure velocity fluctuations at multiple heights, extending its measurement capabilities up to 63.5 mm from the test rig floor. Turbulence intensity (Tu) was determined from the velocity measurements using the following equation:

$$Tu = \frac{u'}{U} \times 100\% \tag{4-1}$$

where u' is the root-mean-square (RMS) value of velocity fluctuations, calculated as

$$u' = \sqrt{\frac{1}{N}\sum_{i=1}^{N}(u_i - \bar{U})^2} \tag{4-2}$$

with u_i representing instantaneous velocity measurement and $\bar{U}$ being the mean velocity over the sampling period, and U is the time-averaged velocity.

To ensure reliable turbulence intensity measurements, data was recorded at a sampling rate of 10 kHz for 30 seconds per measurement location, providing sufficient temporal resolution to capture turbulence fluctuations accurately. This approach enabled the evaluation of turbulence levels at different grid configurations and validated the effectiveness of the turbulence generators in achieving the desired conditions.

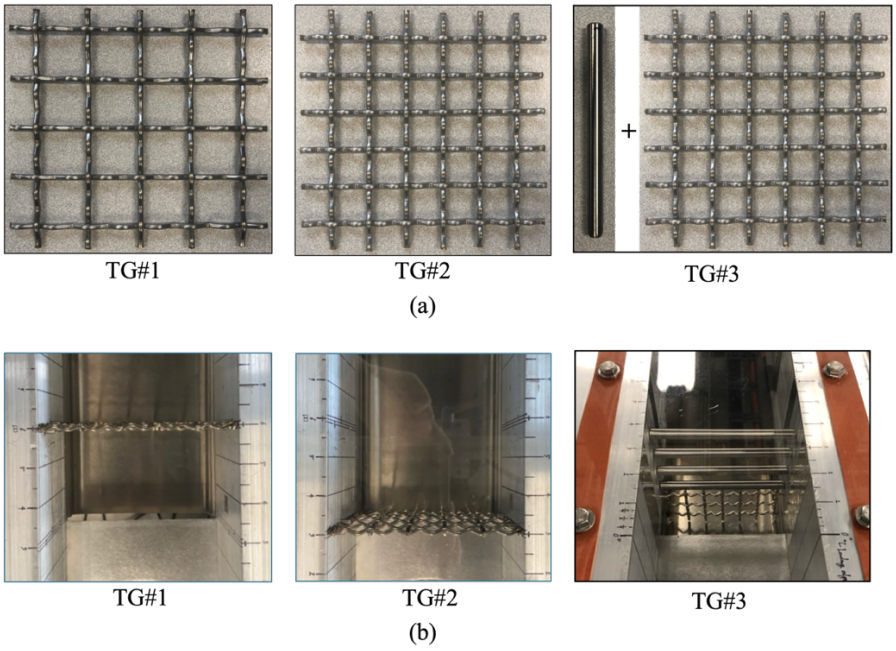

Figure 21. The image of (a) the design and (b) installed of TG#1(left), TG#2(middle), and TG#3(right).

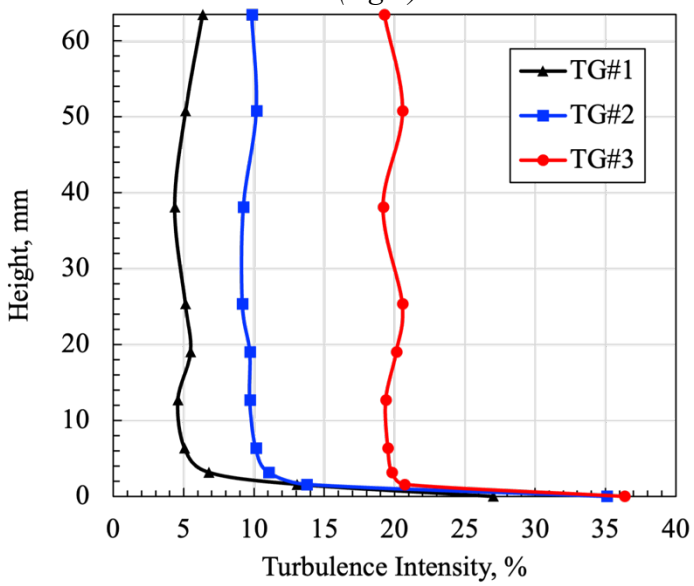

Figure 22. The turbulence intensity profiles are measured at the center of the leading edge of the test coupon installed in the test rig.

The meticulous design, strategic positioning, and rigorous validation of the turbulence generator underscore its indispensability in the experimental setup. By emulating the complex airflow dynamics characteristic of turbine operations, this component not only

enhances the realism of the testing environment but also ensures that conclusions from the study are directly translatable to industrial applications.

4.6 Test Coupons

All test coupons were constructed using stereolithography (SLA) 3D printing with High Temp Resin (Formlabs) to ensure precise fabrication of complex effusion cooling hole geometries. Printing was performed using a Form 3+ printer (Formlabs), chosen for its high resolution and thermal stability suitable for aerodynamic testing. The test coupons were designed to investigate the effects of compound angles on adiabatic film cooling effectiveness (AFE) under different flow conditions.

4.6.1 Test Coupons for the Study of Swirling Flow Effects Near Liner Surface

In a previous study [15], an aluminum test coupon fabricated via conventional machining was used to investigate the directional effects of effusion cooling. The experimental setup, depicted in Figure 14, involved a single circular test coupon that was rotated between tests to align the main flow at different compound angles relative to the effusion cooling jets. This setup aimed to simulate realistic swirling main flow conditions, which are common in gas turbine combustors for flame stabilization.

To verify whether similar results could be reproduced with an SLA 3D-printed test coupon, four configurations—shown in Figure 23(a)—were tested. Each of these configurations used the same single test coupon, but it was installed at discrete rotational angles to achieve compound angles of 0°, 30°, 60°, and 90° relative to the main flow. The 0° compound angle configuration served as the baseline case for comparison.

A key observation from Figure 23(a) is that a swirling main flow not only introduces a nonzero compound angle between the coolant jets and the main flow but also alters the effective pitch of the effusion cooling holes. This occurs because rotating the test coupon changes the projected spacing between holes in the direction of the main flow. To help visualize this, Figure 23(a) includes a zoomed-in schematic of the hole layout and numerical values quantifying the change in effective pitch as a function of compound angle. These changes impact the coolant distribution and film overlap, influencing the measured AFE. To decouple these two effects and study the influence of compound angle in isolation,

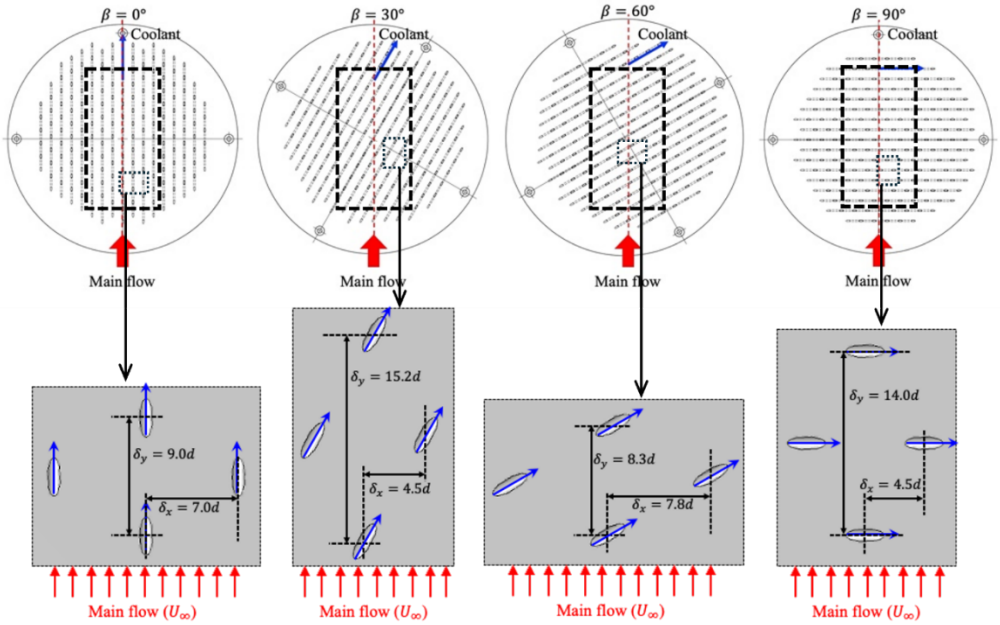

(a)

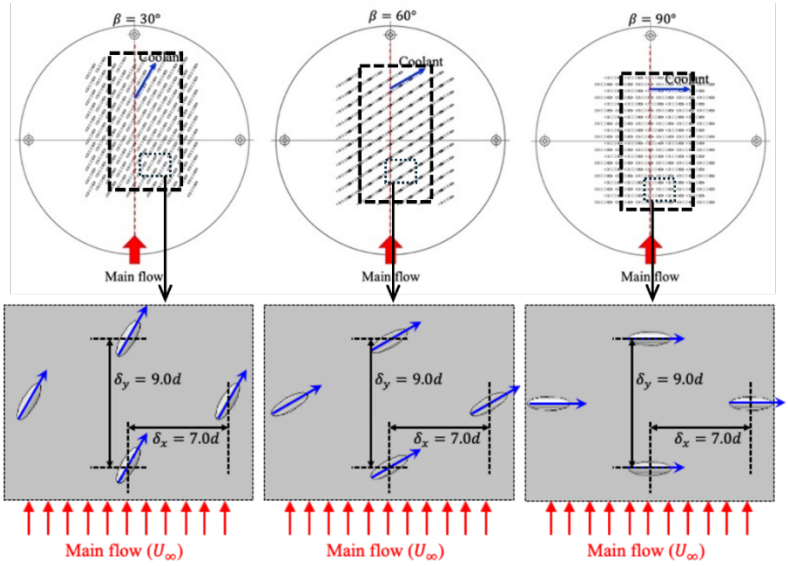

(b)

Figure 23. Effusion cooling test configurations: (a) a single test coupon rotated at four discrete angles relative to the main flow direction (β = 0°, 30°, 60°, and 90°). The co-linear installation (β = 0°, first from the left) serves as the baseline case. Due to rotation, the effective pitch changes as follows: for β = 30°, δ_x= 4.5d and δ_y= 15.2d; for β = 60°, δ_x= 7.8d and δ_y = 8.3d; and for β = 90°, δ_x= 4.5d and δ_y= 14d , and (b) three additional test coupons that have three discrete compound angles (β = 0°, 30°, 60°, and 90°) while maintaining the same hole pitch as the baseline case in (a) such that $\delta_x = 7d$ and $\delta_y = 9d$. All test coupons have a diameter of 123.8 mm and a thickness of 2.54 mm. The black bold dashed box indicates the active effusion cooling area, which is consistent across all test coupons and measures 49d × 90d.

a new set of SLA 3D-printed test coupons was developed. As shown in Figure 23(b), these coupons were designed with fixed hole pitches and compound angles of 0°, 30°, 60°, and 90°, allowing for direct comparisons without the confounding influence of changing hole spacing. This approach eliminates geometric variability and ensures that any differences in adiabatic film cooling effectiveness (AFE) can be attributed solely to the compound angle. To ensure consistency in film cooling comparisons, only the central region of each test coupon—excluding the left and right edges—was considered in the analysis. This approach minimizes uncertainties related to lateral film development and focuses solely on the effect of compound angles on AFE.

4.6.2 Test Coupons for the Study of Optimizing AFE by Varying Compound Angle

A limitation of the previous study was that each test coupon featured a uniform compound angle across its entire surface, which did not reflect the spatial variations in cooling performance observed under realistic swirling flow conditions. As presented in Chapter 5-1, the results indicated that different regions along the flow direction responded differently to compound angle configurations. Specifically, higher compound angles such as 90° were more effective near the leading edge, while lower angles like 30° performed better downstream. These observations led to the hypothesis that a spatially varying compound angle design—tailored to the cooling needs of each region—might further enhance the adiabatic film cooling effectiveness (AFE).

To test this hypothesis, a new set of SLA 3D-printed test coupons was designed with non-uniform compound angles, where the compound angle varies along the mainstream direction to optimize cooling performance. Figure 24 presents a consolidated schematic of the baseline configurations from Figure 23, restructured for visual clarity for the pitch and the active cooling area. This figure serves to summarize the previous test configurations before introducing the new designs, and incorporates visual improvements based on feedback received for Figure 23. Figure 24 shows the baseline designs to compare with the new designed test coupons as shown in Figure 25. This design approach was informed by findings from the author's previous work [32], which demonstrated that compound angles have region-specific cooling benefits—specifically, 90° compound angles enhance cooling near the leading edge, while 30° angles perform better downstream. Based on these insights,

the new test coupons were divided into three longitudinal sections with assigned compound angles of 90°, 60°, and 30°, distributed across the upstream, central, and downstream regions, respectively. As shown in Figure 25, the compound angle distribution was set as follows: 20% of the coupon length for 90° (upstream), 60% for 60° (central), and 20% for 30° (downstream), providing a spatial variation designed to optimize adiabatic film cooling effectiveness (AFE).

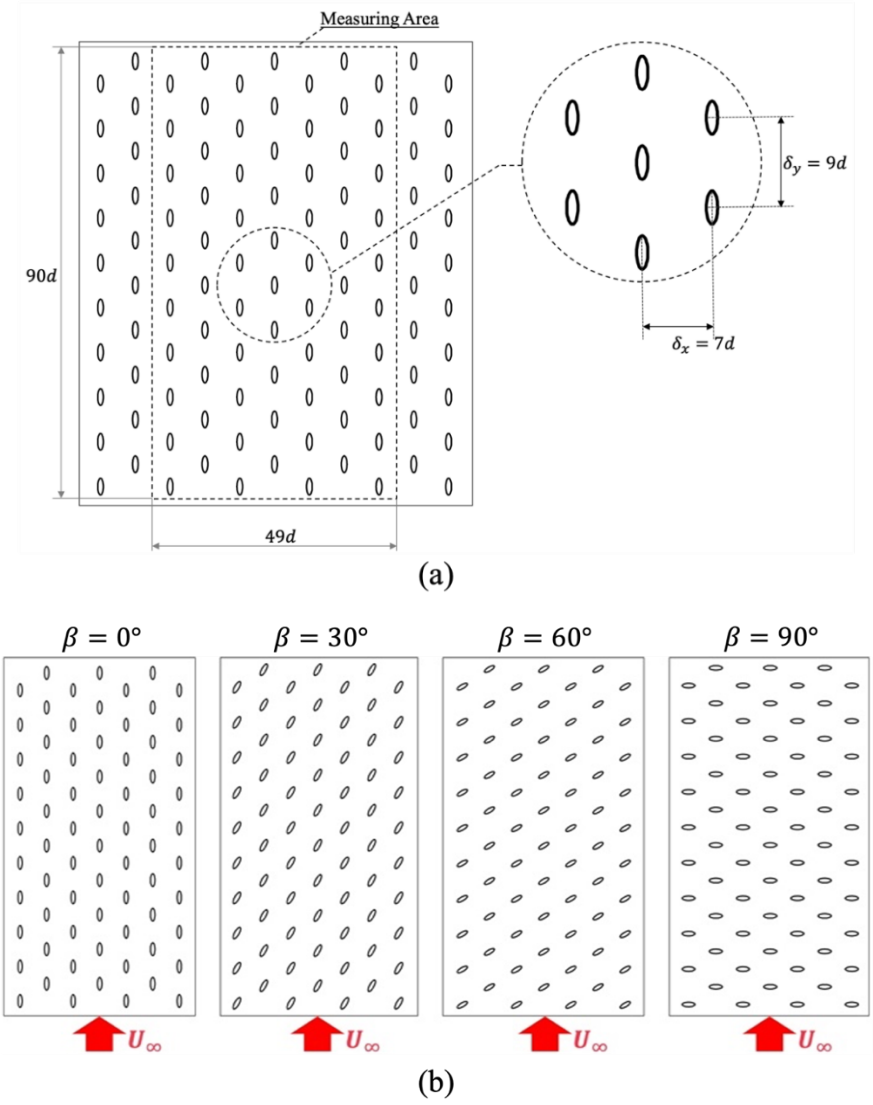

Figure 24. (a) Spanwise (δ_x) and streamwise (δ_y) pitches are denoted for an example effusion cooling configuration ($\beta = 0°$). The black dash-line box means an active effusion cooling area which is the same for all test coupons as 70.83mm × 38.56mm, or 90d ×49d, where d represents the diameter of the effusion cooling holes. (b) effusion cooling test configurations: effusion holes co-linear with the main flow direction ($\beta = 0°$) and three non-zero compound angle cases $\beta = 30°$, $\beta = 60°$, and $\beta = 90°$.

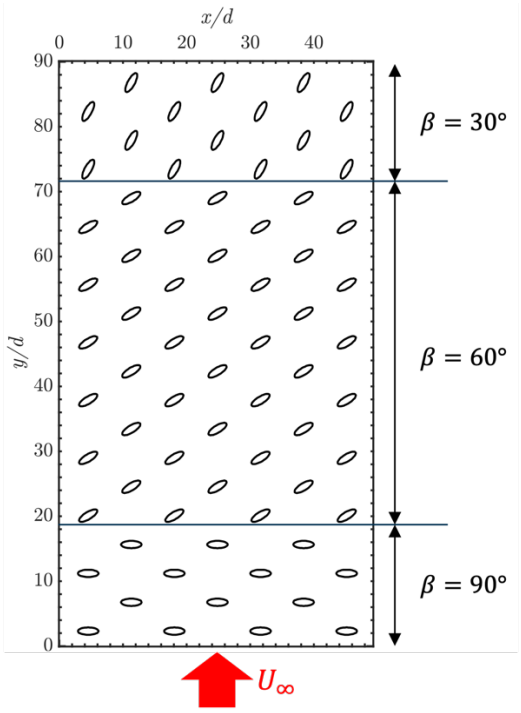

Figure 25. Schematic of test designs using three discrete compound angles. the bottom of the measurement area represents the upstream side.

The longitudinal length of each region for the compound angle of 90, 60, or 30 degrees is inferred from the current author's study [32].

To accurately assess the pressure losses across the effusion cooling test coupons, differential pressure measurements were conducted using static pressure transducers installed in both the test section and the reservoir, as shown in Figure 26.

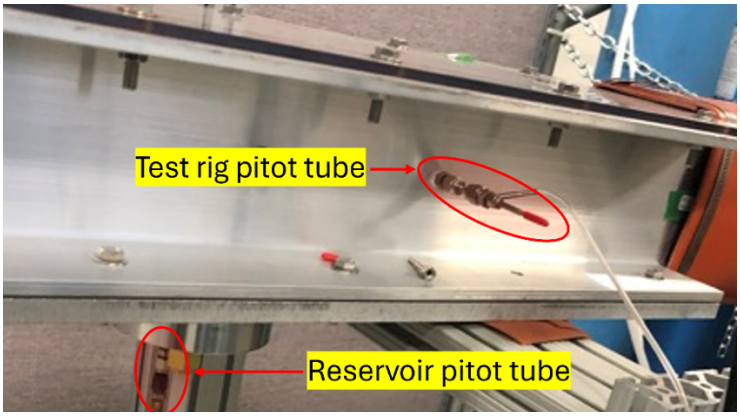

Figure 26. The installed location of the static pressure transducers at the test section and the reservoir to measure the pressure drop through the test coupons.

The pressure drop values were determined to be 0.8%, 1.9%, and 3.8% for blowing ratios (BR) of 0.6, 1.0, and 1.4, respectively, as shown in Figure 27. These values indicate that pressure losses increase with higher blowing ratios, consistent with previous studies on effusion cooling systems. During all experiments, the ambient temperature was maintained at 293 K to ensure consistency in thermal measurements.

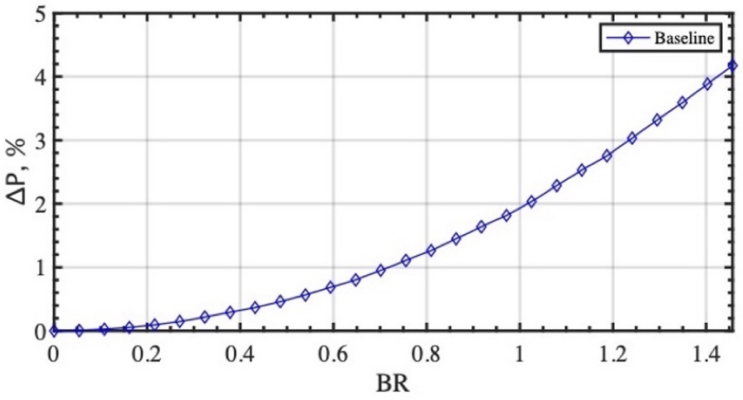

Figure 27. The percentage pressure drop across effusion cooling test coupons were maintained as a fixed function of Blowing Ratio for all test configurations.

4.7 Pressure Sensitive Paint (PSP)

4.7.1 Principle of PSP

In this research, Pressure Sensitive Paint (PSP) has been utilized as a tool for examining aerodynamic behavior and heat/mass transfer mechanisms [45][46], particularly in the realm of effusion cooling [33][47][48][49]. PSP technology is established in the incorporation of oxygen-sensitive molecules within a polymer matrix that is permeable to oxygen. This composition allows for the accurate measurement of oxygen partial pressures across the coated surfaces. Upon UV light activation, these molecules exhibit fluorescence that varies according to the ambient oxygen partial pressures [49]. For the purposes of this study, nitrogen with a purity of 99.99%, serving as a coolant proxy, was chosen due to its negligible oxygen content. This film acts as a barrier or significantly dilutes the main airflow near the cooling surface, enabling a direct correlation between PSP fluorescence intensities and the adiabatic film cooling effectiveness (AFE). The fluorescence intensity and oxygen concentration can be expressed by the Stern-Volmer equation as

$$\frac{I_{max}(T)}{I(T)} = 1 + K(T) \cdot S(T,p) \cdot x \cdot p \tag{4-3}$$

where I is the measured PSP fluorescence intensity, I_{max} is the maximum fluorescence intensity in the absence of oxygen, K is the Stern-Volmer constant depending on temperature, S is Henry's law coefficient that is a function both of temperature and pressure, x is the mole fraction of oxygen in the gas immediately adjacent to the paint, and p is the air pressure at the measurement surface. For calibration of PSP fluorescence intensities, a second-order polynomial equation is employed as:

$$\frac{p}{p_{ref}} = C_1(T)\left(\frac{I_{ref}}{I}\right)^2 + C_2(T)\left(\frac{I_{ref}}{I}\right) + C_3(T) \tag{4-4}$$

where

$$\frac{I}{I_{ref}} = \frac{I_{raw} - I_{dark}}{I_{ref,\ raw} - I_{dark}} \tag{4-5}$$

and the subscript *ref* indicates the standard air condition as the reference point, and I_{ref} is the corrected PSP fluorescence intensity when the paint is surrounded by the standard air. On the other hand, the subscript *dark* denotes the camera reading without UV excitation, which may include some background light. In Equation (4-4), very weak temperature dependency of C_1, C_2, and C_3 is ignored and the polynomial coefficients are treated as constants. Equation (4-5) is for correcting background light leak, where the raw PSP fluorescence intensity I_{raw} is discounted by the recorded camera reading without UV excitation I_{dark} to get corrected PSP fluorescence intensity I.

However, factors such as fluctuations in the illumination intensity and temperature variations during calibration and data collection can impact the accuracy of deriving local oxygen partial pressures from PSP fluorescence. In addition, errors can also arise from temperature variations on the PSP surface due to the fact that the main air (ambient air) could be at a different temperature than that of the coolant proxy (nitrogen), which was discharged from compressed gas bottles. To mitigate these uncertainties, Binary PSP is utilized, featuring a reference molecule for temperature error correction. Unlike single-component PSP, the Binary PSP includes a reference molecule component that enables correction for errors in PSP temperature. Fluorescence intensities can be acquired from both the oxygen-sensitive and reference molecule components allowing the errors induced

by variations in PSP temperature and UV excitation illumination intensities be compensated [49][50]. Figure 28 represents the spectra of UV excitation illumination near the wavelength of 400 nm together with the resulting Binary PSP fluorescence peaks near the wavelength of 650 nm as the pressure-sensitive signal and the wavelength of 560 nm as the reference signal.

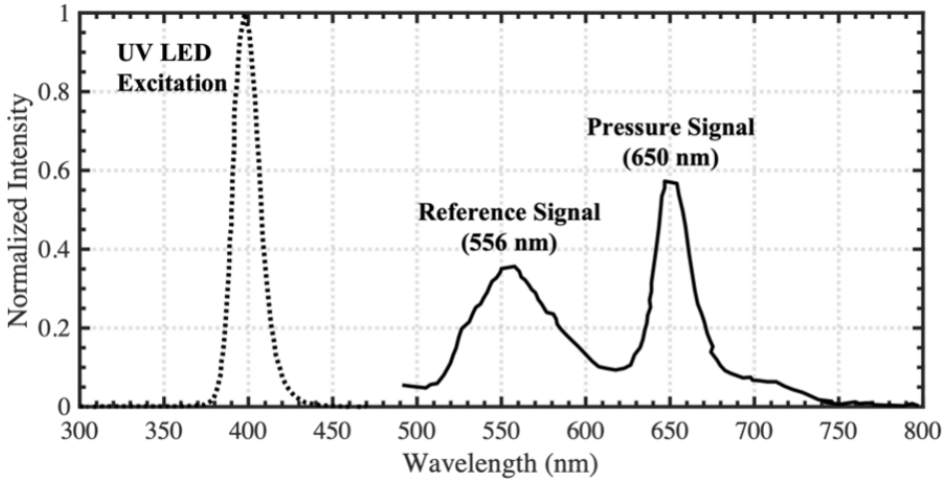

Figure 28. Spectra of UV excitation illumination together with the resulting fluorescence peaks near 650 nm as the pressure-sensitive signal and 560 nm as the reference signal for BinaryFIB PSP from Innovative Scientific Solutions Inc. The plot is reproduced from [51]

The fluorescence emissions at two distinct peaks demonstrate comparable responses to changes in PSP temperature. By computing the ratio between the fluorescence related to pressure sensitivity and the reference fluorescence, it is possible to adjust for errors caused by PSP temperature shifts and variations in the intensity of UV excitation light. McLean [52] highlighted the challenge of accurately accounting for the inhomogeneity of luminophore blending through a straightforward intensity ratio of the two peaks. Consequently, Liu et al. [53] suggested normalizing the fluorescence intensity ratios to the reference condition, specifically the standard ambient air, to correct for uneven luminophore distribution and disparities in paint application thickness. This normalization process, depicted as

$$\frac{r}{r_{ref}} = \frac{(I - I_{dark})_{PT}/(I - I_{dark})_{T}}{(I_{ref} - I_{dark})_{PT}/(I_{ref} - I_{dark})_{T}} \tag{4-6}$$

where r/r_{ref}, the normalized ratio of fluorescence intensities, replaces I/I_{ref}, normalized pressure signal fluorescence intensity introduced in Equation (4-4). The subscript *PT* indicates the pressure signal fluorescence peak near 650 nm which is both pressure and temperature-dependent, while the subscript *T* represents the reference fluorescence peak near 560 nm which is temperature-dependent only.

Building on Equation (4-4), a second-order polynomial formula is employed to calibrate and ascertain the local oxygen partial pressures based on Binary PSP surfaces, as expressed in Equation (4-7):

$$\frac{p_{O_2}}{p_{O_2,ref}} = C_1(T)\left(\frac{r_{ref}}{r}\right)^2 + C_2(T)\left(\frac{r_{ref}}{r}\right) + C_3(T) \tag{4-7}$$

In this scenario, nitrogen, devoid of molecular oxygen, serves as the coolant proxy, while ambient air constitutes the main flow. This setup enables the direct derivation of AFE from the local oxygen partial pressures identified through Binary PSP, as per Equation (4-7), leveraging the heat/mass transfer analogy. This analogy's applicability is contingent upon a turbulent flow scenario, characterized by a turbulent Lewis number nearing unity. Given the high Reynolds numbers typical in gas turbine combustor environments (256,000 in this study), this analogy remains valid across the combustor liner surface [54]. Consequently, AFE, or η_{ad}, can be precisely calculated from the oxygen partial pressures gauged through the normalized fluorescence intensity ratios, as delineated in Equation (4-8):

$$\eta_{ad} = \frac{T_g - T_{aw}}{T_g - T_c} \approx \frac{X_{O_2,g} - X_{O_2,aw}}{X_{O_2,g} - X_{O_2,c}} \tag{4-8}$$

where *T* represents temperature and X denotes the mole fraction of molecular oxygen, respectively. In addition, the subscripts *g*, *aw*, and *c* denote main air flow, adiabatic wall, and coolant, respectively.

4.7.2 Heat and Mass Transfer Analogy for Adiabatic Film Cooling Effectiveness

To accurately evaluate adiabatic film cooling effectiveness (AFE) in this study, the heat and mass transfer analogy is employed, enabling temperature-based definitions of AFE to be expressed in terms of concentration. This analogy is particularly valuable in experiments where temperature measurement is difficult or where mass transfer techniques, such as oxygen-based pressure-sensitive paint (PSP), offer higher sensitivity and spatial resolution.

It begins with the classical definition of adiabatic film cooling effectiveness, written in terms of temperature:

$$\eta = \frac{T_g - T_w}{T_g - T_c} \tag{4-9}$$

where T_g is the mainstream temperature, T_w is the wall (surface) temperature, and T_c is the coolant temperature. This relation measures how effectively the coolant reduces the wall temperature relative to the difference between the mainstream and coolant temperatures.

To derive a concentration-based analog of this equation, it invokes the heat and mass transfer analogy, which relies on the Lewis number (*Le*) being approximately unity. The Lewis number is defined as:

$$Le = \frac{\alpha}{D} = \frac{\nu/Pr}{\nu/Sc} = \frac{Sc}{Pr} \tag{4-10}$$

where α is thermal diffusivity, D is mass diffusivity, ν is kinematic viscosity, Pr is the Prandtl number, and Sc is the Schmidt number. The Prandtl number represents the ratio of momentum diffusivity to thermal diffusivity, while the Schmidt number represents the ratio of momentum diffusivity to mass diffusivity. When $Le = Sc/Pr \approx 1$, the governing transport equations for heat and mass share the same form, allowing for analogous behavior in boundary layer development.

In turbulent gas flows, such as the airflow and nitrogen mixture used in this study, both the Prandtl and Schmidt numbers are typically close to 0.7 under standard temperature and pressure conditions [55]. This similarity arises because turbulent transport is dominated by eddy diffusivity rather than molecular diffusivity, and the turbulent Prandtl and Schmidt numbers tend to converge in such flows. Therefore, it is well established in heat and mass transfer literature [55] that for gases like air and nitrogen, the approximation $Pr \approx Sc \approx 0.7$ holds, which leads to $Le \approx 1$. This justifies the application of the analogy in the present context.

To formalize this analogy, the governing equations for heat and mass transfer are non-dimensionalized. The dimensionless temperature profile is expressed as:

$$\theta(y) = \frac{T_g - T(y)}{T_g - T_c} \tag{4-11}$$

and the dimensionless concentration profile is:

$$\phi(y) = \frac{C_g - C(y)}{C_g - C_c} \tag{4-12}$$

where $T(y)$ and $C(y)$ are the local temperature and concentration at a vertical distance y from the wall, and C_∞ and C_c are the oxygen concentrations in the mainstream and coolant, respectively. When $Le \approx 1$, these profiles are similar, implying $\theta(y) \approx \phi(y)$.

Evaluating both expressions at the wall ($y = 0$) gives:

$$\eta = \frac{T_g - T_w}{T_g - T_c} = \frac{C_g - C_w}{C_g - C_c} \tag{4-13}$$

In this experiment, the coolant used is nitrogen, which is devoid of oxygen, i.e., $C_c = 0$. Thus, with the assumption of the adiabatic wall on the test surface, the expression simplifies further to:

$$\eta_{ad} = \frac{C_g - C_{aw}}{C_g} \tag{4-14}$$

where C_{aw} is the oxygen concentration at the adiabatic wall, and $C_\infty$is the concentration in the freestream. Finally, recognizing that Bi-PSP detects oxygen mole fraction (or volume concentration), the equation becomes:

$$\eta_{ad} = \frac{X_{O_2,g} - X_{O_2,aw}}{X_{O_2,g}} \tag{4-15}$$

In conclusion, by non-dimensionalizing the governing equations for heat and mass transfer and using the empirical and theoretical justification that in turbulent gas flows, the Lewis number approaches unity. This justifies the use of the heat and mass transfer analogy, allowing temperature-based AFE to be equivalently evaluated through oxygen concentration measurements. The supporting relationship between the heat transfer coefficient and mass transfer coefficient reinforces the equivalence, providing a solid foundation for the PSP-based approach used in this thesis.

4.7.3 Application of PSP

In this research, the BinaryFIB PSP [51] provided by ISSI was utilized, characterized by its UV excitation range of 380 to 520 nm and dual emission peaks. One emission peak, sensitive to oxygen partial pressure, is observed near 650 nm, while a reference signal, unaffected by oxygen levels but similarly responsive to temperature variations as the

pressure signal, is detected near 556 nm. The UV excitation required for the Binary PSP, specifically near 400 nm, was supplied by an ISSI LED light source (LM2X-DM). A LaVision ImagerProX 2M camera, coupled with a LaVision Image Doubler, facilitated the capture of both PSP fluorescence signals. This setup, depicted in Figure 29(a), utilizes the image doubler to segregate two distinct wavelengths onto separate image sensors. Filtration of the PSP fluorescence intensity images, as illustrated in Figure 29(c), employs bandpass filters centered at 650 nm and 560 nm, with full-width at half-maximum (FWHM) values of 20 nm and 10 nm, respectively. The filtered images are then juxtaposed by the image doubler, allowing the LaVision camera to record the composite image.

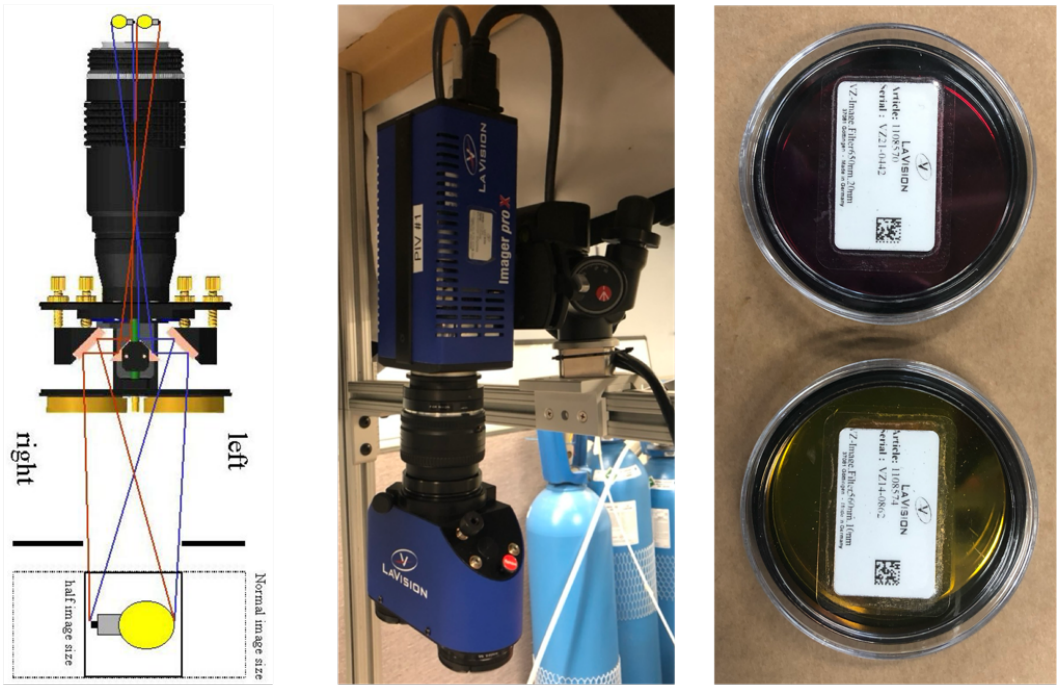

(a) (b) (c)

Figure 29. (a) The schematic of the image doubler which represents how the device works. (b) The image of the image doubler installed with the CCD camera in the test setup. (c) The image of the bandpass filters for the PSP utilization.

The calibration of the Binary PSP, tailored to the specific demands of our experimental arrangement and each unique effusion cooling configuration, was conducted using predefined mixtures of pure nitrogen and compressed air. This calibration procedure involved individually regulating and metering the gas streams before their mixture in a conduit. As detailed in Table 2, calibration points were established across a range of volumetric fractions of compressed air, from 0% to 100%, with pure N2 serving as the

balance gas. During this phase, the wind tunnel's operation ceased, and the test section was isolated, with the calibration gases being introduced to the effusion cooling test coupon via a calibration shroud, as shown in Figure 30, under atmospheric pressure conditions. This process enabled precise pixel-wise calibrations by exposing the Binary PSP on the test coupon surfaces to known oxygen partial pressures, thereby establishing correlations between PSP fluorescence intensities and oxygen levels. Following the calibration for each configuration, the calibration shroud was removed, and the test section reconnected for subsequent experiments, utilizing N2 as the coolant proxy to facilitate PSP-based visualization of cooling films on the effusion cooling test coupon surface.

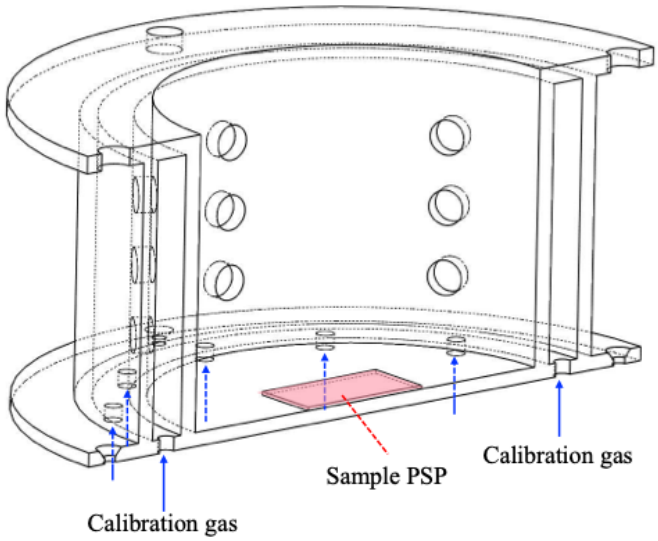

Figure 30. Schematic of the calibration shroud being placed in the test section for isolating the effusion test coupon from the rest of the wind tunnel in the current study.

Table 2 Operating conditions of the calibration gas for the PSP calibration

Overall flow rate, SLPM	Oxygen(O_2) concentration, %	Coolant (N_2) concentration, %
45	20.9	78.1
45	18.6	80.5
45	16.3	83.0
45	13.9	85.4
45	11.6	87.8
45	9.3	90.3
45	7.0	92.7
45	4.6	95.1
45	2.3	97.6

Figure 31 presents a comparative analysis of the calibration curve obtained in this study against those documented in the literature [49][50]. This comparison allows for the pixel-wise determination of oxygen partial pressures, normalized by standard air, based on the ratio of luminescent intensities. Notably, while individual calibration curves exhibit slight variations across the test coupon's active area, the curve featured in Figure 31 represents the averaged calibration curve for all pixels within the measurement zone. The congruence of these calibration curves with those previously published validates the calibration methodology employed in the current investigation.

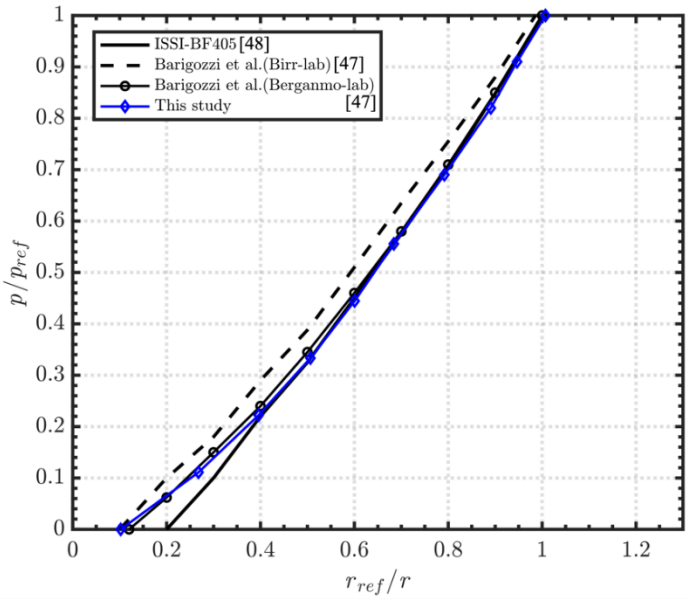

Figure 31. Comparisons of calibration curves. The x-axis is the inverse of normalized ratios of fluorescence intensities as defined by Equation 4-4 while the y-axis is the oxygen partial pressure normalized by standard air.

4.7.4 Uncertainty of PSP Measurement

Accurate quantification of adiabatic film cooling effectiveness (η_{ad}) through Pressure Sensitive Paint (PSP) technology is central to our experimental investigations. However, the precision of PSP measurements can be influenced by various factors, making the understanding and mitigation of associated uncertainties pivotal.

The estimation of the uncertainty for an adiabatic film cooling effectiveness is grounded in the methodological framework established by Kline and McClintock [56], which rigorously assesses the error propagation within experimental measurements. Specifically,

the utilization of binary PSP significantly reduces errors attributed to temperature fluctuations, thanks to pixel-wise calibration curves that tailor the PSP response to specific experimental conditions. Liu and Sullivan [57] further delineated additional sources of uncertainty inherent in PSP measurements, including the stability of illumination, photodegradation of the paint, and spectral leakage. Notably, in the current study, the adoption of a pixel-by-pixel calibration process effectively minimizes the errors stemming from these factors, enhancing the accuracy of cooling film effectiveness measurements. In addition, each PSP image's acquisition process, encompassing an average of 120 frames, significantly diminishes random noise, thereby enhancing measurement fidelity. Moreover, the binary PSP methodology's inherent temperature compensation capabilities, effective across a temperature range of 5 ºC to 45ºC [57], further stabilize the measurement output. The relative uncertainty of cooling film effectiveness has been meticulously evaluated, revealing a variance of ±4.5% at η_{ad} = 0.1, which narrows to ±1.8% as an adiabatic film cooling effectiveness increases to 0.8. This variance underscores the precision attainable through refined calibration and measurement techniques, affirming the reliability of PSP as a diagnostic tool in effusion cooling studies.

5 RESULTS

This chapter presents the results of two different experimental studies. The first study focuses on the effect of the swirling flow by decoupling the influence of varying compound angles and hole pitch during effusion cooling. The second study presents a proposed new design with a non-uniform compound angle in different regions of the test coupon surface along the main streamwise direction in order to improve film cooling performance. Each study is written as a research article and published as a peer-reviewed journal paper, The Aeronautical Journal, and a peer-reviewed technical paper, Proceedings of the ASME Turbo Expo2024.

5.1 Investigation of the Swirling Flow Effects Near Liner Surface

This study addresses the complex interplay between compound angles and pitch variations in effusion cooling configurations under swirling main flow conditions, which are characteristic of gas turbine operations. The focus is on separating the effects of compound angle variations on adiabatic film cooling effectiveness (η_{ad}), distinct from the influences of pitch variations. Through experimentation employing Binary Pressure Sensitive Paint (PSP), the research elucidates the singular impact of non-zero compound angles on AFE, offering insights into how pitch variations contribute to effusion cooling efficiency.

Key findings reveal that non-zero compound angles significantly influence AFE, with swirling main flow conditions prompting a reconsideration of conventional effusion cooling designs. The study demonstrates that by strategically adjusting compound angles independent of pitch variations, enhanced cooling effectiveness can be achieved. This nuanced understanding informs the development of more efficient effusion cooling strategies, optimized for the swirling flow dynamics prevalent in gas turbine engines.

The Aeronautical Journal (2025), 129, pp. 63–83
doi:10.1017/aer.2024.108

RESEARCH ARTICLE

Isolating influences of varying pitch from the effects of non-zero compound angles on effusion cooling

Y. Pyo[1], J. Son[1], P. Richer[2], B. Jodoin[2], M. Broumand[3], S. Yun[3] and Z. Hong[1]

[1]University of Ottawa and National Reseach Council Canada, Ottawa, ON, Canada
[2]Department of Mechanical Engineering, University of Ottawa, Ottawa, ON, Canada
[3]National Research Council Canada, Aerospace Research Centre, Ottawa, ON, Canada
Corresponding author: Z. Hong; Email: zekai.hong@nrc-cnrc.gc.ca

Received: 27 October 2023; **Revised:** 8 August 2024; **Accepted:** 20 September 2024

Keywords: gas turbine; film cooling; effusion cooling; AFE (adiabatic film cooling effectiveness); PSP (pressure sensitive paint); compound angle; pitch

Abstract

Effusion cooling is the state-of-the-art cooling technology for gas turbine hot-gas path components. Typically, effusion cooling holes across the entire combustor liner are aligned with the combustor axis, rendering a nominal zero compound angle between highly directional miniature effusion cooling jets and the main flow direction. The pitch of effusion cooling holes is optimized accordingly. However, the swirling main flow results in a non-zero compound angle and an effectively different pitch from the design. The directional effect of effusion cooling as a result of swirling main flow on the adiabatic film cooling effectiveness (AFE) is a combined effect of a non-zero compound angle and a varied pitch. The current experimental study aims to investigate the isolated effects of compound angle on AFE by excluding the influences of varying pitch. With an improved understanding of the sole effects of non-zero compound angles on AFE, the roles that a varied pitch plays in modifying AFE are further discussed to guide future effusion cooling designs under swirling main flow conditions. Binary Pressure Sensitive Paint (PSP) was used to determine AFE experimentally.

Nomenclature

AFE	adiabatic film cooling effectiveness
BR	blowing ratio
PSP	pressure sensitive paint
C	polynomial constants
d	cooling hole diameter
I	luminescent intensity
r	light intensity ratio
p	air pressure

S	Henry's law coefficient
K	Stern-Volmer constant
x	mole fraction of oxygen in air
T	temperature
U	velocity
X	concentration

Symbols

α	inclination angle
β	compound angle
η	film cooling effectiveness

1.0 Introduction

One of the most effective approaches for improving gas turbine efficiency is to reduce the use of cooling air, as the cooling air for hot gas path components has to be compressed to the highest pressure point of the entire engine. However, the developments of more efficient gas turbine engines are typically associated with higher combustion temperatures, which in turn requires more cooling air if cooling technology remains the same, in addition to the use of advanced high-temperature materials. Furthermore, rising pressure ratios in modern gas turbine engines make the cooling of hot gas path components more challenging because the compressor air is discharged at higher temperatures, making it a less effective coolant for combustor liners and first-stage nozzles. Inadequate cooling available for combustor liners leads to reduced combustor life expectancies and premature engine failures, as reported in the literature [1]. To reduce the metal temperature of combustor liners and to improve the longevity of hot gas path components, previous effusion cooling studies have been focusing on the shape of effusion cooling holes and the pitch of effusion cooling holes [1-4]. In addition, new ceramic materials are being developed as thermal barrier coatings for improved cooling performance [3,4].

Multi-hole effusion cooling provides thermal protection to combustor liners by forcing air at a higher pressure through a series of pinholes, absorbing heat from the liner while forming a protective fluid film layer to insulate heat on the exposed surface [5]. The portion of air that acts as coolant is emanated from the inner surface of the liner through discrete effusion cooling holes as three-dimensional jet columns [6]. The effusion cooling does not affect the location where the coolant is injected, but rather downstream of the cooling holes [6]. Thus, the effusion cooling holes are typically designed to be in the co-linear direction with the hot main flow.

It is well established that the effusion cooling efficiency is highly dependent on the pattern and diameter of the effusion cooling holes, which govern the formation of protective films over the combustor liner. While studies on the pattern or the shape of effusion cooling holes [4-7] and coolant blowing ratios [8-10] are continuously being conducted, the directional effects of effusion cooling on adiabatic film cooling effectiveness (AFE, or η_{ad}) have not received much attention in past studies. The opinion of the authors of this paper is that it is of paramount important to understand the directional effects of effusion cooling under realistic gas turbine combustor conditions for two reasons: 1) the effusion cooling miniature jets are highly directional while the main combustion flow inside gas turbine combustors swirls for flame stabilization; and 2) current

effusion designs predominantly have the effusion cooling holes aligned with the combustor axis. The swirling main flow induces an angular difference between effusion cooling jets and the swirling main flow. Here compound angle (β) is defined as the angular difference between the main flow and the coolant jets as shown in Figure 1.

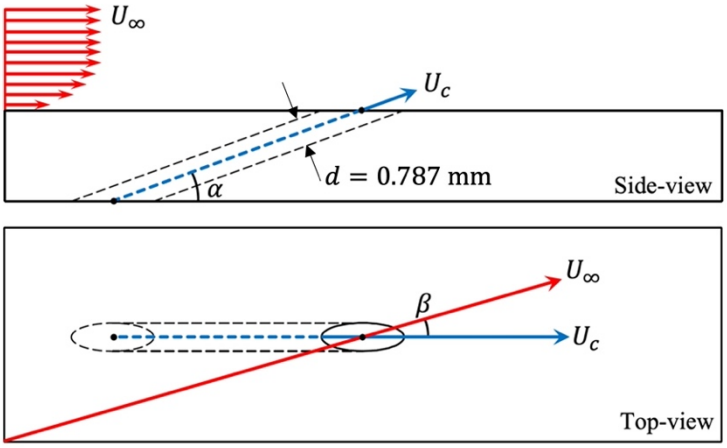

Figure 1. *Diagram of a sample effusion cooling hole with the hole diameter (d), compound angle (β) and inclination angle (α) denoted.*

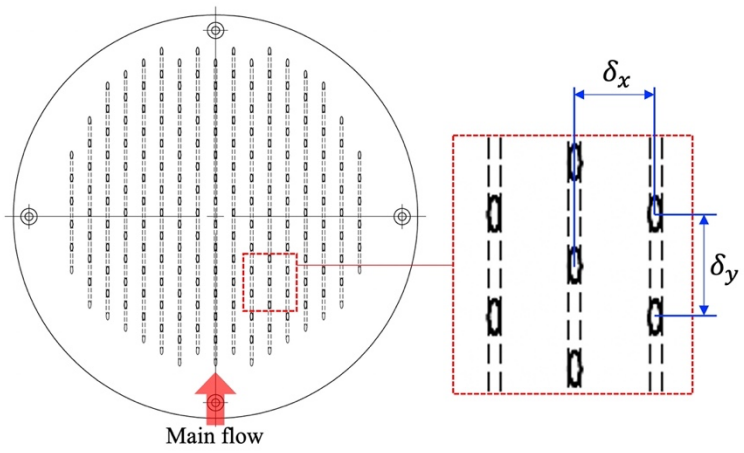

Figure 2. *Spanwise (δ_x) and streamwise (δ_y) pitches are denoted for an example effusion cooling configuration. The effusion cooling holes are staggered in this example.*

The swirling main flow not only induces a non-zero compound angle for effusion cooling, it also alters the effective pitch of effusion cooling holes. Figure 2 illustrates the definition of pitch for an effusion cooling configuration. In the example effusion cooling configuration shown in the figure, the effusion cooling holes are staggered with prescribed spanwise separation between effusion hole columns (δ_x) and streamwise separation between effusion hole rows (δ_y). However, the design pitch is only valid under the condition that the main flow is strictly co-linear with effusion cooling jets, as indicated by the red arrow in the figure. Under swirling main flow conditions, the effective pitch is varied. To see this point, an extreme case can be considered: the main flow is introduced

at 90° to the direct of effusion cooling jet from left to right. In this extreme case, the effective pitch has been altered such that the streamwise and spanwise pitches swapped. In fact, when a swirling main flow induces any non-zero angle between effusion cooling jets and the main flow, the pitch is effectively altered.

When the swirling main flow sweeps on the surface of an effusion cooling plate, both compound angle and effective pitch are altered concurrently. A recent study from this group [11] studied the two combined effects on AFE from swirling main flow as it is most relevant to practical engine operations. However, it is not clear how a non-zero compound angle and a varied pitch contribute separately to the combined directional effects of effusion cooling. The goal of this study is to separate the direction effects on AFE from a non-zero compound angle and from a varied pitch. The approach of this study is to exclude the effects of a varied pitch from the sole effects of non-zero compound angles by fixing the pitch while varying only the compound angle in the experiments. Once the isolated effects of non-zero compound angles are determined, the effects of varying effective pitch will be evaluated to guide future effusion cooling designs under swirling main flow conditions.

2.0 Methodology

Pressure Sensitive Paint (PSP) is a powerful experimental tool for aerodynamic and heat/mass transfer studies [13,14], which was also adopted in previous studies for understanding effusion cooling [15-18]. PSP was formulated by embedding oxygen-sensitive molecules in a polymer binder permeable to oxygen, enabling the inference of localized oxygen partial pressures on the paint surfaces. Upon excitation of a UV light source, the oxygen-sensitive molecules respond with varying fluorescence intensities depending on the oxygen partial pressure [19]. In the current study, nitrogen gas of 99.99% purity was used as the coolant proxy as it has effectively zero oxygen content. If an effusion cooling design is effective in producing a cooling film on the surface of a test article, the main air flow is shielded away or greatly diluted near the effusion cooling surface. Oxygen partial pressures on the surface of a test coupon as revealed by PSP fluorescence intensities can be directly correlated to adiabatic film cooling effectiveness (AFE). The fluorescence intensity and oxygen concentration can be expressed by the Stern-Volmer equation as

$$\frac{I_{max}(T)}{I(T)} = 1 + K(T) \cdot S(T,p) \cdot x \cdot p \qquad \dots (\ 1\ )$$

where I is the measured PSP fluorescence intensity, I_{max} is the maximum fluorescence intensity in the absence of oxygen, K is the Stern-Volmer constant depending on temperature, S is Henry's law coefficient that is a function both of temperature and pressure, x is the mole fraction of oxygen in the gas immediately adjacent to the paint, and p is the air pressure at the measurement surface. A second-order polynomial equation is adopted for calibrating PSP fluorescence intensities as following:

$$\frac{p}{p_{ref}} = C_1(T)\left(\frac{I_{ref}}{I}\right)^2 + C_2(T)\left(\frac{I_{ref}}{I}\right) + C_3(T) \qquad \dots (\ 2\ )$$

where

$$\frac{I}{I_{ref}} = \frac{I_{raw} - I_{dark}}{I_{ref,\ raw} - I_{dark}} \qquad \dots (\ 3\ )$$

and the subscript *ref* indicates the standard air condition as the reference point, and I_{ref} is the corrected PSP fluorescence intensity when the paint is surrounded by the standard air. On the other hand, the subscript *dark* denotes the camera reading without UV excitation, which may include some background light. In Equation (2), very weak temperature dependency of C_1, C_2, and C_3 is ignored and the polynomial coefficients are treated as constants. Equation (3) is for correcting background light leak, where the raw PSP fluorescence intensity I_{raw} is discounted by the recorded camera reading without UV excitation I_{dark} to get corrected PSP fluorescence intensity I.
However, the accuracy of local oxygen partial pressures referred from PSP fluorescence intensities can be affected by other factors, such as fluctuations in excitation illumination intensities and drifts in ambient temperature during calibration and data collection processes. In addition, errors can also arise from temperature variations on the PSP surface due to the fact that main air (ambient air) could be at a different temperature than that of coolant proxy (nitrogen), which was discharged from compressed gas bottles. To minimize uncertainties in oxygen partial pressure determinations from PSP fluorescence intensities due to the aforementioned variations, a Binary PSP was used in this study. Unlike single-component PSP, the Binary PSP includes a reference molecule component that enables correction for errors in PSP temperature. Fluorescence intensities can be acquired from both the oxygen-sensitive and reference molecule components allowing the errors induced by variations in PSP temperature and UV excitation illumination intensities be compensated [18, 19]. Figure 3 shows the spectra of UV excitation illumination near 400 nm together with the resulting Binary PSP fluorescence peaks near 650 nm as the pressure-sensitive signal and 560 nm as the reference signal.

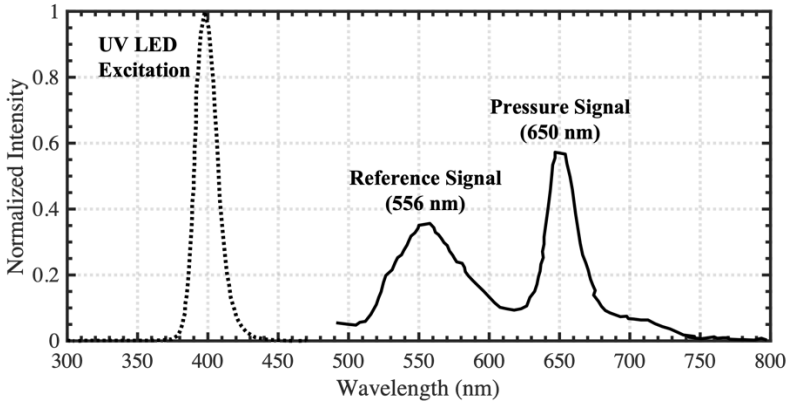

Figure 3. *Spectra of UV excitation illumination together with the resulting fluorescence peaks near 650 nm as the pressure-sensitive signal and 560 nm as the reference signal for BinaryFIB PSP from Innovative Scientific Solutions Inc. The plot is reproduced from [19].*

The two fluorescence peaks exhibit very similar sensitivities to PSP temperature. By taking the ratio of the pressure-sensitive portion of fluorescence to the reference portion, the errors induced by variations in PSP temperature and fluctuations in UV excitation illumination intensities can be compensated. According to McLean [20], due to the imperfect mixing of two luminophores, a simple ratio of the intensities of two fluorescence peaks are insufficient to fully account for luminophore inhomogeneity. Liu et al [21] proposed to normalize ratios of fluorescence intensities by the ratio of fluorescence intensities at the reference condition (i.e., the standard ambient air

condition). The normalized ratio of fluorescence intensities corrects for non-homogeneous luminophore concentrations and variations in paint thickness as

$$\frac{r}{r_{ref}} = \frac{(I - I_{dark})_{PT}/(I - I_{dark})_T}{(I_{ref} - I_{dark})_{PT}/(I_{ref} - I_{dark})_T} \qquad \ldots(\ 4\ )$$

where r/r_{ref}, the normalized ratio of fluorescence intensities, replaces I/I_{ref}, normalized pressure signal fluorescence intensity introduced in Equation 2. The subscript *PT* indicates the pressure signal fluorescence peak near 650 nm that is both pressure and temperature dependent, while the subscript *T* represents the reference fluorescence peak near 560 nm that is temperature dependent only.

Adapting Equation 2 for the normalized ratio of fluorescence intensities, a second order polynomial expression is used for calibrating and determining local oxygen partial pressures on Binary PSP surfaces as follows:

$$\frac{p_{O_2}}{p_{O_2,ref}} = C_1(T)\left(\frac{r_{ref}}{r}\right)^2 + C_2(T)\left(\frac{r_{ref}}{r}\right) + C_3(T) \qquad \ldots(\ 5\ )$$

Nitrogen is used as the coolant proxy, and ambient air is used as the main flow in this study. Since the coolant proxy is free of molecular oxygen, the local oxygen partial pressures that are determined by Binary PSP using Equation 5 can be used to directly infer AFE by adopting heat/mass transfer analogy. The successful adoption of heat/mass transfer analogy requires a turbulent flow field, which is defined as having a turbulent Lewis number close to unity [22]. Due to high Reynolds numbers that are typical to gas turbine combustors (256,000 in this study), the heat/mass transfer analogy is valid over the surface of gas turbine combustor liners [23]. By accepting the heat/mass transfer analogy, AFE (η_{ad}) can be further calculated using the oxygen partial pressures determined from the normalized ratio of Binary PSP fluorescence intensities using the following equation:

$$\eta_{ad} = \frac{T_g - T_{aw}}{T_g - T_c} \approx \frac{X_{O_2,g} - X_{O_2,aw}}{X_{O_2,g} - X_{O_2,c}} \qquad \ldots(\ 6\ )$$

where *T* represents temperature and X denotes mole fraction of molecular oxygen, respectively. In addition, the subscripts *g*, *aw*, and *c* denote main air flow, adiabatic wall, and coolant, respectively.

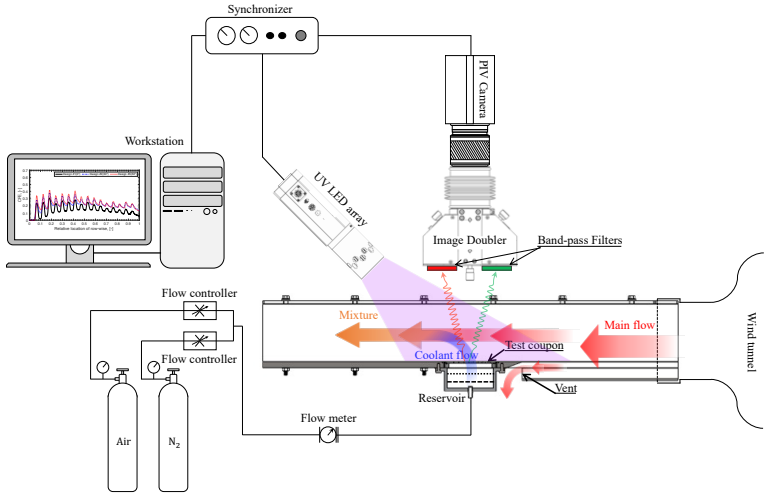

Figure 4. *Schematic of the experimental setup and a sectional view of the test section.*

3.0 Experimental setup

A lab-scale cooling test rig shown in Figure 4 was used to evaluate the effectiveness of the current effusion cooling designs for combustor liners. The present study used a low-speed wind tunnel to accelerate ambient air as the main flow to 33 m/s in order to simulate the flow speed in a typical gas turbine combustor. In the wind tunnel, the Reynolds number and the turbulence intensity are approximately 256,000 and 3%, respectively. The wind tunnel has been described in a previous publication [24]. The wind-tunnel was driven by a 30 kW AC motor that is capable of a maximum mass flow rate of 2.5 kg/s at a pressure rise of 5 kPa.

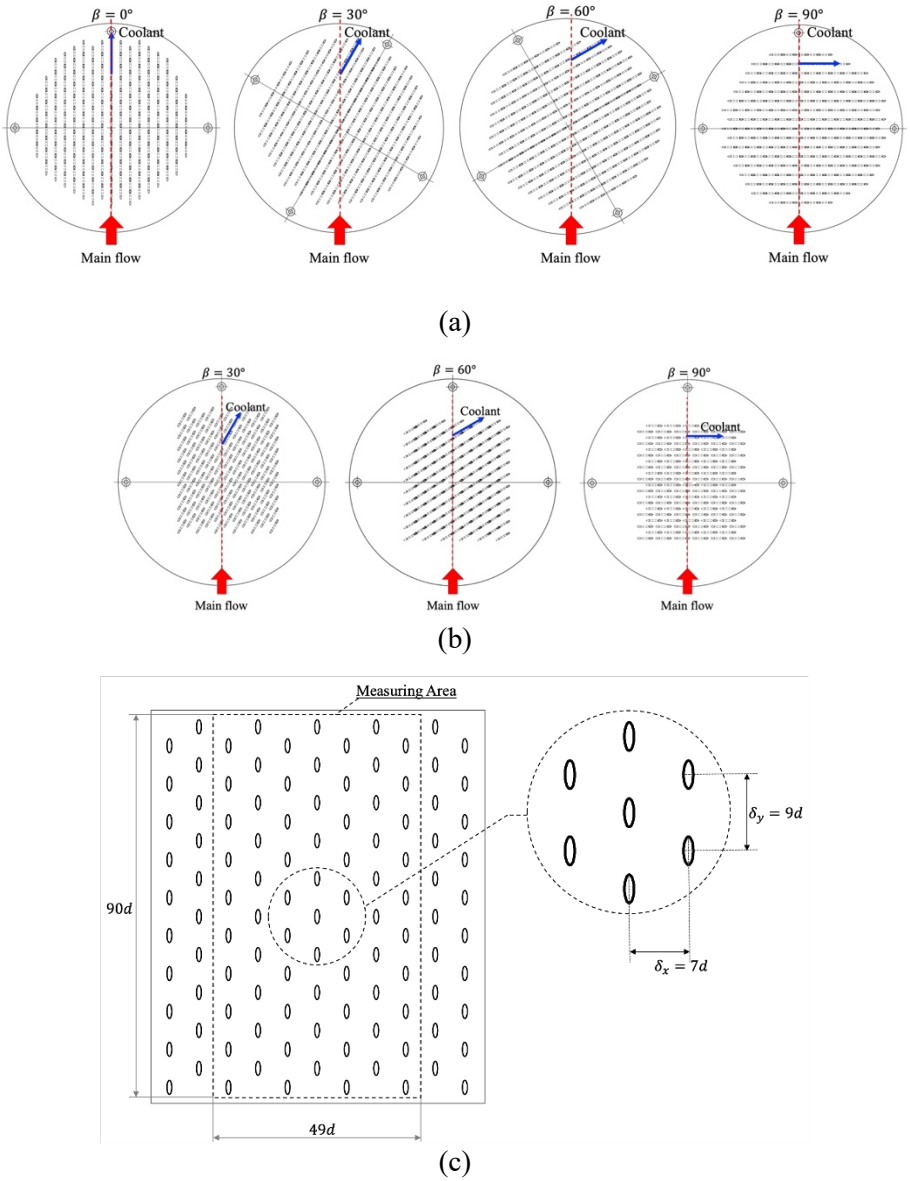

Figure 5. *Effusion cooling test configurations: (a) an identical test coupon rotated at four discrete angles relative to the main flow direction at 0°, 30°, 60°, and 90°; the co-linear installation (β = 0°, first from left) is the baseline case for all other configurations, and (b) three additional test*

coupons that have three discrete compound angles ($\beta = 30°, 60°, and\ 90°$) *while maintaining a fixed pitch as the baseline case* ($\delta_x = 7d$ *and* $\delta_y = 9d$) *as shown in panel (c).*

A transparent polycarbonate top panel covers the test section. After the wind tunnel transition piece that connects the round wind tunnel outlet to the square test section, a Pitot tube is located at the center of the test section and at a distance of 228 mm from the inlet of the test section. A reservoir that has been modified by a perforated plate is used for supplying coolant proxy uniformly to all effusion cooling holes in the test coupon. The reservoir has an inner diameter of 101 mm and an internal height of 44 mm. The center of the reservoir is located 406 mm from the inlet of the test section. Effusion cooling test coupons are installed at the bottom of the test section directly above the reservoir with the inner surface flush with the bottom of the test section.

In consistent with a previous study [11], a single round effusion cooling test coupon was designed and fabricated using stereolithography (SLA) 3D printing. The shrinkage of effusion cooling holes from 3D printing was evaluated and was compensated by post-machining to ensure effusion holes are of exact dimensions as in the previous study. The inclination angle (α) of the effusion holes is 20 degree and the diameter of effusion pinholes (d) is 0.787 mm, as illustrated in Figure 1. The test coupon has staggered effusion cooling holes, with spanwise and streamwise separations between adjacent effusion holes 7 and 9 times of the effusion hole diameter ($\delta_x = 7d$ and $\delta_y = 9d$), as illustrated in Figure 2.

In the previous study, a conventionally machined aluminum test coupon was installed in the test rig shown in Figure 4 for studying the directional effects of effusion cooling. The circular test coupon was rotated so that the main flow could be at an angle with the effusion cooling jets. The arrangement mimics the realistic effusion cooling scenario in a gas turbine combustor as the swirling main flow is common for flame stabilization. To verify that previous results can be reliably reproduced by an SLA 3D printed test coupon, four test configurations shown in Figure 5(a) were first evaluated. The four test configurations shared the same test coupon. By installing the test coupon at discrete rotations, four angles, 0°, 30°, 60°, and 90°, between the effusion cooling jets and the main flow were achieved. The co-linear effusion cooling configuration ($\beta = 0°$) was taken as the baseline case for comparisons throughout this study. It becomes obvious from the figure that a swirling main flow does not only induce a non-zero compound angle between effusion cooling jets and the main flow, it also alters the pitch of effusion cooling holes in effect. The change in effusion cooling AFE induced by a swirling main flow is a combined effect of varied compound angles and altered pitches.

As discussed in the Introduction Section, the goal of the current work is to understand the isolated effects of non-zero compound angles on effusion cooling AFE by excluding the influences of varying pitch. Also taking the co-linear effusion cooling design (first configuration from left in Figure 5(a)) as the baseline case, new effusion cooling test coupons were designed, featuring identical effusion cooling hole pitch while the compound angle is varied as the only parameter. Besides the single test coupon shown in Figure 5(a), three additional test coupons shown in Figure 5(b) were fabricated with SLA 3D printing. Altogether, the comparisons can be made among four effusion cooling configurations of identical pitch and of four compound angles at 0°, 30°, 60°, and 90°. It should be pointed out that for all test configurations shown in Figure 5, only the area near the centerline is chosen for comparisons. By excluding areas on both left and right edges of the

test coupon, we hope to minimize the uncertainties arise from cooling film developments in the horizontal direction.

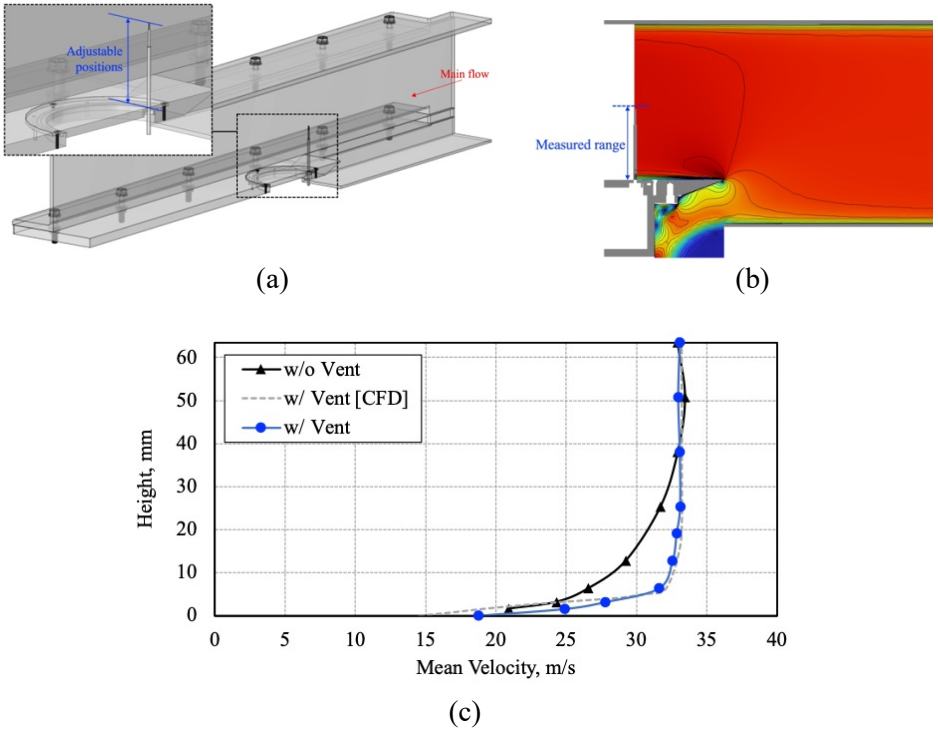

Figure 6. *(a) Cut-away view of the CAD model of the test section; the schematic details the vent for controlling boundary layer thickness on the test coupon and the installation of the hot-wire anemometer in the center of the test section. (b) Cross-sectional view of the velocity contour near the vent for controlling boundary layer thickness from a RANS simulation. (c) Comparison of boundary layer thickness with and without the vent; results from CFD simulations are also included for comparison.*

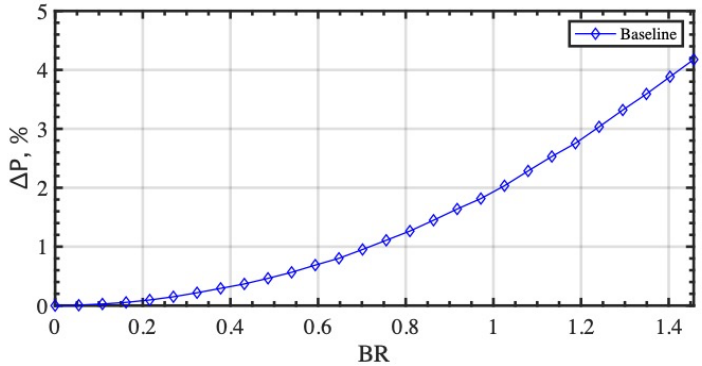

Figure 7. *The percentage pressure drop across effusion cooling test coupons were maintained as a fixed function of Blowing Ratio for all test configurations.*

A vent with adjustable height was designed and placed near the leading edge of the test coupons for boundary layer thickness control; the construction of the vent is shown in Figure 6(a). CFD calculations were performed for designing the vent so that only clean stream is permitted in the test

section, as shown in Figure 6(b). The boundary layer thickness on the test coupon was measured using a hot-wire anemometer located at the leading edge of the test coupon longitudinally and in the middle of the test section horizontally, as shown in Figure 6. In this case, the hot-wire anemometer can be adjusted to cover a height of 63.5 mm from the bottom of the test section. The momentum boundary layer thickness can be inferred from the measured velocity profile, as illustrated in Figure 6(c).

Percentage pressure drop ΔP across effusion cooling coupons is determined by taking static pressures in the coolant reservoir and in the test section, where the static pressure in the test section is taken from the Pitot tube. At blowing ratios of 0.6, 1, and 1.4, the percentage pressure drops are 0.8 %, 1.8 %, and 3.8% respectively. Blowing ratio (BR) is an important parameter for quantifying effusion cooling and is defined by Equation 7 below. Blowing ratio essentially is the momentum ratio between the coolant gas and the main flow.

$$BR = \frac{\rho_c U_c}{\rho_\infty U_\infty} \qquad \ldots (\quad 7 \quad)$$

where ρ_c, ρ_∞ are the densities of coolant and main flow; whereas U_c and U_∞ are the velocities of effusion cooling jets and main flow air, respectively [12]. Figure 7 shows percentage pressure drops measured as a function of BR. The wind tunnel circulates ambient air while the room temperature in the lab was maintained at 293 K.

To calibrate Binary PSP specifically for our experimental setup and each effusion cooling configuration, known mixtures of neat N_2 and compressed air were used as calibration gases. Both neat N_2 and compressed air streams were regulated and metered individually and subsequently mixed in a long line. Ten calibration points were taken with the volumetric fractions of compressed air at 0%, 10%, 20%, 30%, 40%, 50%, 60%, 70%, 80%, 90% and 100% with the balance gas being neat N_2. During the calibration process, the wind tunnel was turned off and the test section was isolated from the rest of the wind tunnel. The effusion cooling test coupon installed in the test section was surrounded by a calibration shroud shown in Figure 8(a) and was purged with calibration gases from the reservoir while maintaining the pressure in the test section at atmospheric pressure. The Binary PSP on test coupon surfaces was exposed to known oxygen partial pressures while pixel-wise calibrations were being performed to get correlations between PSP fluorescence intensities and oxygen partial pressures. Once a calibration was completed for each effusion cooling configuration, the calibration shroud was removed from the test section and the test section was reconnected back to the rest of the wind tunnel. Only N_2 was then supplied to the reservoir as the coolant proxy to visualize cooling films with the help of PSP on the surface of the effusion cooling test coupon.

In the present study, as discussed in the previous section, a Binary PSP from ISSI named as BinaryFIB PSP [19] was used, which has a UV excitation peak between 380 and 520 nm and two emission peaks: 1) the pressure signal that is sensitive to oxygen partial pressure near 650 nm and 2) the reference signal near 556 nm that's insensitive to oxygen partial pressure but of almost identical temperature responses as the pressure signal. A LED light source also from ISSI (LM2X-DM) was adopted to provide UV excitation for the Binary PSP near 400 nm. To acquire both PSP fluorescence signals (both pressure signal and reference signal), a LaVision ImagerProX 2M camera equipped with a LaVison Image Doubler was used. Two PSP fluorescence intensity images were filtered with bandpass filters: the first being a 650 nm center wavelength of 20 nm FWHM

(full-width at half-maximum) and the second a 560 nm center wavelength of 10 nm FWHM. The filtered PSP fluorescence images were then combined together side-by-side by the image doubler; the combined image was subsequently acquired by the LaVision camera.

4.0 Results

4.1 PSP calibration

Figure 8(b) shows the comparisons of the calibration curve of Binary PSP from this study with calibration data published in the literature [48,49]. Using the calibration curve, oxygen partial pressure as normalized by a standard air can be determined pixel-wise from a normalized ratio of luminescent intensities. There are small variations among calibration curves for each pixel on the active area of the effusion cooling test coupon; the curve shown in Figure 8(b) is the average calibration curve for all pixels of the active measurement area. The good comparisons with calibration curves published in the literature indicate the validity of the calibration procedures of the current study.

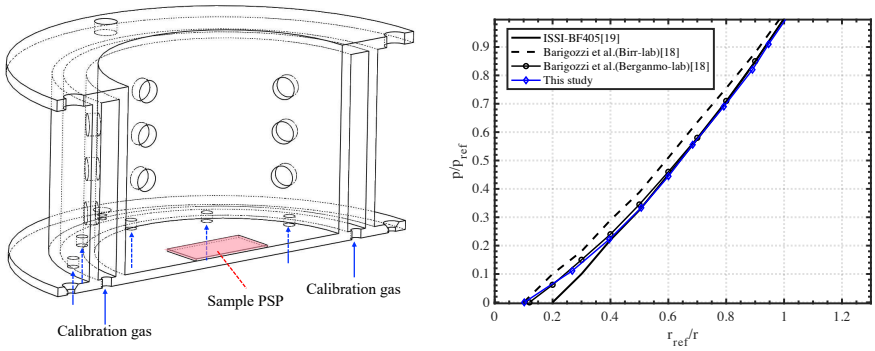

(a) (b)

Figure 8. *(a) Schematic of the calibration shroud being placed in the test section for isolating the effusion test coupon from the rest of the wind tunnel in the current study and (b) comparisons of calibration curves. The x-axis is the inverse of normalized ratios of fluorescence intensities as defined by Equation 4 while the y-axis is the oxygen partial pressure normalized by standard air.*

4.1 Combined effects of compound angle and varying pitch

Figure 9 presents 2D AFE (η_{ad}) maps simulating the baseline effusion cooling design being subject to various swirling main flow conditions, rendering four discrete compound angles between effusion cooling jets and mainstream, at 0°, 30°, 60°, and 90°, with the effusion cooling configuration illustrated in Figure 5. Each effusion cooling configuration was tested at three typical Blowing Ratios (BR), at 0.6, 1.0 and 1.4 respectively. In these 2D AFE maps, as illustrated by the color bar of the figure, red color indicates poor quality of cooling film while blue suggests well-formed cooling film.

The directional effects present in Figure 9 are the results of changing compound angle and effusion cooling hole pitch simultaneously. Although physically the separations between cooling hole rows and columns are maintained, however, in the direction of main flow, the pitch is altered substantially. For example, the design pitch, as is in the co-linear case, is stagged cooling hole with

spanwise and streamwise separations between adjacent effusion holes 7 and 9 times of the effusion hole diameter respectively (δ_x = 7d and δ_y = 9d). However, when the effusion cooling coupon is rotated 90 degrees, the effective pitch, although still stagged, becomes δ_y = 7d and δ_x = 9d, as can be seen from the right-most panel of Figure 5(a). In other cases, for example, in the cases of compound angles being 30° and 60°, the effective pitches cannot be simply defined as the effusion cooling holes after rotation are not perfect aligned with the main flow direction. To the knowledge of the authors, the alteration to effective cooling hole pitch due to swirling main flow has not been studied before.

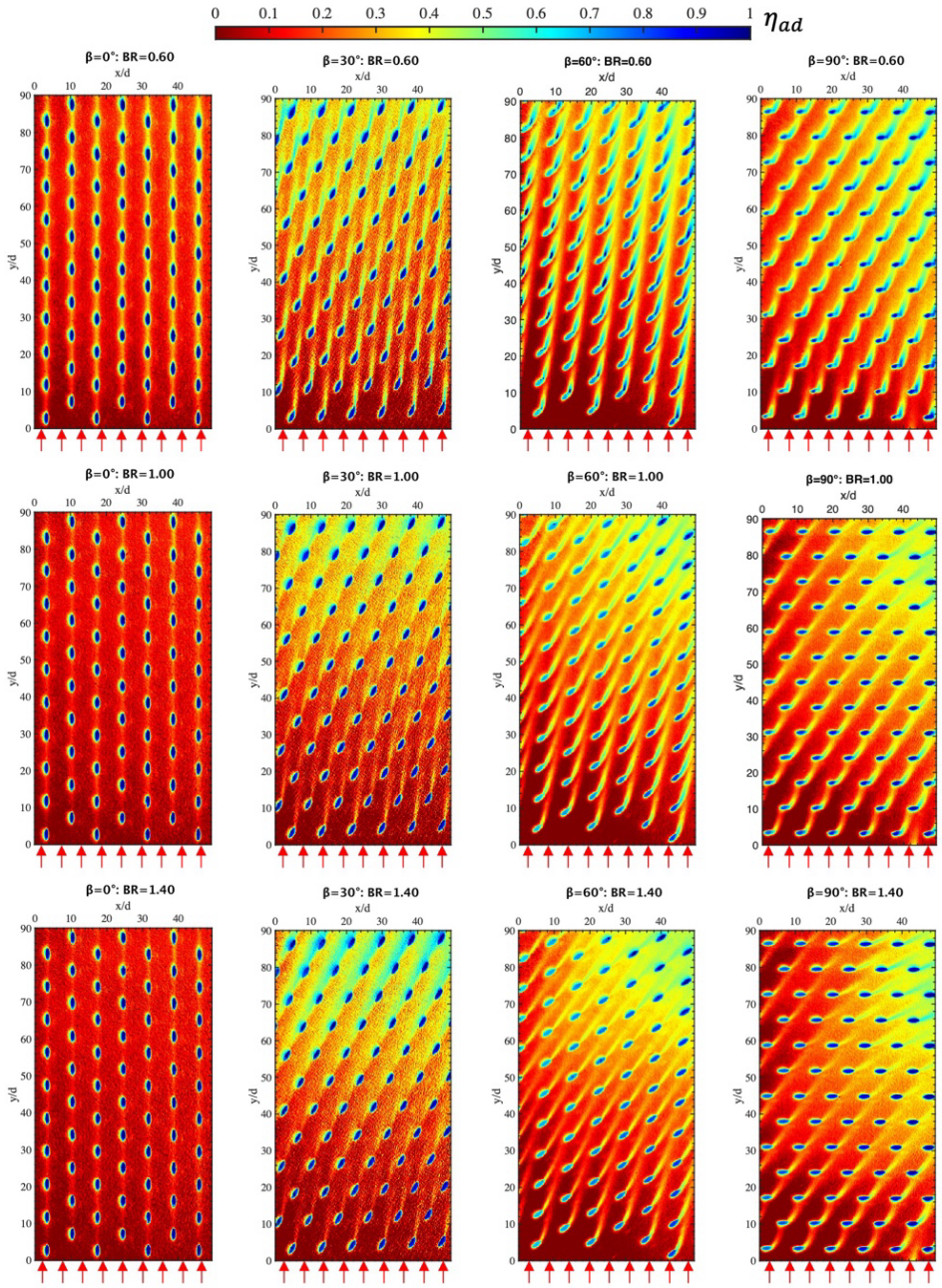

***Figure 9**. Comparisons of 2D AFE distributions as the baseline effusion cooling test coupon is installed at four discrete rotation angles relative to the main flow direction (0°, 30°, 60°, and 90°).*

The comparisons illustrate combined effects of varying compound angle and pitch on AFE that are realistic to engine combustors that are subject to swirling main flows. Red arrows indicate the main flow direction.

Comparing to the co-linear case as the design point of effusion cooling, the combined effects of changing compound angle and pitch enhance film cooling effectiveness at all three BRs studied in this work. In the co-linear case, effusion cooling jets do not penetrate to the gaps between cooling hole columns, leaving large gaps between adject cooling hole columns largely un-protected. The only mechanism for effusion cooling gas to spread out to cover inter-column gaps is mixing, which is a less efficient and less ideal way to produce cooling film as coolant being diluted and dissipated away by the main flow. The ideal method for generating cooling film is for cooling jets to penetrate spanwise while minimizing the mixing between main flow and miniature effusion cooling jets. It is evident that non-zero compound angles make it easier for cooling jet to penetrate into gaps between adjacent cooling hole columns, making effusion cooling more efficient.

Comparing to the co-linear case as the design point of effusion cooling, the combined effects of changing compound angle and pitch enhance film cooling effectiveness at all three BRs studied in this work.

More quantitative analyses of 2D AFE distributions are made by comparing row-wise and column-wise mean AFE. The left panels of Figure 10 are comparisons of row-wise AFE averages at all three Blowing Ratios while the right panels are column-wise means. It is evident that a swirling main flow enhances AFE with its enhancement peaks between 30° and 60° for all BRs studied. This is good news for practical engines that set effusion cooling holes in the direction of the combustor axis. For a typical swirling number of 0.7 and a typical combustor height, the swirling main flow induces an effective compound angle of 45° [16], falling right between the ideal compound angles found in Figure 10 for all BRs. The overall mean AFE values for the entire measurement area shown in Figure 9 that are summarized in Table 3 clearly confirm the above observation from Figure 10. The overall mean AFE values summarized in Table 1 reveal that substantial enhancements to overall cooling film effectiveness between 27% to 135% compared to the co-linear case ($\beta = 0°$) can be achieved by introducing main flow at 30°, 60°, and 90° to effusion cooling jets. The enhancement is more pronounced at high BRs.

Table 1*. The mean and standard deviation of the adiabatic film cooling effectiveness (η_{ad}) of the 2D AFE maps shown in Fig. 9*

Compound angle (β)	$\eta_{ad,\,mean}$			σ		
	BR=0.6	**BR=1**	**BR=1.4**	**BR=0.6**	**BR=1**	**BR=1.4**
0° (baseline)	0.2047	0.1608	0.1430	0.0801	0.0591	0.0540
30°	0.3422	0.3189	0.3373	0.1626	0.1632	0.1831
60°	0.3257	0.3027	0.2898	0.1902	0.1483	0.1439
90°	0.2619	0.2390	0.2273	0.1240	0.1130	0.1136

It is worth a quick discussion of the role that BR plays in affecting AFE at various compound angles. Effusion cooling jets lift-off and reattach back to the surface to form a cooling film, while mixing

with the main flow during this process. When effusion cooling jets are co-linear with the main flow, more pronounced lift-off of cooling jets at higher BRs does not allow the coolant to effectively reattach back to and cool the plate until further downstream [25]. At the same time, enhanced jet mixing between effusion cooling jets and main flow further diminishes the AFE as BR increases. The trend that a higher BR results in less-ideal AFE when $\beta = 0°$ is evident in Figure 10.

However, the role that BR plays at a non-zero compound angle can be more complicated as effusion jets can have a different penetration depth into the gap between effusion cooling hole columns besides the varied lift-off height as BR changes. For instance, the $\beta = 30°$ case shown in Figure 10 reveals this complication. As BR increases from 0.6 to 1.0, as the row-wise AFE mean comparison (the blue curves in top-left panel vs. mid-left panel) indicates, the AFE enhances. This could be explained by the increased penetration depth of effusion jets into the gaps between effusion cooling column, as can be seen from the corresponding AFE 2D maps in Figure 9. As BR further increases to 1.4 from 1.0 (the blue curves in mid-left panel vs. lower-left panel), the AFE recedes. This reduction in AFE while more coolant is being used at an increased BR can be attributed to the fact that the benefits of increased penetration at a higher BR is outweighed by the drawbacks of enhanced jet mixing between effusion cooling jets and main flow at a higher BR, which dilutes coolant substantially. The increased penetration depth of effusion jets is evident by observing the effusion jets leaving the first two rows of cooling holes of three $\beta = 0°$ panels in Figure 9 as BR increases from 0.6 to 1.4.

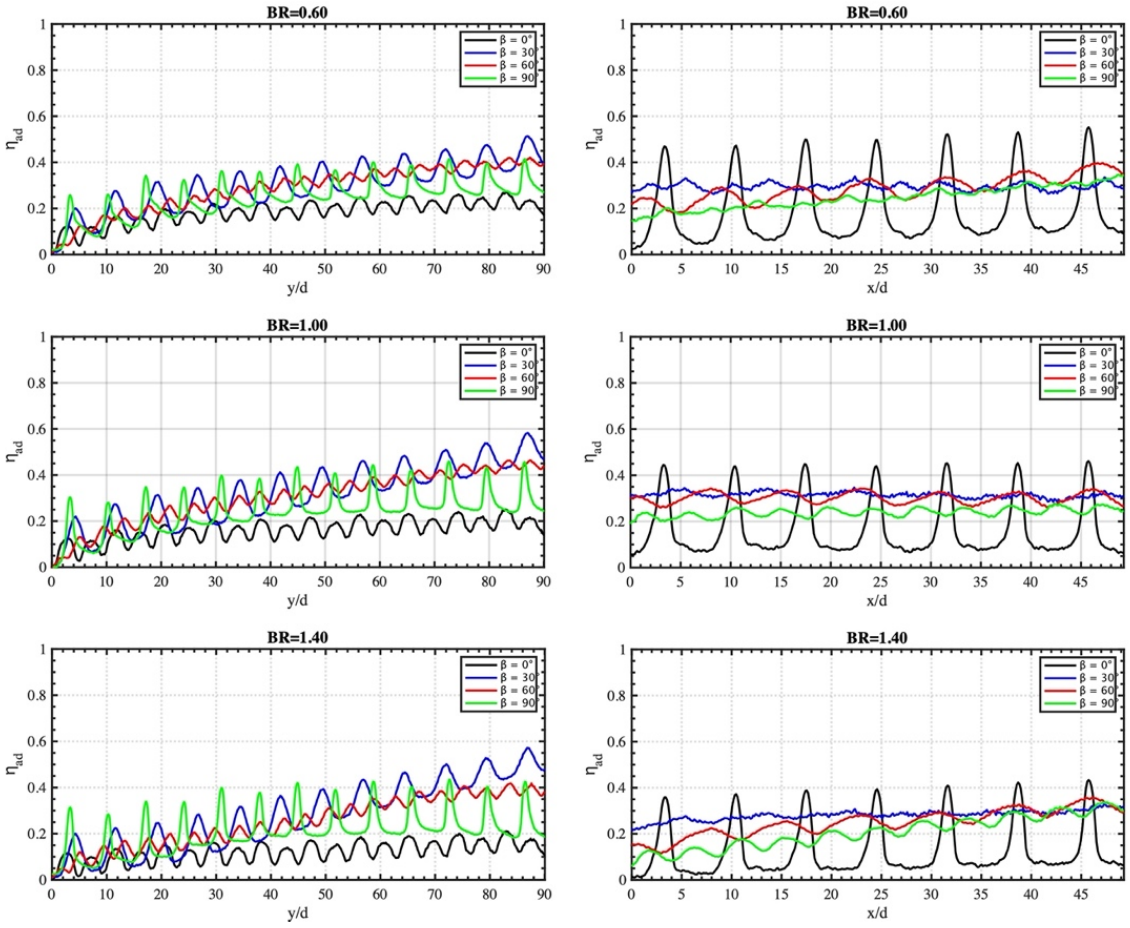

Figure 10. *Comparisons of spanwise averaged AFE (left) and streamwise averaged AFE (right) of the 2D AFE maps shown in Figure 9.*

It should be pointed out that the AFE enhancement observed in Figures 9 and 10 is the combined effects of simultaneously varied compound angle and pitch. As discussed earlier, although the combined effects are of practical importance to engine combustors subjected to swirling main flow, the contributions from each factor need to be isolated and evaluated separately to better guide future effusion cooling designs since effusion cooling performance can be sensitive to cooling hole pitch [7,26].

Revisiting Figure 9, it may be suggested that the most efficient effusion jet penetration depth can vary depending on the effective pitch of effusion cooling holes. For example, examining the right-most panels in Figure 9 with $\beta = 90°$, the effusion jets can penetrate deeper towards the adjacent effusion cooling hole column comparing to smaller compound angles, however, the span-wise separation between effusion cooling hole columns is reduced with the effusion cooling test coupon installed at a 90° rotation relative to the main flow. Cooling film development cannot take full advantage of the increased jet penetration depth due to the reduced separation between effusion cooling hole columns, as effusion jets clearly overshot for all BRs when $\beta = 90°$ in Figure 9. It should be pointed out that the jet penetration increases at larger compound angles at the price of enhanced jet mixing between effusion jets and the main flow. When the jet penetration depth benefits are not fully utilized, overall AFE suffers from the enhanced jet mixing. Therefore, the optimization of effusion cooling should be done by concurrently considering compound angle and the corresponding effective pitch.

4.3 Sole effects of non-zero compound angles on AFE at a fixed pitch

From the discussions in Section 4.2, it is clear that the individual contributions to the combined effects of swirling main flow on AFE from a non-zero compound angle and a varied pitch need to be evaluated separately. As discussed in Section 3, effusion cooling configurations presented in Figure 5(b) were additionally designed and fabricated for studying the sole effects of non-zero compound angles by fixing the effusion cooling hole pitch.

Figure 11 presents 2D AFE distributions for effusion cooling configurations shown in Figure 5(b) at three BRs, 0.6, 1.0 and 1.4. Specifically, these effusion cooling configurations have the compound angles of 30°, 60°, and 90° and a fixed staggered effusion cooling hole pitch ($\delta_x = 7d$ and $\delta_y = 9d$). An identical color legend is used here as that in Figure 9, therefore direct comparisons can be made between corresponding test conditions. To avoid repetency, the 2D AFE maps of the baseline case (β = 0°) shown as the left-most panels of Figure 9 are not reproduced here. However, the comparison can be made by referring to Figure 9. A quick comparison with all the cases in Figure 9, it becomes apparent that without the effects of varying pitch, non-zero compound angle alone can greatly improve AFE comparing to the co-linear case.

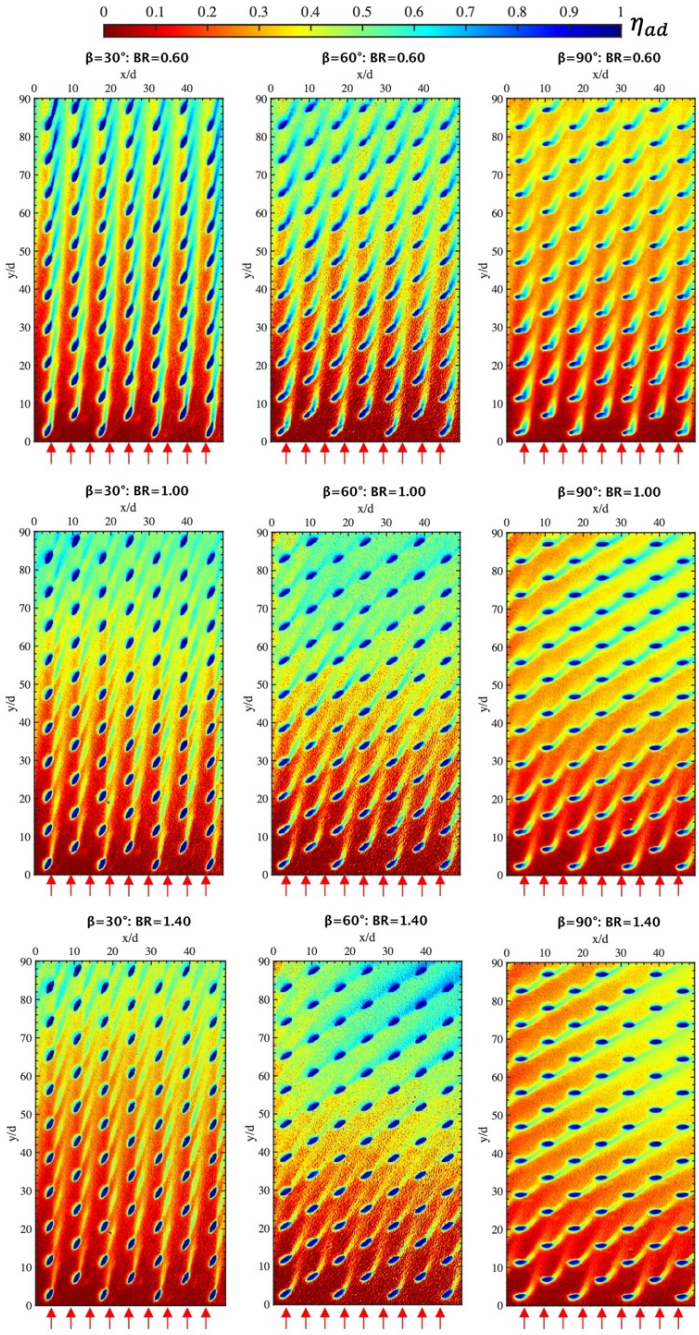

Figure 11. *Comparisons of 2D AFE distributions as a results of varying compound angles (β = 30°, 60°, and 90°), corresponding to the effusion cooling configurations presented in Figure 5(b). As indicated in Figure 5(b), a fixed staggered effusion cooling hole pitch ($\delta_x = 7d$ and $\delta_y = 9d$) was adopted. Red arrows indicate the main flow direction.*

The effects of compound angle alone can be discerned without the complication of varying pitch. At a lower BR of 0.6, the spanwise effusion jet penetration deepens as the compound angle increases from 30° to 90°. At a 30° compound angle, the effusion jets have a span-wise penetration of roughly half of the spanwise pitch. The penetration rises to 3/4 of the spanwise pitch when the

compound angle is increased to 60°. This increase of jet penetration depth is approximately proportional to the ratio of spanwise effusion jet velocity component between two compound angles of 30° and 60° for a given BR. A detailed examination of the top panels of Figure 9 reveals that the effusion jets are more diluted at a 60° compound angle comparing to the 30° configuration due to jet mixing, despite a more significant jet penetration depth. Therefore, the sole effect of compound angle is a trade-off between jet mixing and jet penetration. Row-wise and column-wise means of AFE for the 2D AFE maps of Figure 11 are computed, similar to those shown in Figure 10, and are summarized in Figure 12. Observing the top right panel of Figure 12, which compares the column-wise means of AFE of the low BR case, it is confirmed that the 60° compound angle configuration has deeper penetration than the 30° case, as indicated by the higher trough values of the red curve as well as broader peak features; at the same time, the worsen coolant dilution due to jet mixing at the 60° compound angle configuration is evident by the lower peak value of the red curve comparing to the blue curve.

The row-wise AFE average comparisons with the BR at 0.6 show that the overall performance of two compound angles, 30° and 60°, are nearly identical over the entire streamwise span (red and blue curves in the top-left panel of Figure 12). This indicates that the two competing effects of a non-zero compound angle, jet mixing and jet penetration, are balanced.

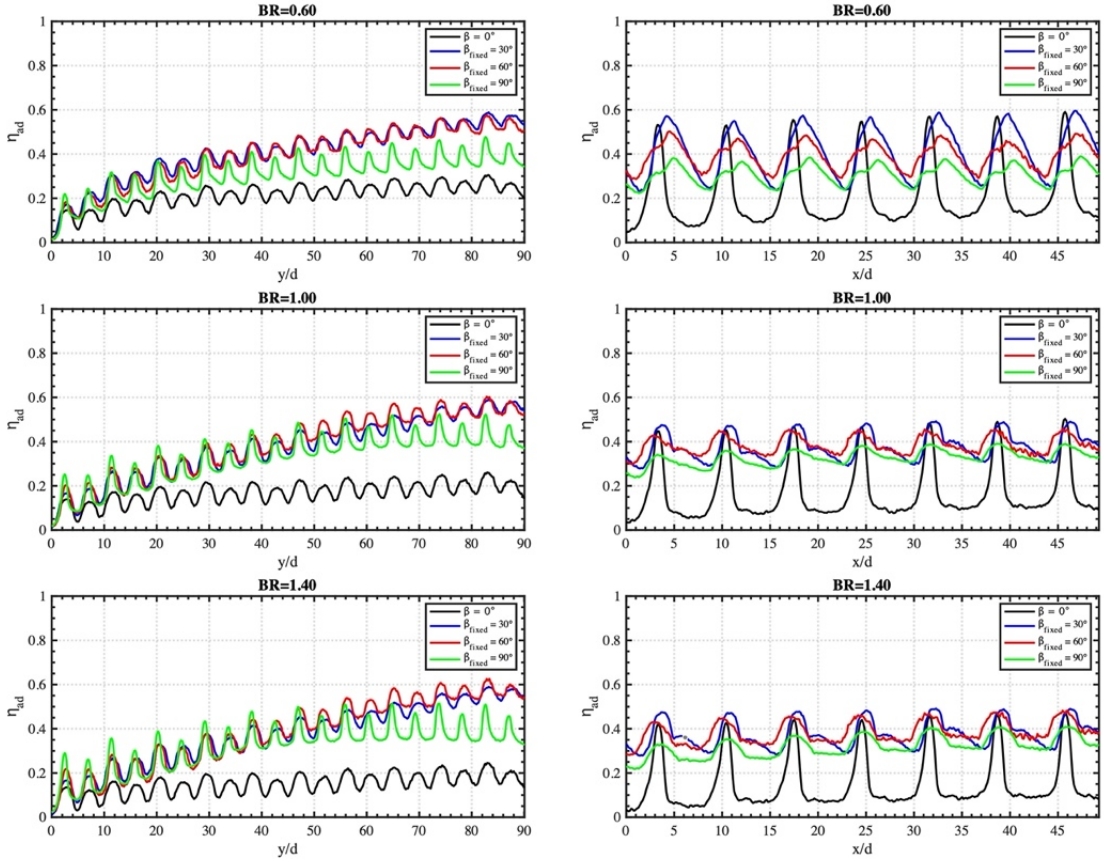

***Figure 12**. Comparisons of spanwise averaged AFE (left) and streamwise averaged AFE (right) of the 2D AFE maps shown in Figure 11 together with the baseline case shown in the left panels of Figure 9.*

As the compound angle is further increased to 90° at BR = 0.6, the effusion jets quickly disappear due to intense jet mixing, as seen from the top-right panel of Figure 11. Since the effusion jets are shortened due to jet mixing, a more considerable jet penetration depth as a potential benefit of a larger compound angle cannot be realized. The top two panels of Figure 12 provide quantitative confirmation of the above observations. The column-wise average shown in the right panel shows that a 90° compound angle does not substantially increase jet penetration depth compared to a smaller 60° compound angle case, by comparing the widths of the peaks of the green and red curves. However, the 90° compound angle case suffers from strong jet mixing as indicated by overall lower AFE. The reduction in effusion cooling effectiveness of the 90° compound angle configuration is clearly shown in the row-wise AFE mean plots (the top left panel of Figure 12). The comparisons of these non-zero compound angle cases clearly reveal the role that compound angle plays in effusion cooling. An ideal compound angle reaches an optimal compromise of jet penetration and jet mixing.

By examining Figure 12 in detail, it is interesting to find that BR has a negligible effect on AFE when a non-zero compound angle is used with a fixed effusion cooling hole pitch. This surprising observation may be attributed to the fact that the pitch being fixed. When the compound angle and pitch are concurrently varied as the case investigated in Section 4.2, larger penetration depths resulting from larger BRs are not fully capitalized due to reduced spanwise pitch when the effusion cooling coupon is rotated. In other words, with reduced spanwise pitch, larger BRs are detrimental to AFE as the effusion jets are penalized for stronger jet mixing but do not benefit from larger jet penetration. With a fixed span-wise pitch, the benefits of larger BRs can be better realized. The invariance of AFE at various BRs when a fixed pitch is used implies two conditions: 1) the span-wise pitch is large enough to take full advantages of larger jet penetration depths at higher BRs, and 2) the disadvantages of stronger jet mixing at larger BRs can be approximately offset by the benefits of larger jet penetrations. It appears that for BRs reasonably close to unity, both conditions can be met. The balance between jet mixing and jet penetration can be seen from the three right panels of Figure 12. As the BR progressively increases from 0.6 to 1.4, all non-zero compound cases see the diminishing of AFE peak amplitudes and the broadening of the peaks.

So far, we improved the understanding of the role that a non-zero compound angle plays in the directional effects of effusion cooling. It is also discussed qualitatively in Sections 4.2 and 4.3 the role that a varied pitch might play in the directional effects of effusion cooling under swirling main flow conditions. Comparisons of AFE values between effusion cooling configurations with fixed and varied pitches at comparable compound angles may reveal pitch effects on AFE quantitatively. Figure 13 compares spanwise and streamwise AFE averages for each compound angle at a representative BR of 1, the comparisons for other BRs are not reported in this paper for simplicity as the same tendency is noted for BR 0.6 and 1.4.

Figure 13 unequivocally reveals that pitch variations induced by a swirling main flow are not beneficial to cooling film effectiveness (AFE). At compound angle of 30°, the fixed pitch has an overall AFE 20% higher than that in the varying pitch scenario by referring to the overall mean AFE values listed in Tables 1 and 2. In the case of 60°compound angle, the enhancement of AFE almost reaches 30%. This revelation is not surprising based on the previous discussions, as all the benefits of a non-zero compound angle can be fully realized as long as the effusion jets do not overreach to the next column of effusion cooling holes. A consideration in determining optimal effusion cooling hole pitch under swirling main flow conditions may have to include the fact that

some of cooling jets may become overlapping under certain pitches, the BR = 1 and β = 90° case in Figure 11. Overlapping effusion cooling jets is apparently less-ideal for producing a uniform cooling film, which could the subject of a future study specifically on pitch optimization under swirling main flow conditions.

Table 2. *The mean and standard deviation of the adiabatic film cooling effectiveness (η_{ad}) of the 2D AFE maps shown in Figure 11.*

Compound angle (β)	$\eta_{ad,\,mean}$			σ		
	BR=0.6	BR=1	BR=1.4	BR=0.6	BR=1	BR=1.4
0° (baseline)	0.2047	0.1608	0.1430	0.0801	0.0591	0.0540
30°	0.4133	0.3852	0.3810	0.2012	0.1781	0.1750
60°	0.4016	0.3953	0.3951	0.1945	0.1871	0.1939
90°	0.2974	0.3132	0.3024	0.1305	0.1315	0.1242

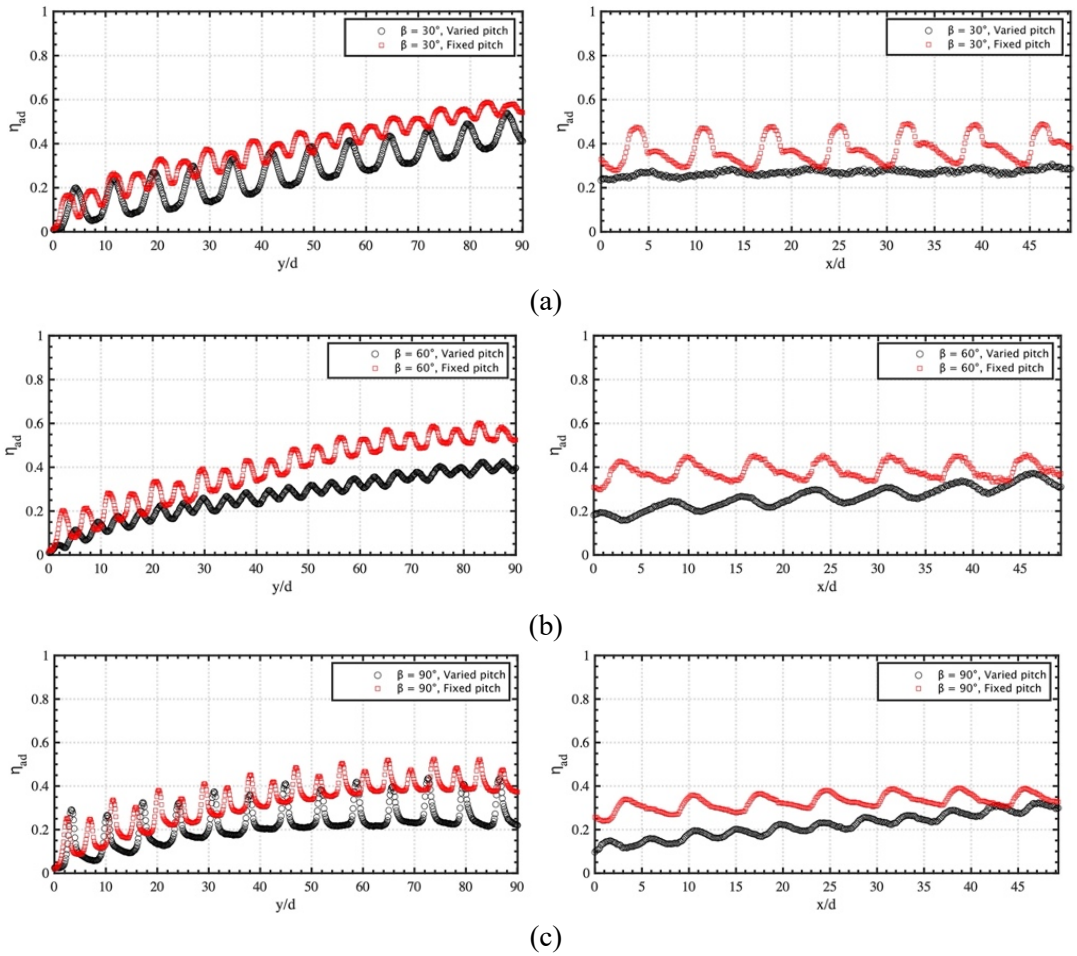

Figure 13. *The comparisons of spanwise (left) and streamwise (right) averaged AFEs between varied pitch and fixed pitch effusion cooling configurations as shown in Figure 5 at three non-zero*

compound angles, (a) 30°, (b) 60° and (c) 90°. A representative BR of 1 is used for these comparisons.

To guide the optimization of compound angle when the fixed pitch shown in Figure 5(b) is used, Figure 14 is compiled based on the 2D AFE maps presented in Figure 11. For each BR and compound angle combination, a 2D AFE map in Figure 11 is equally divided along the flow direction into 10 sub-regions and a mean AFE value is computed for each sub-region. By plotting the mean AFEs for each sub-region along the main flow direction as histograms, the optimal compound angles for the prescribed fixed pitch can be determined. Three observations can be made for the fixed pitch configuration investigated in this study from Figure 14: 1) two compound angles, 30° and 60°, appear to be optimal for enhancing AFE, 2) regardless of BR, the optimal compound angle remains the same, and 3) regardless the cooling film development stage along the main flow direction, the optimal compound angle remains the same. These observations indicate that for the fixed pitch studied here, the choice of optimal compound angle is simple and universal: a compound angle between 30° and 60°.

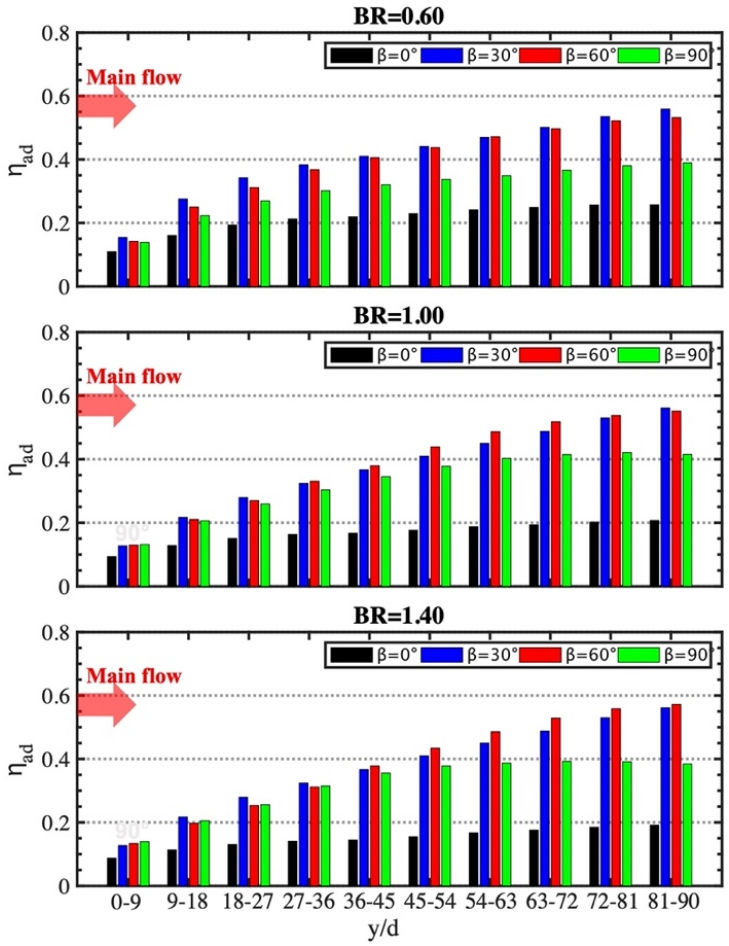

Figure 14. *Mean AFE for 10 equal blocks along the mean flow direction for each 2D AFE map shown in Figure 11.*

4.4 Other discussions

It should be pointed out that the experiments of this study were conducted with the coolant to mainstream density ratio near unity (DR ≈ 1) while for engine conditions the typical value is DR ≈ 2. Higher AFE values can be achieved under engine conditions with higher density ratios, because higher density ratios lead to lower coolant velocity at fixed BRs. Consequently, the results presented in this study is a conservative representation of AFE performance under engine conditions. However, the difference in AFE due to variations in DR is expected to be small, with the difference in AFE less than 20% for coolant DR ≈ 2 compared to DR ≈ 1.2 in the vicinity to the effusion hole but was essentially zero farther downstream [27-29].

In addition, the turbulence level of the experiments performed in this study is estimated to be 3%. The turbulence level of a gas turbine combustor was previously measured to be 6% and 9% at non-reacting and combustion conditions, respectively, along the combustor centreline [30]. The impact of turbulence intensity on cooling film effectiveness has been well-established [31, 32]: at the optimal momentum flux ratio, a high turbulence level of $Tu = 17\%$ caused a factor of two decrease in film effectiveness near the effusion hole comparing to a low turbulence level flow ($Tu = 0.3\%$), and almost a complete loss of cooling for $x/d > 25$ [32].However, it should be pointed out that the combustor investigated by the previous study have strong impinging jets in crossflow in the forms of dilution air jets. It has been established that a primary source of turbulence in a gas turbine combustor is impinging jets in crossflow [33]. Other than rich-burn/quick–mix/lean-burn (RQL) combustor, modern gas turbine combustors have largely moved away from large impinging dilution air jets, therefore, a reduced turbulence level in combustors could be expected. In addition, the earlier study also found that the difference in cooling film effectiveness between two main flows of higher turbulence levels ($Tu = 10\%$ vs. $Tu = 17\%$) is insignificant. Therefore, we believe the findings of this study is valid for realistic engine conditions. Nevertheless, a future study is warranted to confirm that the proposed optimal compound angle is also valid for modestly high turbulence levels (6-9%).

5.0 Conclusions

Typically, gas turbine combustors featuring effusion cooling have the effusion cooling holes aligned with the axis of the combustor. However, the main flow in gas turbine combustors swirls for flame stabilization, which induced a non-zero compound angle between main flow and effusion cooling jets. The swirling main flow also alters the effective pitch of effusion cooling holes. The directional effects of effusion cooling induced by a swirling main flow are the results of a non-zero compound angle and a varied pitch simultaneously acting on effusion jets. Surprisingly, these important directional effects induced by a swirling main flow received little attention in the literature.

Two sets of experiments were designed. The first set of experiment mimics the scenario that a piece of effusion cooled engine combustor liner subjects to various swirling levels of main flow, rendering four discrete compound angles: 0°, 30°, 60° and 90°. The pitch of effusion cooling holes is defined when the compound angle β is 0° (co-linear baseline case) as $\delta_x = 7d$ and $\delta_y = 9d$, staggered. The same effusion cooling test coupon was rotated to achieve three non-zero compound angles: 30°, 60°, and 90°. Due to the rotation of test coupon, the effective pitch of the effusion

cooling plate is concurrently varied with compound angle. It is confirmed that non-zero compound angles make it easier for cooling jet to penetrate into gaps between adjacent cooling hole columns, making effusion cooling more efficient. Substantial enhancements to overall cooling film effectiveness between 27% to 135% was observed compared to the co-linear baseline case ($\beta = 0°$) by introducing the main flow at 30°, 60°, and 90° to effusion cooling jets; the AFE enhancement peaks between 30° and 60° for all BRs studied. In addition, the AFE enhancement due to swirling main flow is more pronounced at high BRs.

Although the first set of experiments is more relevant to engine realties, the combined effects of non-zero compound angle and varied pitch on AFE makes it difficult to determine the contributions from each factor separately. The second set of experiments were performed with a fixed pitch ($\delta_x = 7d$ and $\delta_y = 9d$, staggered) that doesn't vary with compound angle. Three additional effusion cooling coupons were fabricated to achieve three non-zero compound angles: 30°, 60°, and 90°. Without the complication of varying pitch, the effects of compound angle alone can be clearly discerned: a non-zero compound angle leads to a trade-off between jet mixing and jet penetration. Larger jet penetration depths usually can result from larger compound angles, promoting the spreading of coolant into the gaps between adjacent effusion cooling hole columns and enhancing AFE. However, the competing effect of adopting larger compound angles is that stronger jet mixing can occur, resulting in excessive losses of coolant to the main flow, diminishing AFE.

When the effects of varying pitch are excluded, a good balance of jet penetration and jet mixing can be achieved for two moderate compound angles, 30° and 60°, regardless of BR or the cooling film development stage. Therefore, the choice of optimal compound angle is simple and universal: a compound angle between 30° and 60°. The invariant of AFE at various BRs when a fixed pitch is used implies two conditions: 1) the span-wise pitch is large enough to take full advantages of larger jet penetration depths at higher BRs, and 2) the disadvantages of stronger jet mixing at larger BRs can be approximately offset by the benefits of larger jet penetrations. We propose a 45° compound angle as the starting point for future effusion cooling design optimizations.

It is hypothesized that a varying pitch affects AFE by potentially limiting the benefits of larger jet penetration depths resulting from larger compound angles. When the effusion cooling coupon is rotated and the spanwise pitch is reduced, the effusion jets resulting from larger compound angles not only fully penetrates the gap between adjacent effusion cooling hole columns, but also overshoot. When effusion jets overshoot the reduced spanwise pitch, the effusion jets are penalized for coolant losses due to stronger jet mixing but do not benefit from larger jet penetration. The similar reduction in AFE at higher BRs can be observed when the spanwise pitch is reduced, because at larger BRs the effusion jets are again penalized for stronger jet mixing but do not benefit from larger jet penetration. With a fixed span-wise pitch that can take full advantage of increased jet penetration depth, the benefits of a larger BR or a larger compound angle up to 60° can be better realized.

With the optimal compound angle proposedly set at 45°, the next step is to search for an optimal pitch. As discussed earlier, one factor may have to be considered in determining optimal effusion cooling hole pitch is that some of effusion jets may overlap at certain BR. Overlapping effusion cooling jets is apparently less-ideal and inefficient for producing a uniform cooling film. This factor may be investigated in the future when pitch optimization is studied.

Finally, in future effusion cooling design optimizations, the swirling effect of the main flow has to be taken into account. The optimal compound angle of 45° that we proposed here should be achieved considering the combustor swirl number. In addition, it is the effective pitch, resulting from the nominal pitch and swirling main flow, that should be optimized, instead of the nominal one.

Acknowledgements. The work is supported by the National Research Council of Canada (NRC)'s National Program Office under the Ideation New Beginnings Program (No. 577) and Postdoctoral Fellowship Program (PDF2021-06). Additional funding for the work is provided by the NRC's Aerospace Research Center under the LEAP Program (LEAP-012). The authors would like to thank NRC Technical Officers Mart Jonathan Regalado & Yin Yang for their technical support.

References

[1] S AHMED, P SINGH, AND S V EKKAD, "Comparison of Different Combustion Liner Cooling Techniques under Non-Reacting Conditions for a Lean Pre-Mixed Fuel Nozzle," *AIAA Scitech 2019 Forum*, pp. 1-13, 2019.

[2] D G RITCHIE, A J CLICK, P M LIGRANI, F LIBERATORE, R PATEL, AND Y H HO, "Double Wall Cooling of an Effusion Plate with Cross Flow and Impingement Jet Combination Internal Cooling: Comparisons of Main Flow Contraction Ratio Effects," *AIAA Propulsion and Energy 2019 Forum*, pp. 1-18, 2019.

[3] P W SCHILKE, "Advanced Gas Turbine Materials and Coatings," Report GER-3569G, GE Energy, Schenectady, NY, 2004.

[4] B GOSWAMI, S K SAHAY, AND A K RAY, "Application of Thermal Barrier Coatings on Combustion Chamber Liners – A Review," *High Temperature Materials and Processes*, vol. 23, no. 3, pp. 211-236, 2004.

[5] P GROOTENHUIS, "The Mechanism and Application of Effusion Cooling*," *The Journal of the Royal Aeronautical Society*, vol. 63, no. 578, pp. 73–89, 1959.

[6] K M B GUSTAFSSON, "Experimental Studies of Effusion Cooling," Ph. D. Dissertation, Department of Thermo and Fluid Dynamics, Charlmers University of Technology, Göteborg, Sweden, 2001.

[7] H H CHO, D H RHEE, AND R J GOLDSTEIN, "Effects of Hole Arrangements on Local Heat/Mass Transfer for Impingement/Effusion Cooling with Small Hole Spacing," *Journal of Turbomachinery*, vol. 130, no. 4, 2008.

[8] R KREWINKLE, "A Review of Gas Turbine Effusion Cooling Studies," *International Journal of Heat and Mass Transfer,* vol. 66, pp. 706–722, 2013.

[9] G CERRI, A GIOVANNELLI, L BATTISTI, AND R FEDRIZZI, "Advances in Effusive Cooling Techniques of Gas Turbines," *Applied Thermal Engineering*, vol. 27, no. 4, pp. 692–698, 2007.

[10] D G BOGARD, "Gas Turbine Film Cooling," *Journal of Propulsion and Power,* vol. 22, no. 2, pp. 249–270, 2006.

[11] L C PAITICH, P RICHER, B JODOIN, Y PYO, S YUN, AND Z HONG, "Directional Effects of Effusion Cooling on the Cooling Film Effectiveness," *AIAA Journal*, pp.1-12, 2021.

[12] D G BOGARD, "4.2.2.1 - Airfoil Film Cooling," *Gas Turbine Handbook*, National Energy Techonolgy Laboratory, 2004, pp. 309–321.

[13] T LIU, B T CAMPBELL, S P BURNS, AND J P SULLIVAN, "Temperature- and Pressure-Sensitive Luminescent Paints in Aerodynamics," *Applied Mechanics Reviews,* vol. 50, no. 4, pp. 227–246, 1997.

[14] J W GREGORY, K ASAI, M KAMEDA, T LIU, AND J P SULLIVAN, "A review of pressure-sensitive paint for high-speed and unsteady aerodynamics," *Proceeding of the Institution of Mechanical Engineers, Part G: Journal of Aerospace Engineering,* vol. 222, no. 2, pp. 249-290, 2008.

[15] A ANDREINI, B FACHHINI, A PICCHI, L TARCHI, AND F TURRINI, "Experimental and Theoretical Investigation of Thermal Effectiveness in Multi-Perforated Plates for Combustor Liner Effusion Cooling," *Journal of Turbomachinery,* vol. 136, no. 9, pp. 1-13, 2014.

[16] G WANG, G LEDEZMA, J DELANCEY, AND A WANG, "Experimental Study of Effusion Cooling with Pressure-Sensitive Paint," *Journal of Engineering for Gas Turbines and Power*, vol. 139, no. 5, 2017.

[17] L ANDREI, A ANDREINI, C BIANCHINI, G CACIOLLI, B FACHHINI, A PICCHI, L TARCHI, AND F TURRINI, "Effusion cooling plates for combustor liners: experimental and numerical investigations on the effect of density ratio," *Energy Procedia*, no. 45, pp. 1402-1411, 2014.

[18] G BARIGOZZI, C MUCIGNAT, H ABDEH, D SCANDELLA AND G DOLCI, "Assessment of binary PSP technique for film cooling effectiveness measurement on nozzle vane cascade with cutback trailing edge," *Experimental Thermal and Fluid*, vol. 97, no. 201, pp. 431-443, 2014.

[19] Innovative Scientific Solutions Inc. Binary Pressure-Sensitive Paint (http://www.psp-tsp.com). Accessed 20 April 2023.

[20] D MCLEAN, "Referenced pressure paint and the ratio of ratios," *Proceedings of the Sixth Annual Pressure Sensitive Paint Workshop*, The Boeing Company, Seattle, Washington, pp. 11–1:35, 1998

[21] T LIU, T BEN AND J P SULLIVAN, " Pressure Sensitive Paints," *NASA Review Article*, 2000

[22] T V JONES, " Theory for the Use of Foreign Gas in Simulating Film Cooling," *International Heat and Fluid Flow*, vol. 20, no. 3, pp. 349–354, 1999

[23] J C HAN AND A P RALLABANDI, "Turbine Blade Film Cooling Using PSP Technique," *Front. Heat Mass Transfer,* vol. 1, no. 1, p. 013001, 2010

[24] Z LEI, A MAHALLATI, M CUNNINGHAM, AND P GERMAIN, "Influence of Inlet Swirl on the Aerodynamics of a Model Turbofan Lobed Mixer," *ASME International Mechanical Engineering Congress and Exposition*, pp. 807–819, 2010.

[25] J J SCRITTORE, K A THOLE AND S W BURD, "Investigation of Velocity Profiles for Effusion Cooling of a Combustor Liner," *Journal of Turbomachinery*, vol. 129, pp. 518-526, 2007.

[26] A M A DABAGH, G E ANDREWS, R A A ABDUL HUSAIN, C I HUSAIN, A NAZARI AND J WU, "Impingement/Effusion Cooling: The Influence of the Number of Impingement Holes and Pressure Loss on the Heat Transfer Coefficient," *Journal of Turbomachinery*, vol. 112, no. 3, pp. 367-476, 1990.

[27] S BALDAUF, M SCHEURLEN, A SCHULZ AND S WITTING, "Correlation of Film-Cooling Effectiveness from Thermographic Measurements at Enginelike Conditions," *Journal of Turbomachinery*, vol. 124, pp. 686-698, 2002.

[28] A K SINHA, D G BOGARD AND M E CRAWFORD, "Film Cooling Effectiveness Downstream of a Single Row of Holes with Variable Density Ratio," *Journal of Turbomachinery*, vol. 113, no. 3, pp. 442-449, 1991.

[29] D R PEDERSEN, E ECKERT AND R GOLDSTEIN, "Film Cooling with Large Density Differences Between the Mainstream and the Secondary Fluid Measured by the Heat-Mass Transfer Analogy," *ASME Journal of Heat Transfer*, vol. 99, pp. 620-627, 1977.

[30] C J MAREK, "Combustor Turbulence," Transition in Turbines, NASA Conference Publication, 2386.

[31] X CHEN, J KRAWCIW, H XIA, P A DENMAN, C BONHAM AND J F CARROTTE, "Study of an effusion-cooled plate with high level of upstream fluctuation," *Applied Thermal Engineering*, vol. 184, 2021.

[32] D L SCHMIDT AND D G BOGARD, "Effects of Free-Stream Turbulence and Surface Roughness on Film Cooling," ASME Paper 96-GT-462, 1996.

[33] M FOLK, R J MILLER AND J D COULL, "The Impact of Combustor Turbulence on Turbine Loss Mechanisms," *Journal of Turbomachinery*, vol. 142, no. 9, 091009, 2020.

5.2 Optimizing Adiabatic Film Cooling Effectiveness through Varying Compound Angles

This paper explores innovative effusion cooling designs featuring varying compound angles to optimize adiabatic film cooling effectiveness (AFE) along the main flow direction of gas turbine combustor liners. Leveraging the recent advancements in understanding the directional effects of effusion cooling, the study proposes a novel approach by setting discrete compound angles at successive regions along the flow direction. Experimental evaluations, conducted using Pressure Sensitive Paint (PSP) to determine AFE, illustrate that the new design with varying compound angles significantly improves cooling film uniformity and enhances AFE compared to traditional designs with fixed and uniform compound angles.

The investigation underscores the potential of varying compound angles in effusion cooling designs to achieve more uniform cooling coverage and a slight enhancement in AFE. These results contribute to the ongoing efforts to refine cooling technologies for gas turbines, emphasizing the role of compound angle variations in advancing effusion cooling efficiency.

DOI: 10.1115/GT2024-122413

Proceedings of the ASME Turbo Expo2024
Turbomachinery Technical Conference and Exposition
GT2024
June 24-28, 2024, London, England, United Kingdom

GT2024-122413

ENHANCED ADIABATIC FILM COOLING EFFECTIVENESS BY VARYING COMPOUND ANGLE

Yeongmin Pyo
National Research Council of Canada, Ottawa, Canada
University of Ottawa
Ottawa, Canada

Mohsen Broumand
National Research Council of Canada, Ottawa, Canada

Juchan Son
National Research Council of Canada, Ottawa, Canada
University of Ottawa
Ottawa, Canada

Patrick Richer
University of Ottawa
Ottawa, Canada

Bertrand Jodoin
University of Ottawa
Ottawa, Canada

Sean Yun
National Research Council of Canada, Ottawa, Canada

Zekai Hong*
National Research Council of Canada, Ottawa, Canada
University of Ottawa
Ottawa, Canada

ABSTRACT

Effusion cooling is the state-of-the-art cooling technology for gas turbines. However, the compound angle of effusion cooling holes is commonly set as a fixed value in prior studies. In particular, the compound angle is mostly set to zero in practice by assuming that highly directional miniature effusion cooling jets are aligned with the main flow. A recent study from our group has examined the directional effects of effusion cooling on adiabatic film cooling effectiveness (AFE) subjecting to a swirling main flow. It was found that a large compound angle initially facilitates a quick build-up of cooling film and the optimal compound angle reduced to smaller values downstream where the cooling film is further developed. The current study exploits the recent findings in the directional effects of effusion cooling by proposing novel effusion cooling designs with varying compound angles of cooling holes which are optimized for improving AFE along the main flow direction. In the present study, AFE was experimentally determined using Pressure Sensitive Paint (PSP) through invoking the heat/mass transfer analogy. A new effusion cooling design was evaluated by setting the compound angles of effusion cooling holes to three discrete values of 90, 60, and 30 degrees at three successive regions along the direction of the main flow. 2D AFE maps resulting from the proposed design were compared with those of conventional effusion cooling designs with fixed compound angles under identical conditions. It was found that the new effusion cooling design featuring varying compound angles produces a more uniform cooling film coverage and a small enhancement to AFE comparing to the conventional effusion cooling designs.

Keywords: Effusion cooling, Blowing ratio, Compound angle, PSP (Pressure sensitive paint), AFE (Adiabatic film cooling effectiveness)

NOMENCLATURE

BR	Blowing Ratio
δ_y	Longitudinal hole pitch
δ_x	Transverse hole pitch
d	Hole diameter
T_g	Main flow temperature
T_{aw}	Adiabatic surface temperature
T_c	Coolant temperature
U_∞	Main flow velocity at a leading edge on test coupons
U_c	Coolant velocity at an outlet of effusion cooling holes
$c_{O2,g}$	Oxygen concentration in with the presence of main flow
$c_{O2,aw}$	Oxygen concentration near a wall with the presence of mixture flow of the main airflow and foreign coolant gas
p	Static pressure
α	Inclination angle
β	Compound angle
η_{ad}	Adiabatic film cooling effectiveness

1. INTRODUCTION

One of the strategies for improving the efficiency of gas turbine engines is to reduce the use of cooling air for their combustor liners and first stage nozzles, as the cooling air for these hot gas path components has to be compressed to the highest-pressure point of the entire engine. However, the developments of more efficient gas turbine engines are typically correlated with higher combustion temperatures, which in turn requires the use of more cooling air, if the cooling technology used remains the same, in addition to the use of advanced high-temperature resistant materials. Furthermore, rising pressure ratios in modern gas turbine engines make the cooling of hot gas path components more challenging since the compressor air is discharged at higher temperatures, making it a less effective coolant for combustor liners and first-stage nozzles.

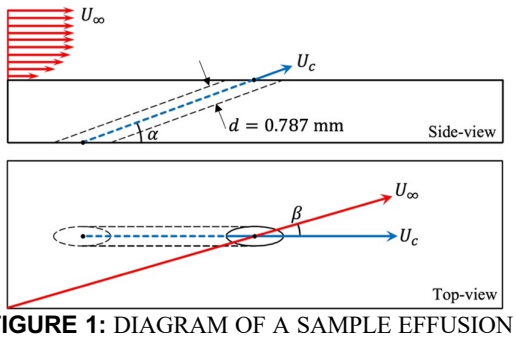

FIGURE 1: DIAGRAM OF A SAMPLE EFFUSION COOLING HOLE WITH THE HOLE DIAMETER (d), COMPOUND ANGLE (β), AND INCLINATION ANGLE (α) DENOTED.

Inadequate cooling available for combustor liners reduces their life expectancies and can cause premature failures of combustor components, as reported in the literature [1]. To reduce the metal temperature of the combustor liner and improve the longevity of the component, changing various cooling parameters including the shape of cooling holes and the amount of cooling air has been the main focus of previous studies [1-4]. In addition, new materials for providing thermal barriers are suggested for improved cooling performance [3,4].

Multi-hole effusion cooling is the state-of-the-art cooling method by forcing a pressurized coolant through an array of pinholes, thereby absorbing heat from a combustor liner while forming a protective fluid film subsequently to insulate heat exposed metal surfaces [5]. The pressurized coolant is injected into the inner surface of the liner through discrete effusion cooling holes as three-dimensional jet columns or through slots as two-dimensional sheets [6].

It is established that the effusion cooling efficiency is highly dependent on cooling hole pattern, shape, and size, as they govern the formation of cooling films. The diameter of effusion cooling holes ranging from 1.18 to 2.16mm was studied by Andrews et al [7] while maintaining a fixed inclination angle (α). The effects of inclination angles between 30 and 90 degrees were studied by Venkatesh et al [8]. In the current study, the choice of the cooling hole diameter d = 0.787 mm and the inclination angle α = 20 degrees are according to commonly adopted values [9,10]. All test coupons have a thickness of 2.54 mm. Therefore, a constant length-to-diameter (l/d) ratio of effusion holes is kept at 9.4 for all test coupons.

While studies on the pattern or shape of effusion cooling holes [4-6,11] and coolant blowing ratios [12-14] are continuously being conducted, studies with a focus on the compound angle (β) of effusion cooling holes are limited. By compound angle, we mean the angular difference between the main flow and the coolant flow/jet as shown in Figure 1.

The compound angle (β) is expected to significantly impact the overall film cooling

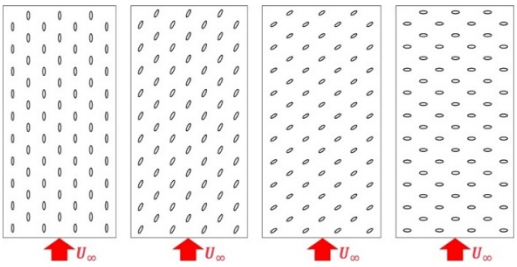

(a) (b) (c) (d)

FIGURE 2: EFFUSION COOLING TEST CONFIGURATIONS: (a) EFFUSION HOLES CO-LINEAR WITH THE MAIN FLOW DIRECTION (β = 0°) AND THREE NON-ZERO COMPOUND ANGLE CASES (b)β = 30°, (c)β = 60°, AND (d)β = 90°.

effectiveness over the inner surface of a combustor liner. A recent study [15] investigated the directional effects of effusion cooling induced by the swirling main flow on the adiabatic film cooling effectiveness (AFE) by rotating an effusion cooling plate to be at 30, 60, and 90-degree angles with the main flow. The study suggests that angles as large as 90 degrees between effusion jets and main flow are preferred for developing cooling film initially; once the cooling film is fully developed, the angle between effusion jets and main flow can be reduced to 30 degrees for optimal performance. The main goal of the current study is to evaluate an effusion cooling design concept by varying compound angles along the direction of the main flow. Specifically, the effusion cooling plate was divided into three successive regions along the main flow direction, three discrete compound angles were applied to each region, with the effusion holes of a 90-degree compound angle in the leading-edge region and the ones of a 30-degree compound angle in the trailing-edge region.

Additionally, a 2023 study [16] isolated the directional effects of effusion cooling originated from non-zero compound angles from those resulting from variations in the effective pitch of effusion cooling holes. Figure 2 illustrates the effusion cooling configurations tested in the study, where only the compound angle was varied while the pitch of the effusion holes was kept identical. The study reveals that the swirling main flow has two separate effects on effusion cooling: 1) the compound angle is varied and 2) the effective pitch of the effusion cooling holes is also altered. The alteration in the effective pitch of effusion cooling holes was identified as a major factor in the effectiveness of the resulting cooling film. Therefore, in evaluating the aforementioned concept of varying compound angles along the direction of the main flow, it is determined that the pitch of effusion cooling holes should be kept identical as those of the fixed compound angle configurations as shown in Figure 2. It should be noted that the main flow direction is indicated by the red arrows at the bottom of Figure 2.

Specifically, the pitch of effusion holes that was adopted in the reference [16] and in this study is detailed in the section of Experimental Setup, where the longitudinal separation between two adjacent holes δ_y is 9 times of the effusion hole diameter and the transverse separation δ_x is 7 times of the effusion hole diameter. A staggered arrangement of effusion holes was adopted.

2. METHODOLOGY

Pressure sensitivity paint (PSP) was adopted in the study to measure adiabatic film cooling effectiveness for effusion cooling. The application of PSP primarily exploits the heat/mass transfer analogy. Instead of using a heated or cooled secondary stream of gas of different temperature from the main flow as coolant proxy, a gas of different oxygen content from the main flow can be readily used as the coolant proxy. PSP measurement in this context involves the injection of foreign gases like nitrogen or carbon dioxide at ambient temperature. However, small errors can arise from temperature variations on the PSP surface, particularly when the main air (ambient air) temperature differs from that of the coolant proxy (nitrogen), which is typically discharged from compressed gas bottles. To address these challenges and minimize uncertainties in oxygen partial pressure determinations from PSP fluorescence intensities, the current study employs a binary PSP. Unlike the single-luminophore PSP, the dual-luminophore PSP (binary PSP) allows for the acquisition of fluorescence intensities from both oxygen-sensitive and reference molecule components, thus compensating for errors induced by variations in PSP temperature and UV excitation illumination intensities [17,18].

Binary PSP exhibits fluorescence peaks at distinct wavelengths, typically near 650 nm for the pressure-sensitive signal and 560 nm for the reference signal, as shown in Figure 3. These peaks demonstrate similar sensitivities to PSP temperature changes. By taking the ratio of the pressure-sensitive portion of fluorescence to the reference portion, Binary PSP effectively compensates for errors induced by variations in PSP temperature and fluctuations in UV excitation illumination intensities. However, as

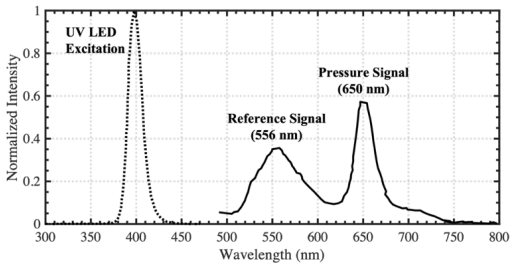

FIGURE 3: SPECTRA OF UV EXCITATION ILLUMINATION TOGETHER WITH THE RESULTING FLUORESCENCE PEAKS NEAR 650 NM AS THE PRESSURE-SENSITIVE SIGNAL AND 560 NM AS THE REFERENCE SIGNAL FOR BINARY-FIB PSP FROM INNOVATIVE SCIENTIFIC SOLUTIONS INC. THE PLOT IS REPRODUCED FROM [19].

McLean [17] notes, due to the imperfect mixing of two luminophores, a simple ratio of the intensities of the two fluorescence peaks may not fully account for luminophore inhomogeneity. To address this, Liu et al [18] proposed normalizing the ratios of fluorescence intensities by the ratio at the reference condition (standard ambient air condition as wind-off). This normalized ratio corrects for non-homogeneous luminophore concentrations and variations in paint thickness as following:

$$\frac{r}{r_{ref}} = \frac{(I - I_{dark})_{PT}/(I - I_{dark})_T}{(I_{ref} - I_{dark})_{PT}/(I_{ref} - I_{dark})_T} \quad (4)$$

where r/r_{ref}, the normalized ratio of fluorescence intensities, replaces I/I_{ref}, normalized pressure signal fluorescence intensity in a second-order polynomial equation [19]. The subscript PT indicates the pressure signal fluorescence peak near 650 nm which is both pressure and temperature-dependent, while the subscript T represents the reference fluorescence peak near 560 nm which is temperature-dependent only. The second-order polynomial expression is revised for calibrating and determining local oxygen partial pressures on Binary PSP surfaces as

$$\frac{p_{O_2}}{p_{O_2,ref}} = A\left(\frac{r_{ref}}{r}\right)^2 + B\left(\frac{r_{ref}}{r}\right) + C \quad (5)$$

In the current study, nitrogen is used as the coolant proxy, and ambient air serves as the main flow. As the coolant proxy is devoid of molecular oxygen, the local oxygen partial pressures determined by Binary PSP can directly infer AFE by adopting the heat and mass transfer analogy [20] as

$$\eta_{ad} = \frac{T_g - T_{aw}}{T_g - T_c} \approx \frac{c_{O_2,g} - c_{O_2,aw}}{c_{O_2,g}} \quad (6)$$

where c and T denote oxygen concentration and temperature, respectively. In addition, the subscripts g, aw, and c represent main air flow, adiabatic wall, and coolant, respectively. For this analogy to hold, a turbulent flow field is required, characterized by a Lewis number being equal to 1, indicating that the thermal and concentration boundary layer equations share similar diffusion terms, which is typically the case in turbulent flow conditions (Re=256,000 in this study) common in gas turbine applications.

Figure 4 shows the comparison results of the calibration curve of Binary PSP between the current study and the references [19,21]. The calibration curves are small variations among the curves for each pixel on the measurement area of the effusion cooling test coupon; the curve is the average calibration curve for all pixels of the active measurement area. Therefore, the good comparisons declare the validity of the current calibration procedures for the spatial variation of intensity. The calibration method depends on the uncertainty in the calibration constant A, B, and C and in the CCD camera resolution [21,22]. To further reduce the experimental uncertainty of the PSP measurement, the current study uses the pixel-by-pixel calibration method, not for all pixels by one averaged calibration curve. The experimental procedure for the calibration of the

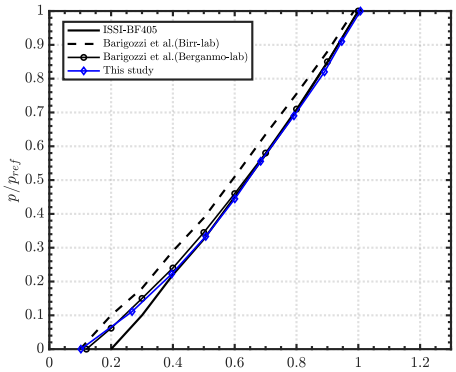

FIGURE 4: COMPARISONS OF CALIBRATION CURVES. THE X-AXIS IS THE INVERSE OF NORMALIZED RATIOS OF FLUORESCENCE INTENSITIES WHILE THE Y-AXIS IS THE OXYGEN PARTIAL PRESSURE NORMALIZED BY STANDARD AIR.

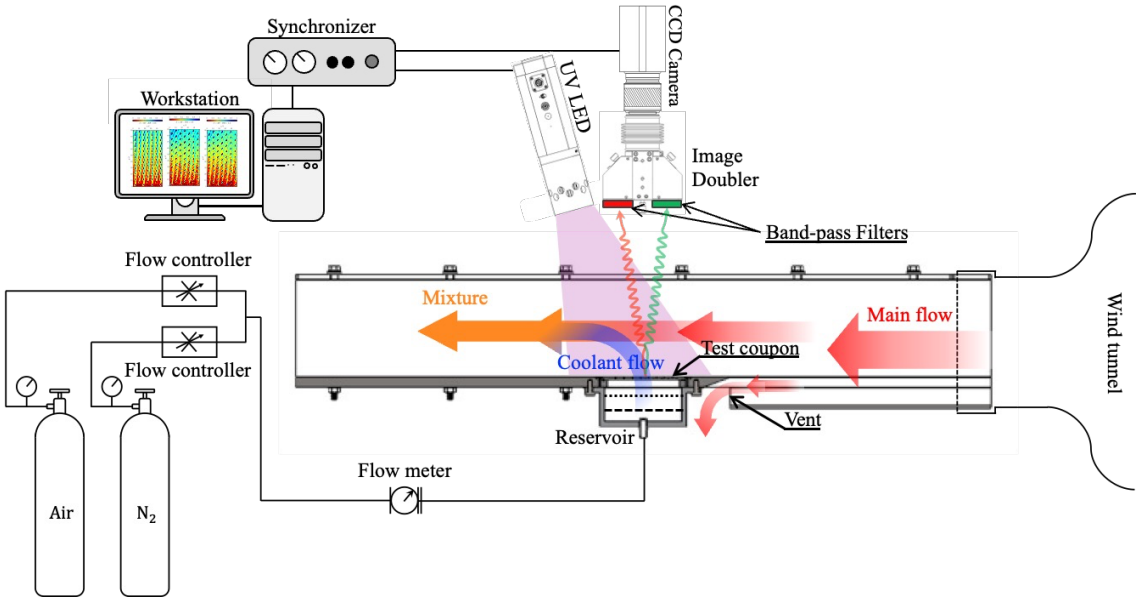

FIGURE 5: SCHEMATIC OF THE EXPERIMENTAL SETUP AND A SECTIONAL VIEW OF THE TEST SECTION.

current study is explained in the following section.

3. EXPERIMENTAL SETUP

Experiments for evaluating the effectiveness of the two new designs of effusion cooling, as advanced cooling methods for combustor liners, were performed in a lab-scale cooling test rig shown in Figure 5. In the present study, to simulate the flow speed in a typical gas turbine combustor, a low-speed wind tunnel was adjusted for accelerating the main flow of air to 33 m/s. The Reynolds number and the turbulence intensity for the wind-tunnel flow are approximately 256000 and 3%, respectively. A 30 kW AC motor drives a fan that is capable of delivering a maximum mass flow rate of approximately 2.5 kg/s at a pressure rise of 5 kPa [23].

The test section has a transparent polycarbonate top panel with a 127-mm square cross-section. The Pitot tube is located 228.6 mm from the inlet of the square test section after the wind tunnel transition piece that connects the round wind tunnel outlet to the square test section. The reservoir, which supplies the cooling gas as uniform distribution using the perforated plate to all the effusion cooling holes, is mounted on the bottom panel of the test section with an inner

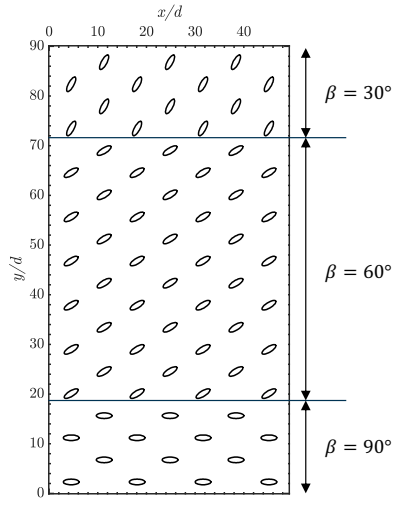

FIGURE 6: SCHEMATIC OF TEST DESIGNS USING THREE DISCRETE COMPOUND ANGLES. THE BOTTOM OF THE MEASUREMENT AREA REPRESENTS THE UPSTREAM SIDE

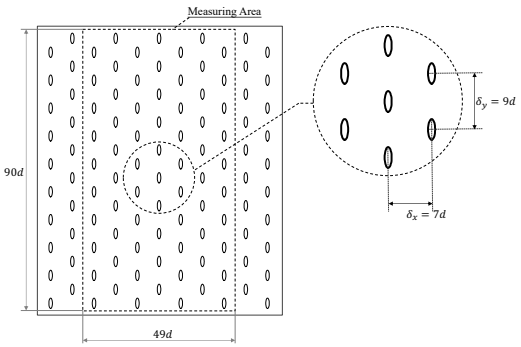

FIGURE 7: SPANWISE (δ_x) AND STREAMWISE (δ_y) PITCHES ARE DENOTED FOR AN EXAMPLE EFFUSION COOLING CONFIGURATION. THE EFFUSION COOLING HOLES ARE STAGGERED IN THIS EXAMPLE.

diameter of 101.6 mm and an internal height of 44.45 mm. The center of the reservoir is located 406.4 mm from the inlet of the test section. Each test coupon shown in Figure 2 and Figure 6 is installed on the bottom panel of the test section directly above the reservoir with the inner surface flush with the bottom panel of the test section. Test coupon configurations were briefly mentioned in the Introduction Section; additional information about the test coupon preparation is described here. As reported in the reference [16], a test coupon has an active effusion cooling area of 70.83mm x 38.56mm, or 90d x 49d, as shown in Figure 7. In the circular coupon, the active area is confined to the central square section, which is equipped with effusion cooling holes. Furthermore, only the middle section of the active area was used for studying effusion cooling so that edge effects from both sides can be minimized. In this study, the exact same test coupon layout was adopted as used in the previous study by only altering the effusion cooling hole configurations. As shown in Figure 6, the actual measurement area of the test coupon studied in this work is with varying compound angles; three discrete compound angles (30, 60, and 90 degrees) were arranged in three discrete regions along the direction of the main flow. In Figure 6, the bottom side of the measurement area represents the upstream side.

The longitudinal length of each region is inferred from the previous study [16]. Figure 8 shows spatially averaged AFE along the mainstream direction for three compound angles at varying blowing ratios (BR). The blowing ratio is defined as

$$BR = \frac{\rho_c U_c}{\rho_\infty U_\infty} \qquad (7)$$

where ρ_c, ρ_∞ are the densities of coolant and main flow and U_c and U_∞ are the velocities of effusion cooling jets and main flow air, respectively [14]. For all BRs, a compound angle of 90 degrees outperforms other compound angles in AFE at the initial stage of cooling film developments near the leading edge while the 30-degree compound angle offers the best AFE towards the trailing edge. Therefore, three discrete compound angles of 90, 60, and 30 degrees were designed to occupy regions of 20, 60, and 20% of the longitudinal spans along the mainstream direction.

The test coupons were constructed using stereolithography (SLA) 3D printing. Figure 9 shows the measured pressure drops across an

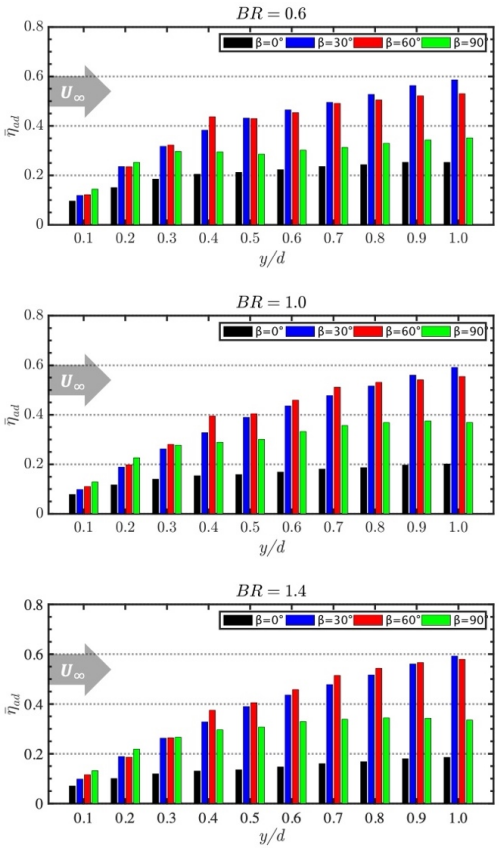

FIGURE 8: COMPARISONS OF LONGITUDINAL SPATIALLY AVERAGED ADIABATIC FILM COOLING EFFECTIVENESS OF BASELINE DESIGN MEASURING AT THE SPECIFIC AREA FOR DIFFERENT BLOWING RATIOS: BR=0.6(TOP), BR=1.0(MIDDLE), AND BR=1.4(BOTTOM).

effusion cooling test coupon. Using static pressure transducers installed in the test section and the reservoir as shown in Figure 5, pressure drops were determined to be 0.8 %, 1.9 %, and 3.8% for BR of 0.6, 1, and 1.4, respectively. In addition, the ambient temperature in the lab was maintained at 293 K.

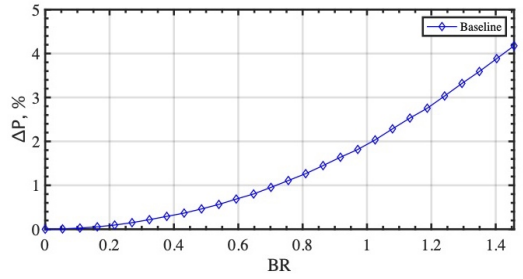

FIGURE 9: PRESSURE DROP ACROSS THE EFFUSION PLATE AS A FUNCTION OF BR.

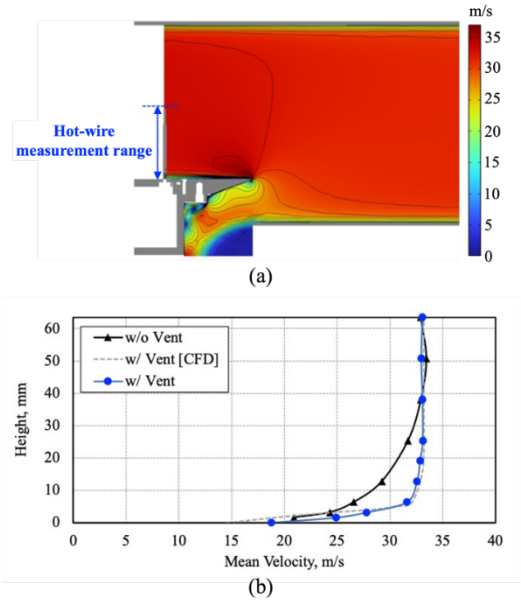

FIGURE 10: (A) COMPUTED VELOCITY CONTOUR NEAR THE VENT FOR BOUNDARY LAYER REJECTION. (B) COMPARISON OF MEASURED BOUNDARY LAYER THICKNESS WITH AND WITHOUT THE BOUNDARY LAYER VENT; RESULTS FROM CFD SIMULATIONS ARE ALSO INCLUDED FOR COMPARISON.

The main flow in the test section was conditioned before the test coupon. An adjustable vent, as illustrated in Figure 5, was installed immediately upstream to the test coupons, so that the boundary layer developed in the test section upstream to the test coupon could be vented out. A CFD simulation based on the RANS turbulency model shows that the boundary layer developed in the test section prior to the test coupon can be fully rejected by the vent, as demonstrated in Figure 10(a). Boundary layer thickness measurements were conducted at the test coupon's leading edge by adjusting the height of a hot-wire anemometer in the center plane of the test section. The hot-wire measurements show excellent agreement with CFD simulation results, as illustrated in Figure 10(b). It is apparent that the vent can effectively reject the boundary layer developed prior to the test coupon.

The current study carefully calibrated the binary PSP for each specific effusion cooling setup, utilizing blends of pure nitrogen (N2) and compressed air as the calibration gases. The calibration procedure involved individually regulating and metering the streams of N2 and compressed air, which were then blended in a controlled manner. This study established ten calibration points, with the volumetric fractions of compressed air ranging from 0% to 100% in 10% increments and nitrogen being the balance. Throughout the calibration process, the wind tunnel was turned off, and the test section was effectively isolated. The effusion cooling test coupon within the test section was encased in a calibration enclosure and was subjected to known calibration gases at ambient pressure. This process allowed the binary PSP painted on the coupon surfaces to be fully exposed to predetermined oxygen partial pressures, enabling a precise pixel-by-pixel calibration procedure. The calibration process establishes correlations between the PSP fluorescence intensities and oxygen partial pressures. Following the calibration for each configuration, the enclosure was removed, and the test section reconnected to the wind tunnel, preparing the system for subsequent effusion cooling experiments with nitrogen as the sole coolant proxy. Table 1 summarizes test conditions for studying AFE of the effusion cooling configuration featuring varying compound angles. Reynolds number of coolant (N_2) inside the effusion cooling hole is 1067, 1778, and 2490 at the blowing ratios of 0.6, 1, and 1.4, respectively.

The AFE uncertainty is estimated using the method reported by Kline and McClintock [24] while pixel-wise calibration curves for binary PSP essentially eliminate errors from temperature variations. Liu and Sullivan [25] also assessed other sources of uncertainty in PSP measurements, such as stability of illumination, photodegradation, and spectral leakage. Nevertheless, the pixel-by-pixel calibration process mitigated errors from these uncertainty sources. The relative uncertainty of cooling film effectiveness was evaluated to be ±4.5% for AFE = 0.1 and ±1.8% for AFE = 0.8.

For UV excitation of the Binary PSP, we utilized the ISSI LM2X-DM LED light source, calibrated to operate around 400 nm. The PSP fluorescence signals, both the pressure-sensitive and reference signals, were captured using a LaVision ImagerProX 2M camera, equipped with a LaVision Image Doubler. To isolate the required fluorescence signals, we employed two specific bandpass filters: one centered at 650 nm with a 20 nm FWHM, and another at 560 nm with a 10 nm FWHM. These filtered signals were then merged side-by-side via the Image Doubler, enabling the LaVision camera to capture a comprehensive image combining both fluorescence intensity spectra.

TABLE 1 SUMMARY OF TEST CONDITIONS

BR	Main flow rate, m/s	N_2, m/s
0.6	33.0	20.5
1.0	33.0	34.1
1.4	33.0	47.8

4. RESULTS AND DISCUSSIONS

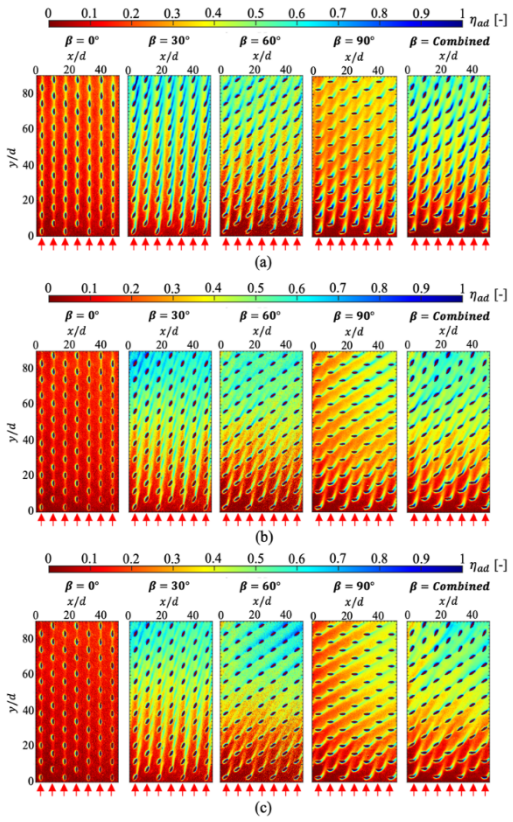

FIGURE 11: COMPARISONS OF 2D AFE DISTRIBUTIONS AS A RESULT OF THE CASES OF A SINGLE COMPOUND ANGLE ($\beta = 0°$, 30°, 60°, AND 90°) AND THE CASE OF COMBINING COMPOUND ANGLES AT DIFFERENT BRS (BR=(a)0.6, (b)1, AND (c)1.4), CORRESPONDING TO THE MEASURING AREA OF EFFUSION COOLING TEST COUPONS IN FIGURE. 3. ALL TEST COUPONS HAVE THE SAME PITCHES ($\delta_x = 7d$ AND $\delta_y = 9d$).

Figure 11 presents 2D AFE distributions at all three BRs. The comparison is between configurations of fixed compound angles (from 0 to 90 degrees) and the configuration of varying compound angles as shown in Figure 2 and Figure 6. As discussed earlier, the pitches of all five configurations are of the same pitch of effusion holes. As expected, the configuration of varying

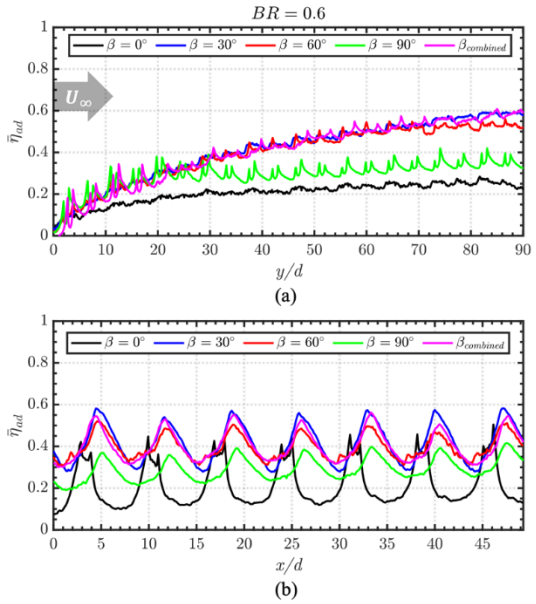

FIGURE 12: COMPARISONS OF (a) SPANWISE AVERAGED AFE AND (b) STREAMWISE AVERAGED AFE OF THE BR = 0.6 CASE, CORRESPONDING TO THE 2D AFE DISTRIBUTIONS SHOWN IN FIGURE 10(a).

compound angles demonstrates overall superior performance than any fixed compound angle configurations. Specifically, the varying compound angle configuration can quickly develop the cooling film initially with a 90-degree

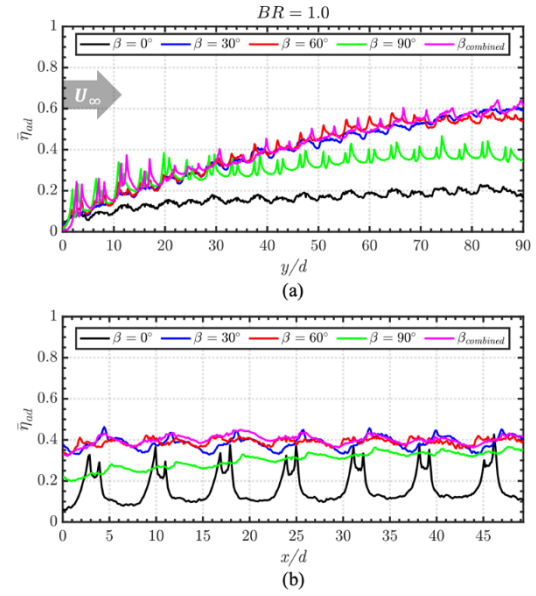

FIGURE 13: COMPARISONS OF (a) SPANWISE AVERAGED AFE AND (b) STREAMWISE AVERAGED AFE OF THE BR = 1.0 CASE, CORRESPONDING TO THE 2D AFE DISTRIBUTIONS SHOWN IN FIGURE 10(b).

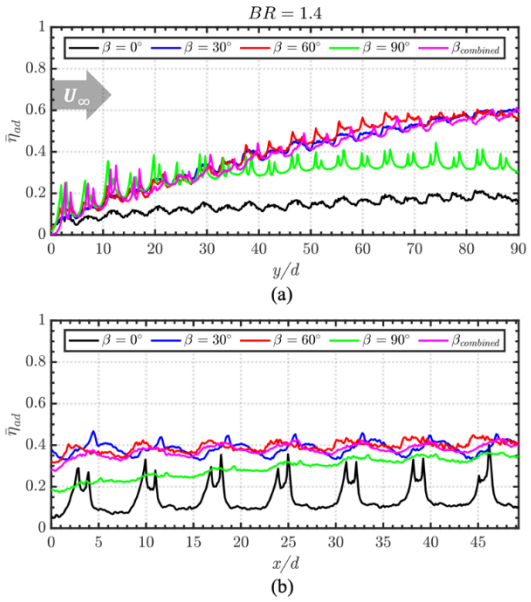

FIGURE 14: COMPARISONS OF (a) SPANWISE AVERAGED AFE AND (b) STREAMWISE AVERAGED AFE OF THE BR = 1.4 CASE, CORRESPONDING TO THE 2D AFE DISTRIBUTIONS SHOWN IN FIGURE 10(c).

compound angle. However, as can be seen from the comparisons, the 90-degree compound angle is not optimal overall. In fact, the 90-degree fixed compound angle configuration obviously under-performs compared to two other fixed compound angle cases (30 degrees and 60 degrees) because a compound angle as large as 90 degrees results in strong mixing between coolant jets and the main flow. The mixing is undesirable because the coolant is effectively dissipated once it mixes with the main flow. The benefit of large transverse penetration depths resulting from a large compound angle at the onset of the cooling film is quickly outweighed by the negative effects of strong coolant dissipations. Quickly after the onset of the cooling film, smaller compound angles (30 degrees and 60 degrees) are preferred as these compound angles reach a good balance between good transverse penetrations and suppressed coolant dissipations due to mixing with the main flow. Figure 11 suggests that the varying compound angle configuration provides optimal cooling film among possible compound angle variations.

The observations of Figure 11 can be quantitively confirmed by comparisons of AFE means in the spanwise direction, as shown in Figures 12-14. The AFE mean in the spanwise direction is computed by averaging the AFE values determined from a horizontal row of pixels

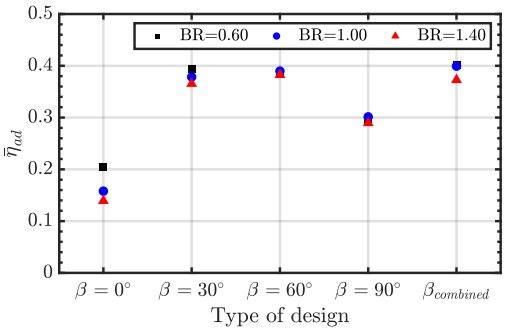

FIGURE 15: COMPARISONS OF AFE AVERAGED OVER THE ENTIRE MEASURING AREA FOR ALL CONFIGURATIONS AT VARYING BRS.

as shown in Figure 11, excluding the pixels representing effusion holes. A row of pixels for calculating spanwise AFE mean is perpendicular to the direction of the main flow. Similarly, the streamwise means of AFE were computed by averaging the AFE values determined from a vertical column of pixels as shown in Figure 11, again, excluding the pixels representing effusion holes. The comparisons of the spanwise averages for all BRs, as shown in Figures 11-13, clearly indicate that the varying compound angle configuration for effusion cooling is optimized for all stages of the cooling film development. At the early stages of cooling film developments (y between 0-20d), the varying compound angle configuration outperforms configurations of two smaller fixed compound angles of 30- and 60-degree and is comparable to the one of a fixed 90-degree compound angle. As the cooling film is more developed (y>30d), the varying compound angle configuration substantially outperforms the one of a 90-degree fixed compound angle, while being comparable to the two configurations featuring smaller fixed compound angles of 30- and 60-degree. It should be pointed out that a zero-compound angle configuration substantially underperforms any configurations tested in this study featuring non-zero compound angles, whether it being fixed or varying values.

Figure 15 shows comparisons of AFE averaged over the entire measuring area for all configurations at varying BRs. Unlike the colinear effusion jets case (β=0°) where high BRs are detrimental to the effectiveness of cooling film, all configurations featuring non-zero compound angles are rather insensitive to BR changes. In addition, the varying compound angle configuration does not significantly improve the overall AFE as evidenced by the comparisons in the Figure. It can be therefore concluded that the

main advantage of the effusion configuration featuring varying compound angles is improved AFE near the leading edge over two configurations of fixed compound angles of 30 and 60 degrees without incurring additional costs.

5. CONCLUSION

An effusion cooling configuration featuring varying compound angles was proposed and evaluated in this study. The design was intended to take advantage of the findings of a recent study [12] that compound angles as large as 90 degrees are beneficial for initially starting the cooling film while such large compound angles are less ideal for AFE after the initial stages of cooling film developments due to strong coolant dissipations from mixing with the main flow. Smaller compound angles such as 30 and 60 degrees are preferred for optimal AFE after the initial stages of cooling film developments. This preference of later stage compound angle can be attributed to the comprise that cooling film benefits from effusion jets' enhanced transverse penetrations as the compound angle increases but suffers from strong coolant dissipations due to mixing with the main flow at the same time. Therefore, the proposed effusion cooling configuration features three discrete compound angles: 90, 60, and 30 degrees along the direction of the main flow. Specifically, from the leading edge of the effusion cooling plate to 20d, a 90-degree compound angle is adopted. The compound angle is then reduced to 60 degrees between 20d and 70d. After 70d, the compound angle is further reduced to 30 degrees. To remove the directional effects resulting from varying pitches of effusion holes, an identical pitch of effusion holes was maintained among all effusion cooling configurations to facilitate the comparison. Five effusion cooling configurations were compared in total: one proposed configuration of varying compound angles and four configurations of the same pitch but of fixed compound angles ranging between 0 and 90 degrees.

Experimental studies of 2D AFE distributions of the effusion cooling configurations were performed using pressure sensitive paint (PSP). Upon comprehensive evaluation, it is observed that the combined compound angle design demonstrates an insignificant enhancement in adiabatic film cooling effectiveness (AFE) when compared to the 30º and 60º single compound angle designs. Although the varying compound angle configuration does not significantly improve the overall AFE, the design achieves optimal performance everywhere, particularly near the leading edge of an effusion cooling plate where the cooling film is being initiated. Specifically, when the cooling film is being initiated, the varying compound angle design attains the AFE of a 90-degree compound angle configuration, outperforming smaller fixed compound angles. When the cooling film goes beyond the initial development stage, the varying compound angle configuration attains the level of AFE performance of smaller fixed compound angle configurations.

ACKNOWLEDGEMENTS

The work is supported by the National Research Council of Canada (NRC)'s National Program Office under the Ideation New Beginnings Program (No. 577) and Postdoctoral Fellowship Program (PDF2021-06). Additional funding for the work is provided by the NRC's Aerospace Research Center under the LEAP Program (LEAP-012).

REFERENCES

[1] Ahmed, S., Singh, P., and Ekkad, S. V. " Numerical Investigations For Different Combustion Liner Cooling Techniques Under Non-Reacting Conditions Through A Lean Pre-Mixed Fuel Nozzle." *AIAA Scitech 2019 Forum*. pp. 1-13. 2019. DOI: 10.2514/6.2019-0532.

[2] Ritchie, D. G., Click, A. J., Ligrani, P. M., Liberatore, F., Patel, R., and Ho, Y. H. "Double Wall Cooling of an Effusion Plate with Cross Flow and Impingement Jet Combination Internal Cooling: Comparisons of Main Flow Contraction Ratio Effects." *AIAA Propulsion and Energy 2019 Forum*. pp. 1-18. 2019. DOI: 10.2514/6.2019-3967.

[3] Schilke, P. W. "Advanced Gas Turbine Materials and Coatings." Report GER-3569G. GE Energy. Schenectady. NY. 2004.

[4] Goswami, B., Sahay, S. K., and Ray, A. K. "Application of Thermal Barrier Coatings on Combustion Chamber Liners – A Review." *High Temperature Materials and Processes*. Vol. 23 NO.3 (2004): pp. 211-236. DOI: 10.1515/HTMP.2004.23.3.211.

[5] Grootenhuis, P. "The Mechanism and Application of Effusion Cooling*." *The Aeronautical Journal*. Vol. 63 No. 578 (1959): pp. 73–89. DOI: 10.1017/S0368393100070632.

[6] Gustafsson, K. M. B. "Experimental Studies of Effusion Cooling." PhD Thesis. Charlmers University of Technology. Göteborg. Sweden. 2001.

[7] Andrews, G. E., Asere, A. A., Gupta, M. L., and Mkpadi, M. C., "Full Coverage Discrete

Hole Film Cooling: The Influence of Hole Size." *International Journal of Turbo and Jet Engines*. Vol. 2 No. 3 (1985): pp. 213-226. DOI: 10.1515/TJJ.1985.2.3.213.

[8] Venkatesh, V., Sriraam, J., Bala, V. D., Subash, K., Ratna, K. V., Srikrishnan, A. R., Ramakrishnananda, B., and Suresh, B., "Studies on effusion cooling: Impact of geometric parameters on cooling effectiveness and coolant consumption." *Aerospace Science and Technology*. Vol. 1 No. 232 (2018): pp. 1-9. DOI: 10.1016/j.ast.2017.12.044.

[9] Woodcock, G. O., Ertz, T., and Koch, B., "Effusion Cooling Techniques for Combustors in Engine Assemblies," US Patent US8104288B2, 31 Jan. 2012.

[10] Dai, Z., Pearson, M. R., and Cohen, J. M., "Combustor Liner Effusion Cooling Holes," European Patent EP3056816A1, 17 Aug.

[11] Cho, H. H., Rhee, D. H., and Goldstein, R. J. "Effects of Hole Arrangements on Local Heat/Mass Transfer for Impingement/Effusion Cooling with Small Hole Spacing." *Journal of Turbomachinery*. Vol. 130 No. 4. (2008). DOI: 10.1115/1.2812325.

[12] Krewinkle, R. "A Review of Gas Turbine Effusion Cooling Studies." *International Journal of Heat and Mass Transfer*. Vol. 66 (2013): pp. 706–722. DOI: 10.1016/j.ijheatmasstransfer.2013.07.071.

[13] Cerri. G., Giovannelli, A., Battisti, L., and Fedrizzi, R. "Advances in Effusive Cooling Techniques of Gas Turbines." *Applied Thermal Engineering*. Vol. 27 No. 4 (2007): pp. 692–698. DOI: 0.1016/j.applthermaleng.2006.10.012.

[14] Bogard, D. G. "Gas Turbine Film Cooling." *Journal of Propulsion and Power*. Vol. 22 No. 2 (2006): pp. 249–270. DOI: 10.2514/1.18034.

[15] Paitich, L. C., Richer, P., Jodoin, B., Pyo, Y., Yun, S., and Hong, Z. "Directional Effects of Effusion Cooling on the Cooling Film Effectiveness." *AIAA Journal*, (2021): pp.1-12. DOI: 10.2514/1.J060625.

[16] Pyo, Y., Son, J., Richer, P., Jodoin, B., Broumand, M., Yun, S. and Hong, Z., "Isolating Influences of Varying Pitch from the Effects of Non-Zero Compound Angles on Effusion Cooling," *The Aeronautical Journal* (2024). (Under reviewing)

[17] Mclean, D., "Referenced pressure paint and the ratio of ratios," *Proceedings of the Sixth Annual Pressure Sensitive Paint Workshop*, The Boeing Company, Seattle, Washington, pp. 11–1:35, (1998).

[18] Liu. T., Ben, T. and Sullivan, J. P., "*Pressure Sensitive Paints*," NASA Review Article, 2000.

[19] Innovative Scientific Solutions Inc. Binary Pressure-Sensitive Paint (http://www.psp-tsp.com). Accessed 20 Nov (2023).

[20] Jones, T. V., "Theory for the Use of Foreign Gas in Simulating Film Cooling," *International Heat and Fluid Flow*, vol. 20, no. 3, pp. 349–354, (1999) DOI: 10.1016/S0142-727X(99)00017-X.

[21] Barigozzi, G., Mucignat, C., Abdeh, H., Scandella, D. and Dolci, G., "Assessment of binary PSP technique for film cooling effectiveness measurement on nozzle vane cascade with cutback trailing edge," *Experimental Thermal and Fluid*, vol. 97, no. 201, pp. 431-443, (2018) DOI: 10.1016/j.expthermflusci.2018.05.015.

[22] Chen, X., Krawciw, J., Xia, H., Denman, P.A., Bonham, C. and Carrotte, J.F., "Study of an effusion-cooled plate with high level of upstream fluctuation," Applied Thermal Engineering, Vol. 184 (2021): 115126. DOI: 10.1016/j.applthermaleng.2020.116126.

[23] Lei, Z., Mahallati, A., Cunningham, M., and Germain, P. "Influence of Inlet Swirl on the Aerodynamics of a Model Turbofan Lobed Mixer." *ASME International Mechanical Engineering Congress and Exposition*. pp. 807–819. (2012) DOI: 10.1115/IMECE2010-39.

[24] S. Kline and F. McClintock, "Describing the uncertainties in single-sample experiments," *Mech. Eng*. 75 (1953).

[25] T. Liu and J. Sullivan, "Pressure and Temperature Sensitive Paints," Springer, (2005). DOI: 10.1007/978-3-030-68056-5.

6 CONCLUSIONS AND FUTURE WORK

6.1. Conclusions

The investigation into advanced effusion cooling technologies for gas turbine combustor liners, as presented in this thesis, offers significant insights into optimizing gas turbine efficiency amidst the evolving demands for reduced emissions and enhanced durability of components in the hot gas path. The primary conclusions drawn from this study are:

1) Directional Effects of Swirling Main Flow: The research underscores the critical impact of swirling main flow on effusion cooling effectiveness. It is conclusively demonstrated that non-zero compound angles, induced by the swirling nature of the main flow, significantly enhance adiabatic film cooling effectiveness (AFE) by facilitating more efficient jet penetration into the gaps between adjacent cooling hole columns. This phenomenon results in substantial improvements in overall cooling film effectiveness, with observed enhancements ranging between 27% to 135% when compared to the co-linear baseline case.
2) Optimal Compound Angle: The isolated effects of compound angles on AFE, devoid of the complicating factors of varied pitch, indicate a trade-off between jet penetration depth and jet mixing. An optimal balance of these effects is achievable at moderate compound angles of 30° and 60°, leading to the recommendation of a 45° compound angle as a starting point for future effusion cooling design optimizations.
3) Pitch Optimization: The study further posits that pitch optimization, particularly under swirling main flow conditions, remains an essential factor for enhancing effusion cooling performance. The introduction of varying pitch has been hypothesized to potentially limit the benefits of larger jet penetration depths afforded by larger compound angles, suggesting a nuanced approach to pitch design in future studies.
4) Varying Compound Angle Design: Experimental investigations into a novel effusion cooling design featuring varying compound angles reveal that, while significant improvements in AFE were not universally observed, the design achieves optimal performance near the leading edge of the effusion cooling plate. This suggests a potential for targeted enhancements in cooling film initiation stages.

6.2. Future Work

Building on the foundational insights garnered through this thesis, several avenues for future research emerge:

1) Pitch Optimization Under Swirling Conditions: Future studies should endeavor to systematically explore the optimization of pitch under varying swirling main flow conditions. This includes investigating the potential overlapping effects of effusion jets at different blowing ratios (BRs) and the resultant impact on cooling film uniformity.
2) Comprehensive Evaluation of Varying Compound Angles: While this thesis initiates the exploration of varying compound angles along the main flow direction, further research is warranted to comprehensively evaluate the performance of such designs across a broader spectrum of operational conditions, particularly focusing on the initiation stages of cooling film development.
3) Integration with Computational Fluid Dynamics (CFD): The integration of experimental findings with CFD simulations presents a promising avenue for enhancing the predictive accuracy of effusion cooling performance under realistic operational conditions, facilitating more refined design optimizations.
4) Material Innovations: Alongside aerodynamic optimizations, material innovations, particularly in the development of advanced thermal barrier coatings, should be pursued to complement the aerodynamic advancements in effusion cooling strategies.
5) Swirl Number Considerations: Finally, considering the swirling effect of the main flow, future designs should incorporate swirl number considerations to ensure the proposed optimal compound angle of 45° and the effective pitch are realistically achievable within the operational dynamics of gas turbine combustors.

The current thesis represents a step forward in the ongoing journey to enhance the efficiency and longevity of gas turbine systems through advanced cooling technologies. The findings and future directions outlined herein contribute to the broader discourse on sustainable and efficient energy production in the face of global environmental challenges.

REFERENCES

[1] K. Hunecke, “Jet Engines: Fundamentals of Theory, Design and Operation,” Airlife, Shrewsbury, England, 2010.

[2] “Fossil and Alternative Fuels - Energy Content,” https://www.engineeringtoolbox.com/fossil-fuels-energy-content-d_1298.html (accessed Feb 2, 2024).

[3] A. Ulvestad, “A Brief Review of Current Lithium Ion Battery Technology and Potential Solid State Battery Technologies,” Mar. 2018. [Online], http://arxiv.org/abs/1803.04317.

[4] H. Kobayashi, A. Hayakawa, K.D. Somarathne, and E. Okafor, “Science and technology of ammonia combustion,” *Proceedings of the Combustion Institute*, Vol. 37, no. 1, 2019, pp. 109-133. https://doi.org/10.1016/j.proci.2018.09.029.

[5] S. Naik, “Basic Aspects of Gas Turbine Heat Transfer [Internet],” *Heat Exchangers - Design, Experiment and Simulation.* InTech; 2017. http://dx.doi.org/10.5772/67323.

[6] S. Ahmed, P. Singh, and S. V. Ekkad, "Comparison of Different Combustion Liner Cooling Techniques under Non-Reacting Conditions for a Lean Pre-Mixed Fuel Nozzle," *AIAA Scitech 2019 Forum*, pp. 1-13, 2019. https://doi.org/10.2514/6.2019-0532.

[7] D. G. Ritchie, A. J. Click, P. M. Ligrani, F. Liberatore, R. Patel, and Y. H. Ho, "Double Wall Cooling of an Effusion Plate with Cross Flow and Impingement Jet Combination Internal Cooling: Comparisons of Main Flow Contraction Ratio Effects," *AIAA Propulsion and Energy 2019 Forum*, pp. 1-18, 2019. https://doi.org/10.2514/6.2019-3967.

[8] B. Goswami, S. K. Sahay, and A. K. Ray, "Application of Thermal Barrier Coatings on Combustion Chamber Liners – A Review," *High Temperature Materials and Processes*, vol. 23, no. 3, pp. 211-236, 2004. https://doi.org/10.1515/HTMP.2004.23.3.211.

[9] P. Grootenhuis, "The Mechanism and Application of Effusion Cooling,” *The Journal of the Royal Aeronautical Society*, vol. 63, no. 578, pp. 73–89, 1959. https://doi.org/10.1017/S0368393100070632.

[10] K. M. B. Gustafsson, "Experimental Studies of Effusion Cooling," Ph. D. Dissertation, Department of Thermo and Fluid Dynamics, Charlmers University of Technology, Göteborg, Sweden, 2001.

[11] H. H. Cho, D. H. Rhee, and R. J. Goldstein, "Effects of Hole Arrangements on Local Heat/Mass Transfer for Impingement/Effusion Cooling with Small Hole Spacing," *Journal of Turbomachinery*, vol. 130, no. 4, 2008. https://doi.org/10.1115/1.2812325.

[12] R. Krewinkle, "A Review of Gas Turbine Effusion Cooling Studies," *International Journal of Heat and Mass Transfer*, vol. 66, pp. 706–722, 2013. https://doi.org/10.1016/j.ijheatmasstransfer.2013.07.071.

[13] G. Cerri, A. Giovannelli, L. Battisti, and R. Fedrizzi, "Advances in Effusive Cooling Techniques of Gas Turbines," *Applied Thermal Engineering*, vol. 27, no. 4, pp. 692–698, 2007. https://doi.org/10.1016/j.applthermaleng.2006.10.012.

[14] D. G. Bogard, "Gas Turbine Film Cooling," *Journal of Propulsion and Power*, vol. 22, no. 2, pp. 249–270, 2006. https://doi.org/10.2514/1.18034.

[15] L. C. Paitich, P. Richer, B. Jodoin, Y. Pyo, S.Yun, and Z. Hong, "Directional Effects of Effusion Cooling on the Cooling Film Effectiveness," *AIAA Journal*, pp.1-12, 2021. https://doi.org/10.2514/1.J060625.

[16] A. H. Lefebvre and D. R. Ballal, "Gas Turbine Combustion: Alternative Fuels and Emissions," CRC Press, Boca Raton, FL, 2010.

[17] C. Borgnakke and R. E. Sonntag, "Fundamentals of Thermodynamics 10th Ed.," Wiley, Hoboken, New Jersey, 2019.

[18] "Airplane Flying Handbook," U.S. Department of Transportation, Federal Aviation Administration, Oklahoma City, OK, volume FAA-H-8083-3C, 2021.

[19] R. S. Bunker, "Evolution of turbine cooling," Proc. ASME Turbo Expo, vol. 1, pp. 1–26, 2017. https://doi.org/10.1115/GT2017-63205.

[20] G. Cerri, A. Giovannelli, L. Battisti, and R. Fedrizzi, "Advances in effusive cooling techniques of gas turbines," Appl. Therm. Eng., vol. 27, no. 4, pp. 692–698, Mar. 2007. https://doi.org/10.1016/j.applthermaleng.2006.10.012.

[21] L. Mazzei, S. Puggelli, D. Bertini, A. Andreini, B. Facchini, I. Vitale and A. Santoriello, "Numerical and Experimental Investigation on an Effusion-Cooled Lean Burn Aeronautical Combustor: Aerothermal Field and Emissions," *ASME. Turbo Expo: Power for Land, Sea, and Air, Vols. Volume 4B: Combustion, Fuels, and Emissions*, 2018. https://doi.org/10.1115/1.4041676.

[22] K. M. B. Gustafsson, "Experimental Studies of Effusion Cooling, "PhD Thesis, Department of Thermo and Fluid Dynamics, Chalmers University of Technology, Goteborg, Sweden, 2001.

[23] D. Dupuy, A. Perrot, N. Odier, L.Y.M. Gicquel and F. Duchaine, "Boundary-condition models of film-cooling holes for large-eddy simulation of turbine vanes," *International Journal of Heat and Mass Transfer*, Volume 166, 2021, 120763, ISSN 0017-9310. https://doi.org/10.1016/j.ijheatmasstransfer.2020.120763.

[24] H. Wang and L. M. Wright, "TPIV Experimental Investigation of Film Coolant-to-Mainstream Interaction from Shaped Cooling Holes with Various Inlet Geometries." *Journal of Turbomachinery*, May 2024; 146(5): 051006. https://doi.org/10.1115/1.4064261.

[25] M. Gritsch, A. Schulz and S. Wittig, "Adiabatic Wall Effectiveness Measurements of Film-Cooling Holes with Expanded Exits." *Journal of Turbomachinery*, July 1998; 120(3): 549–556. https://doi.org/10.1115/1.2841752.

[26] R. P. Schroeder and K. A. Thole, "Adiabatic Effectiveness Measurements for a Baseline Shaped Film Cooling Hole." *Journal of Turbomachinery,* December 2022; 144(12): 121003. https://doi.org/10.1115/1.4055271.

[27] R. Krewinkel, A review of gas turbine effusion cooling studies, International Journal of Heat and Mass Transfer, Volume 66, 2013, Pages 706-722, ISSN 0017-9310, https://doi.org/10.1016/j.ijheatmasstransfer.2013.07.071.

[28] A. Andreini, R. Becchi, B. Facchini, A. Picchi and A. Peschiulli, "The effect of effusion holes inclination angle on the adiabatic film cooling effectiveness in a three-sector gas turbine combustor rig with a realistic swirling flow," *International Journal of Thermal Sciences*, Vol. 121, 2017, Pages 75-88, ISSN 1290-0729, https://doi.org/10.1016/j.ijthermalsci.2017.07.003.

[29] H. H. Cho, D. H. Rhee, and R. J. Goldstein, "Effects of Hole Arrangements on Local Heat/Mass Transfer for Impingement/Effusion Cooling with Small Hole Spacing,"

Journal of Turbomachinery, Vol. 130, no. 4, 2008. https://doi.org/10.1115/1.2812325.

[30] T. Lenzi, A. Picchi, R. Becchi, A. Andreini and B. Facchini, "Swirling main flow effects on film cooling: Time resolved adiabatic effectiveness measurements in a gas turbine combustor model," *International Journal of Heat and Mass Transfer*, Vol. 200, 2023. https://doi.org/10.1016/j.ijheatmasstransfer.2022.123554.

[31] Y. Ji, B. Ge and S. Zang, "Analysis of effusion cooling under realistic swirl reacting flow in gas turbine combustor," *Applied Thermal Engineering*, Vol. 216, 2022. https://doi.org/10.1016/j.applthermaleng.2022.119101.

[32] Y. Pyo, J. Son, P. Richer, B. Jodoin, M. Broumand, S. Yun and Z. Hong, "Isolating Influences of Varying Pitch from the Effects of Non-Zero Compound Angles on Effusion Cooling," *The Aeronautical Journal* (2024). https://doi.org/10.1017/aer.2024.108.

[33] G. Wang, G. Ledezma, J. Delancey and A. Wang, "Experimental Study of Effusion Cooling with Pressure-Sensitive Paint," *Journal of Engineering for Gas Turbines and Power*, vol. 139, no. 5, 2017. https://doi.org/10.1115/1.4034943.

[34] X. Chen, J. Krawciw, H. Xia, P.A. Denman, C. Bonham and J.F. Carrotte, "Study of an effusion-cooled plate with high level of upstream fluctuation," *Applied Thermal Engineering,* Vol. 184, 2021.https://doi.org/10.1016/j.applthermaleng.2020.116126.

[35] Paitich, L. C., Richer, P., Jodoin, B., Pyo, Y., Yun, S., and Hong, Z. "Directional Effects of Effusion Cooling on the Cooling Film Effectiveness." *AIAA Journal*, (2021): pp.1-12. DOI: 10.2514/1.J060625.

[36] Y. Pyo, J. Son, P. Richer, B. Jodoin, M. Broumand, S. Yun and Z. Hong, "Enhanced Adiabatic Film Cooling Effectiveness by Varying Compound Angle," 2024 *ASME Turbo Expo*, 2024.

[37] Z. Lei, A. Mahallati, M. Cunningham and P. Germain, "Influence of Inlet Swirl on the Aerodynamics of a Model Turbofan Lobed Mixer." *ASME International Mechanical Engineering Congress and Exposition*. pp. 807–819, 2012. https://doi.org/10.1115/IMECE2010-39.

[38] D. G. Bogard and K. A. Thole, "Gas turbine film cooling," *Journal of Propulsion and Power*, vol. 22, no. 2, pp. 249–270, 2006. https://doi.org/10.2514/1.18034.

[39] A. K. Sinha, D. G. Bogard, and M. E. Crawford, "Film-cooling effectiveness downstream of a single row of holes with variable density ratio," *Journal of Turbomachinery*, vol. 113, no. 3, pp. 442–449, 1991. https://doi.org/10.1115/1.2929110.

[40] D. L. Schmidt, B. Sen, and D. G. Bogard, "Film cooling with compound angle holes: Adiabatic effectiveness," *Journal of Turbomachinery*, vol. 118, no. 4, pp. 807–813, 1996. https://doi.org/10.1115/1.2840947.

[41] DANTEC Website: https://www.dantecdynamics.com/product/cable-equipped-wire-probe/ (accessed Mar 5, 2024).

[42] D. R. Ballal and A. H. Lefebvre, "Flame quenching in turbulent flowing gaseous mixtures," Symposium (International) on Combustion, Volume 16, Issue 1, Pages 1689-1698, 1977. https://doi.org/10.1016/S0082-0784(77)80447-5.

[43] T. Bacci, A. Picchi, T. Lenzi and B. Facchini, "Turbulence Intensity Measurements across a NGV cooled cascade with representative lean burn combustor outflow". In:

2019. URL: http://www.euroturbo.eu/

[44] M. Folk, R. J. Miller and J. D. Coull, "The Impact of Combustor Turbulence on Turbine Loss Mechanisms." *Journal of Turbomachinery*. September 2020; 142(9): 091009. https://doi.org/10.1115/1.4047615.

[45] T. Liu, B. T. Campbell, S. P. Burns, and J. P. Sullivan, "Temperature- and Pressure-Sensitive Luminescent Paints in Aerodynamics," *Applied Mechanics Reviews*, vol. 50, no. 4, pp. 227–246, 1997. https://doi.org/10.1115/1.3101703.

[46] J. W. Gregory, K. Asai, M. Kameda, T. Liu and J. P. Sullivan, "A review of pressure-sensitive paint for high-speed and unsteady aerodynamics," *Proceeding of the Institution of Mechanical Engineers, Part G: Journal of Aerospace Engineering*, vol. 222, no. 2, pp. 249-290, 2008. https://doi.org/10.1243/09544100JAERO2.

[47] A. Andreini, B. Fachhini, A. Picchi, L. Tarchi and F. Turrini, "Experimental and Theoretical Investigation of Thermal Effectiveness in Multi-Perforated Plates for Combustor Liner Effusion Cooling," *Journal of Turbomachinery*, vol. 136, no. 9, pp. 1-13, 2014. https://doi.org/10.1115/1.4026846.

[48] G. Wang, G. Ledezma, J. Delancey and A. Wang, "Experimental Study of Effusion Cooling with Pressure-Sensitive Paint," *Journal of Engineering for Gas Turbines and Power*, vol. 139, no. 5, 2017. https://doi.org/10.1115/1.4034943.

[49] L. Andrei, A. Andreini, C. Bianchini, G. Caciolli, B. Fachhini, A. Picchi, L. Tarchi and F. Turrini, "Effusion cooling plates for combustor liners: experimental and numerical investigations on the effect of density ratio," *Energy Procedia*, no. 45, pp. 1402-1411, 2014. https://doi.org/10.1016/j.egypro.2014.01.147.

[50] G. Barigozzi, C. Mucignat, H. Abdeh, D. Scandella and G. Dolci, "Assessment of binary PSP technique for film cooling effectiveness measurement on nozzle vane cascade with cutback trailing edge," *Experimental Thermal and Fluid*, vol. 97, no. 201, pp. 431-443, 2014. https://doi.org/10.1016/j.expthermflusci.2018.05.015.

[51] Innovative Scientific Solutions Inc. Binary Pressure-Sensitive Paint (http://www.psp-tsp.com). Accessed 20 April 2023.

[52] D. Mclean, "Referenced pressure paint and the ratio of ratios," *Proceedings of the Sixth Annual Pressure Sensitive Paint Workshop,* The Boeing Company, Seattle, Washington, pp. 11–1:35, 1998.

[53] T. Liu, T. Ben and J. P. Sullivan, " Pressure Sensitive Paints," NASA Review Article, 2000. (https://ntrs.nasa.gov/api/citations/20000000191/downloads/20000000191.pdf)

[54] T. V. Jones, "Theory for the Use of Foreign Gas in Simulating Film Cooling," *International Heat and Fluid Flow*, vol. 20, no. 3, pp. 349–354, 1999. https://doi.org/10.1016/S0142-727X(99)00017-X.

[55] T. L. Bergman, A. S. Lavine, F. P. Incropera and D. P. Dewitt, "Fundamentals of Heat and MassTransfer - Seventh Edition," John Wiley & Sons, 2012.

[56] S. Kline and F. McClintock, "Describing the uncertainties in single-sample experiments," *Mech. Eng*. 75 , 1953.

[57] T. Liu and J. P. Sullivan, K. Asai, C. Klein and Y. Egami "Pressure and Temperature Sensitive Paints," Springer, 2005. https://doi.org/10.1007/978-3-030-68056-5.

Appendix – A: CFD Simulations of Vent and Reservoir System Designs

A.1 Reservoir Simulation

The CAD design and meshing of the reservoir were performed within COMSOL Multiphysics 6.0, setting a foundation for detailed flow analysis (as depicted in Figure 16). Utilizing the Standard k-omega model within the RANS (Reynolds Averaged Navier-Stokes) simulation framework, the boundary conditions were aligned with experimental parameters, specifically targeting a blowing ratio of 0.6.

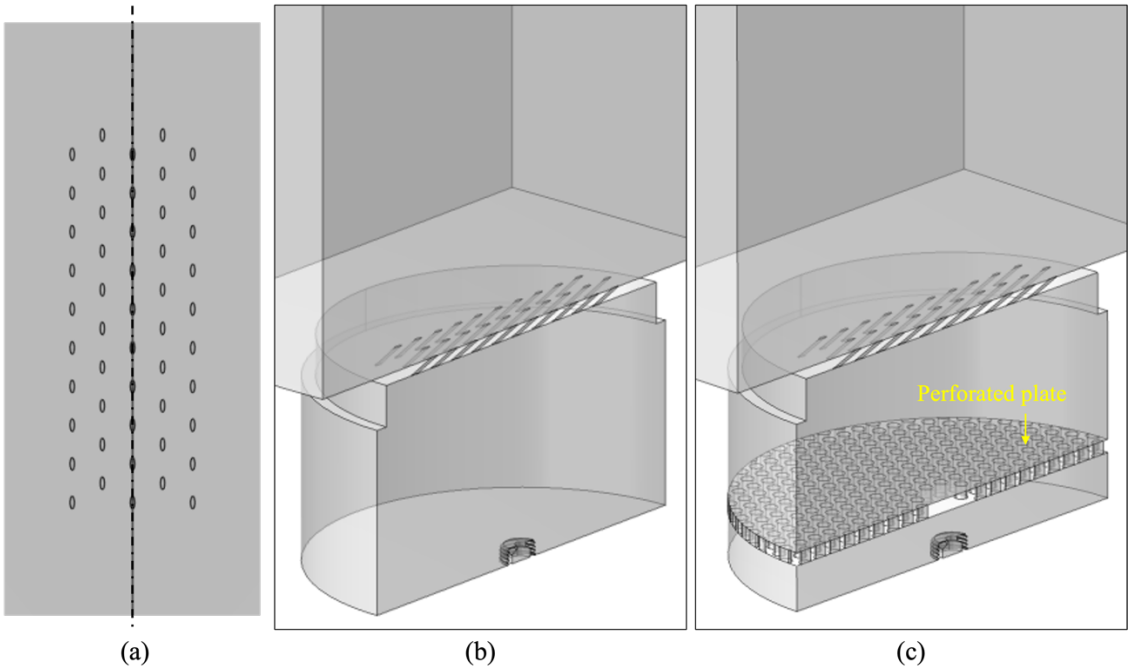

Figure 32. The 2D and 3D domains of the numerical simulation: (a) the cooling hole distribution, (b) the geometry of the design without the perforated plate in the reservoir, and (c) the geometry of the design with the perforated plate in the reservoir. The 3D domain is shown as a cross-section view.

The CFD results, illustrated in Figures A.2(a) and A.2(b), compare the velocity contours and streamlines for configurations with and without the perforated plate. In the absence of the perforated plate (Figure A.1(a)), swirling flows and uneven cooling flow distributions were observed, notably near the inlet of upstream and downstream effusion cooling holes. This non-uniformity was further exacerbated by jetting of the cooling flow inlet, leading to high-speed turbulent flows directly impinging on the cooling holes.

Conversely, the inclusion of the perforated plate significantly mitigated these flow disturbances, as shown in Figure A.2(b). As shown in Figure A.3, the biased high swirling flow and direct high-speed flow impacts were substantially reduced, enhancing flow uniformity across the test samples, and reducing the maximum coolant flow velocity difference between holes from 9.2% to 1%. Further refinement was achieved by installing a honeycomb structure near the top of the reservoir, ensuring a highly uniform distribution of coolant flow (refer to Figure 16).

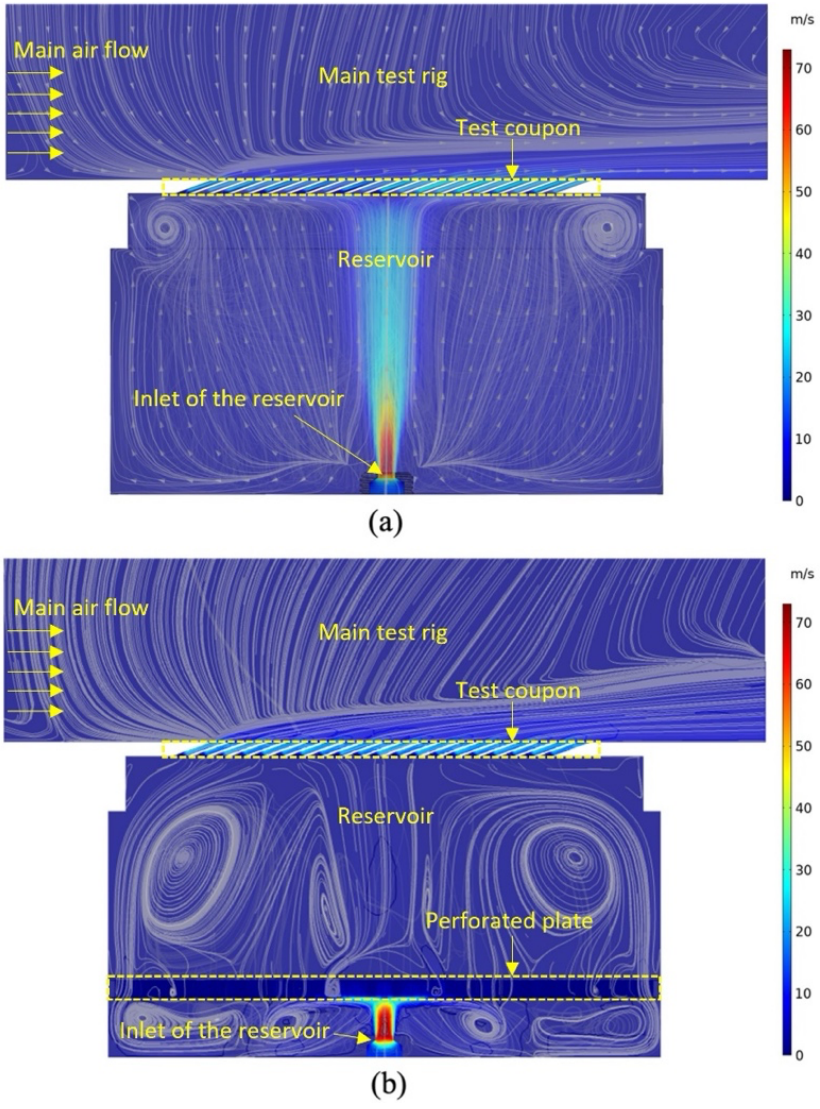

Figure 33. The side-view of the velocity contour and streamlines for the case (a) without the perforated plate and (b) with the perforated plate.

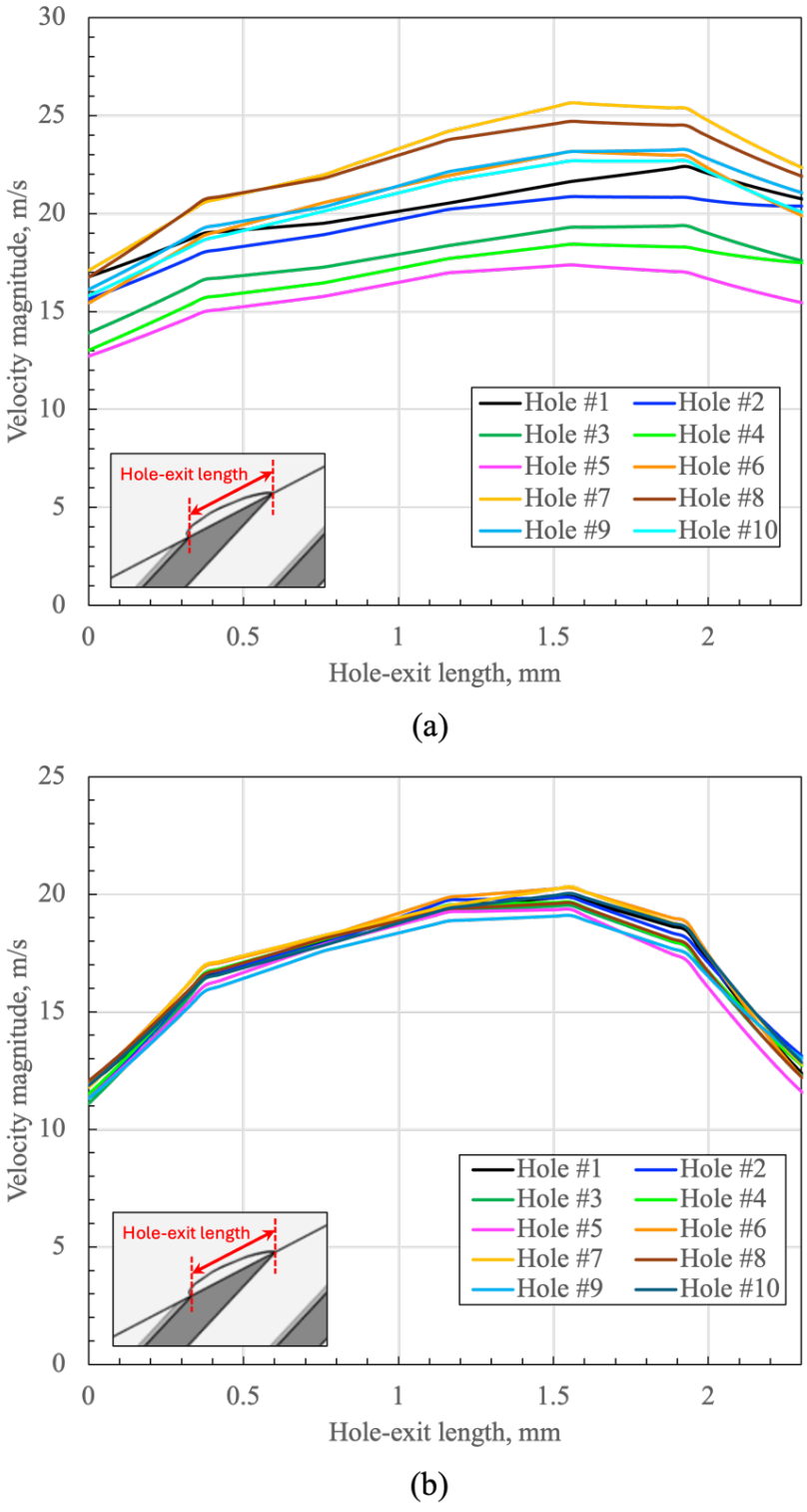

Figure 34. The velocity profiles at the exit of each cooling hole for the case (a) without the perforated plate and (b) with the perforated plate.

A.2 Vent System Simulation

Prior to empirical testing, the vent system's design underwent validation via CFD simulations using COMSOL Multiphysics 6.0, ensuring accurate representation of the test rig's geometry (illustrated in Figure A.4). These simulations were conducted to evaluate the effectiveness of the vent system in controlling boundary layer thickness, aiming for a target thickness of 10 mm and a momentum thickness Reynolds number in the range of 1000-1500, both of which align with experimental objectives and conditions typically found in gas turbine combustor liners.

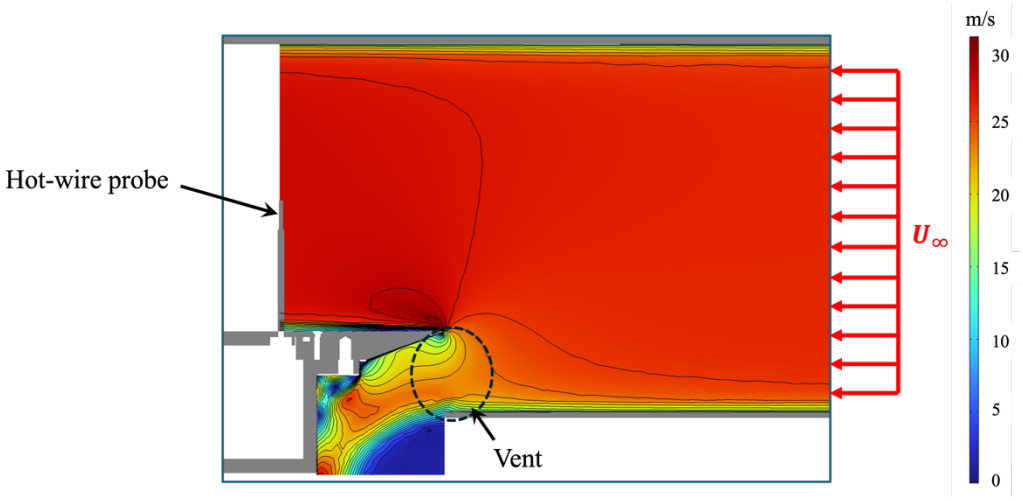

Figure 35. The 2D contour of the velocity profile at the cross-section of the test rig including the vent system.

The CFD methodology was based on a steady-state (stationary) simulation using the k- ω turbulence model, selected for its robustness in capturing near-wall turbulence effects and boundary layer behavior. A velocity inlet of 33m/s and a relative pressure outlet of 0Pa were applied as boundary conditions at the inlet and outlet, respectively, while all solid surfaces were assigned no-slip boundary conditions to accurately model wall interactions. The CFD solver in COMSOL Multiphysics 6.0 utilizes a finite element method (FEM) to solve the steady-state, incompressible Navier–Stokes equations, coupled with the k–ω turbulence model. The incompressibility assumption is valid given the subsonic (low Mach number, << 0.3) conditions of the vent system.

The mesh resolution in critical regions near the vent and wall boundaries reached approximately 50 µm, allowing accurate resolution of boundary layer velocity gradients.

A low background turbulence intensity (< 1%) was specified at the inlet to reflect wind tunnel conditions and ensure consistency with hot-wire measurements performed experimentally.

To ensure sufficient resolution of turbulence effects, particularly near the vent region, a structured mesh was generated with a total of 1,284,322 elements. The mesh was refined near the vent opening and along the test section walls to accurately capture velocity gradients and boundary layer development. A y+ between 1 and 5 was maintained near the walls to satisfy the resolution requirements of the k-omega model.

A mesh independence study was conducted by comparing results across three mesh densities: coarse (642,456 elements), medium (1,284,322 elements), and fine (2,115,949 elements). The mean velocity profiles in the boundary layer, located at the hot wire installed position, were compared for each mesh configuration. As shown in Figure A.5, the medium and fine mesh results are nearly identical, with a velocity and boundary layer thickness deviation of less than 2%, confirming mesh independence. The medium mesh was therefore selected for the remainder of the simulations, balancing accuracy and computational cost.

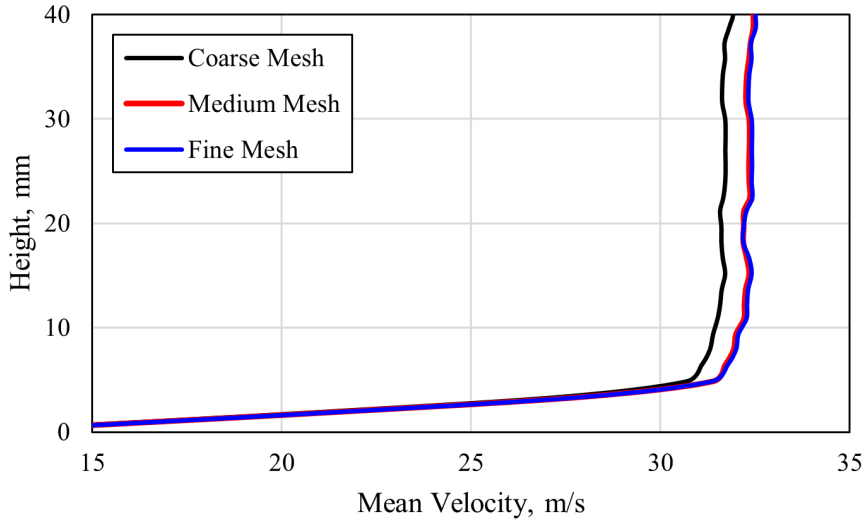

Figure 36. Comparison of boundary layer velocity profiles for three mesh densities: coarse (black), medium (red), and fine (blue). The results confirm mesh independence as the medium and fine mesh curves overlap closely.

Appendix – B

The Matlab code used to calibrate and analyze the PSP raw data capturing by CCD camera with Image Doubler. The below is the example of the Matlab code used for the study of Optimizing Adiabatic Film Cooling Effectiveness through Varying Compound Angles.

```
%%-------- Calibration of Binary-PSP for the CCD camera ----------
%%%% Location: M10_Co-axial_round_room, NRC-CNRC, Ottawa, ON, Canada
%%%% Yeongmin Pyo

clc
clear
close all

% Design: Combined-BETA

%% Call Spreadsheet-files(.csv) --- The raw data was already processed as R_ref/R in
DaVis software
Rref_R_01 = readtable('varying_20231109_air00.csv') ;
Rref_R_02 = readtable('varying_20231109_air05.csv') ;
Rref_R_03 = readtable('varying_20231109_air10.csv') ;
Rref_R_04 = readtable('varying_20231109_air15.csv') ;
Rref_R_05 = readtable('varying_20231109_air20.csv') ;
Rref_R_06 = readtable('varying_20231109_air25.csv') ;
Rref_R_07 = readtable('varying_20231109_air30.csv') ;
Rref_R_08 = readtable('varying_20231109_air35.csv') ;
Rref_R_09 = readtable('varying_20231109_air40.csv') ;
Rref_R_10 = readtable('varying_20231109_air45.csv') ;

Rref_R_060 =readtable('varying_20231109_br060.csv')  ;
Rref_R_100 =readtable('varying_20231109_br100.csv')  ;
Rref_R_140 =readtable('varying_20231109_br140.csv')  ;

%% Cell to Matrix
x_01 = Rref_R_01{:,:} ;
x_02 = Rref_R_02{:,:} ;
x_03 = Rref_R_03{:,:} ;
x_04 = Rref_R_04{:,:} ;
x_05 = Rref_R_05{:,:} ;
x_06 = Rref_R_06{:,:} ;
x_07 = Rref_R_07{:,:} ;
x_08 = Rref_R_08{:,:} ;
x_09 = Rref_R_09{:,:} ;
x_10 = Rref_R_10{:,:} ;

x_060 = Rref_R_060{:,:} ;
x_100 = Rref_R_100{:,:} ;
x_140 = Rref_R_140{:,:} ;

%% C/C_ref = a1*(r_ref/r)^2 + a2*(r_ref/r) + a3
C_Cref = [0.0000 0.1111 0.2222 0.3333 0.4444 0.5556 0.6667 0.7778 0.8889 1.0000] ; % Be
careful of the order

n = length(x_060(1,:));
m = length(x_060(:,1));

%---------- beta = Combined ------------------------------------------------------------
-------------------------------------------------------
y_060 = ones(m,n);
y_100 = ones(m,n);
y_140 = ones(m,n);
for j=1:n
    for i=1:m
        % Setup the components of the fitting function
```

```
        x = [x_01(i,j) x_02(i,j) x_03(i,j) x_04(i,j) x_05(i,j) x_06(i,j) x_07(i,j)...
             x_08(i,j) x_09(i,j) x_10(i,j)];
        y = C_Cref;
        a = polyfit(x,y,2); % Coefficients of the polytropic fitting function

        % Polytropic curve fitting function for Binary-PSP
        f_060 = a(1)*x_060(i,j).^2 + a(2)*x_060(i,j) + a(3);
        f_100 = a(1)*x_100(i,j).^2 + a(2)*x_100(i,j) + a(3);
        f_140 = a(1)*x_140(i,j).^2 + a(2)*x_140(i,j) + a(3);

        % To fit [0<η<1]
        if f_060 < 0
            y_060(i,j) = 0;
        elseif f_060 > 1
            y_060(i,j) = 1;
        else
            y_060(i,j) = f_060;
        end

        if f_100 < 0
            y_100(i,j) = 0;
        elseif f_100 > 1
            y_100(i,j) = 1;
        else
            y_100(i,j) = f_100;
        end

        if f_140 < 0
            y_140(i,j) = 0;
        elseif f_140 > 1
            y_140(i,j) = 1;
        else
            y_140(i,j) = f_140;
        end
    end
end

eta_060 = 1 - y_060;
eta_100 = 1 - y_100;
eta_140 = 1 - y_140;

%% Post-processing
L_span = 38.779; % mm
L_stream = 70.866; % mm

l_span = length(x_060(1,:));
l_stream = length(x_060(:,1));
l_st = linspace(0, L_stream/0.787, l_stream);
l_st_inv_comb = linspace(L_stream/0.787, 0, l_stream) ;
l_sp_comb = linspace(0, L_span/0.787, l_span) ;

n_st_sum_060_beta45_fix = sum(eta_060,2) ;
n_st_060_beta45_fix = n_st_sum_060_beta45_fix./l_span;
n_sp_sum_060_beta45_fix = sum(eta_060,1) ;
n_sp_060_beta45_fix = n_sp_sum_060_beta45_fix./l_stream;
n_st_sum_100_beta45_fix = sum(eta_100,2) ;
n_st_100_beta45_fix = n_st_sum_100_beta45_fix./l_span;
n_sp_sum_100_beta45_fix = sum(eta_100,1) ;
n_sp_100_beta45_fix = n_sp_sum_100_beta45_fix./l_stream;
n_st_sum_140_beta45_fix = sum(eta_140,2) ;
n_st_140_beta45_fix = n_st_sum_140_beta45_fix./l_span;
n_sp_sum_140_beta45_fix = sum(eta_140,1) ;
n_sp_140_beta45_fix = n_sp_sum_140_beta45_fix./l_stream;

eta_060_ave_beta45_fix =
(sum(n_st_060_beta45_fix(:))+sum(n_sp_060_beta45_fix(:)))./(l_span+l_stream) ;
eta_060_std_n_beta30_fix = std(eta_060);
eta_060_std_beta45_fix =
sum(eta_060_std_n_beta30_fix(:))./length(eta_060_std_n_beta30_fix) ;
```

```
eta_100_ave_beta45_fix =
(sum(n_st_100_beta45_fix(:))+sum(n_sp_100_beta45_fix(:))./(l_span+l_stream) ;
eta_100_std_n_beta45_fix = std(eta_100);
eta_100_std_beta45_fix =
sum(eta_100_std_n_beta45_fix(:))./length(eta_100_std_n_beta45_fix) ;
eta_140_ave_beta45_fix =
(sum(n_st_140_beta45_fix(:))+sum(n_sp_140_beta45_fix(:))./(l_span+l_stream) ;
eta_140_std_n_beta45_fix = std(eta_140);
eta_140_std_beta45_fix =
sum(eta_140_std_n_beta45_fix(:))./length(eta_140_std_n_beta45_fix) ;

%% Overall Averaged AFE
ave = array2table([eta_060_ave_beta45_fix eta_100_ave_beta45_fix
eta_140_ave_beta45_fix],...
                  'VariableNames', {'BR=0.60' 'BR=1.00' 'BR=1.40'},...
                  'RowName',{'With_Holes'}) ;
disp(ave)
```